Stony Brook University

Molecular Mechanisms of Ionotropic Glutamate Receptor Assembly

A Dissertation Presented

by

Catherine Lourdes Salussolia

to

The Graduate School

in Partial Fulfillment of the

Requirements

for the Degree of

Doctor of Philosophy

in

Neuroscience

Stony Brook University

May 2012

Stony Brook University

The Graduate School

Catherine Lourdes Salussolia

We, the dissertation committee for the above candidate for the

Doctor of Philosophy degree, hereby recommend

acceptance of this dissertation.

Lonnie P. Wollmuth - Dissertation Advisor
Professor, Department of Neurobiology and Behavior

Maurice Kernan - Chairperson of Defense
Associate Professor, Department of Neurobiology and Behavior

David Talmage
Associate Professor, Department of Pharmacological Sciences

Hiro Furukawa
Assistant Professor, Neuroscience, Cold Spring Harbor Laboratory

Myles Akabas
Professor, Department of Physiology and Biophysics,
Albert Einstein College of Medicine

This dissertation is accepted by the Graduate School

Charles Taber
Interim Dean of the Graduate School

Abstract of the Dissertation

Molecular Mechanisms of Ionotropic Glutamate Receptor Assembly

by

Catherine Lourdes Salussolia

Doctor of Philosophy

in

Neuroscience

Stony Brook University

2012

Fast excitatory neurotransmission mediated by the neurotransmitter glutamate via ionotropic glutamate receptors (iGluRs) is essential to central nervous system function. Perturbations in glutamatergic signaling – including alterations in iGluR membrane expression – have been implicated in numerous nervous system diseases including psychiatric, developmental, acute excitotoxic and chronic neurodegenerative disorders. iGluR biogenesis is a complex process that requires many coordinated events – biosynthesis, folding, oligomerization of subunits (dimerization and tetramerization), post-translational modification, and insertion into the plasma membrane. iGluR subtypes form preferential (AMPA, kainate) or obligate (NMDA) heterotetramers that assemble as a dimer of dimers to yield functional receptors.

Functional NMDA receptors (NMDARs) are obligate heteromers composed of two GluN1 and typically two GluN2 subunits; however, the arrangement of subunits in functional tetrameric complexes – whether identical subunits are positioned adjacent to

(N1/N1/N2/N2) or diagonal to (N1/N2/N1/N2) one another – was controversial. In my first project, I addressed the arrangement of subunits in functional NMDARs by utilizing the recent insight that individual subunits within a homotetrameric AMPA receptor adopt two distinct conformations – termed A/C and B/D. Using cysteine mutagenesis, immunoblots, and functional assays, I showed that GluN subunits adopt distinct subunit-specific conformations with the GluN1 and GluN2 subunits approximating the A/C and B/D conformations, respectively, demonstrating that GluN subunits are positioned in a N1/N2/N1/N2 arrangement.

In contrast to prokaryotic iGluR subunits, all eukaryotic iGluRs have an additional transmembrane segment, the M4 segment, located C-terminal to the ion channel core (M1-M3). Surprisingly, in the AMPAR structure, the M4 segment of one subunit was associated with the ion channel core of an adjacent subunit. My second project addressed the functional implications of the M4 transmembrane segment. I showed that disruption of a specific face of M4 that is closely apposed to the adjacent M1 and M3 segments in the crystal structure results in a loss of AMPAR surface expression. These data suggest that the M4/ion channel core interaction is necessary for iGluR expression and may represent a novel mechanism regulating iGluR assembly. Overall my work provides novel insights into the biogenic mechanisms regulating the structure/function of iGluRs and suggests possible therapeutic targets for modulating dysfunctional glutamatergic activity.

To my loving family – my parents, Nicholas, and my grandparents - for all of the support, encouragement, and inspiration you have provided me throughout my education.

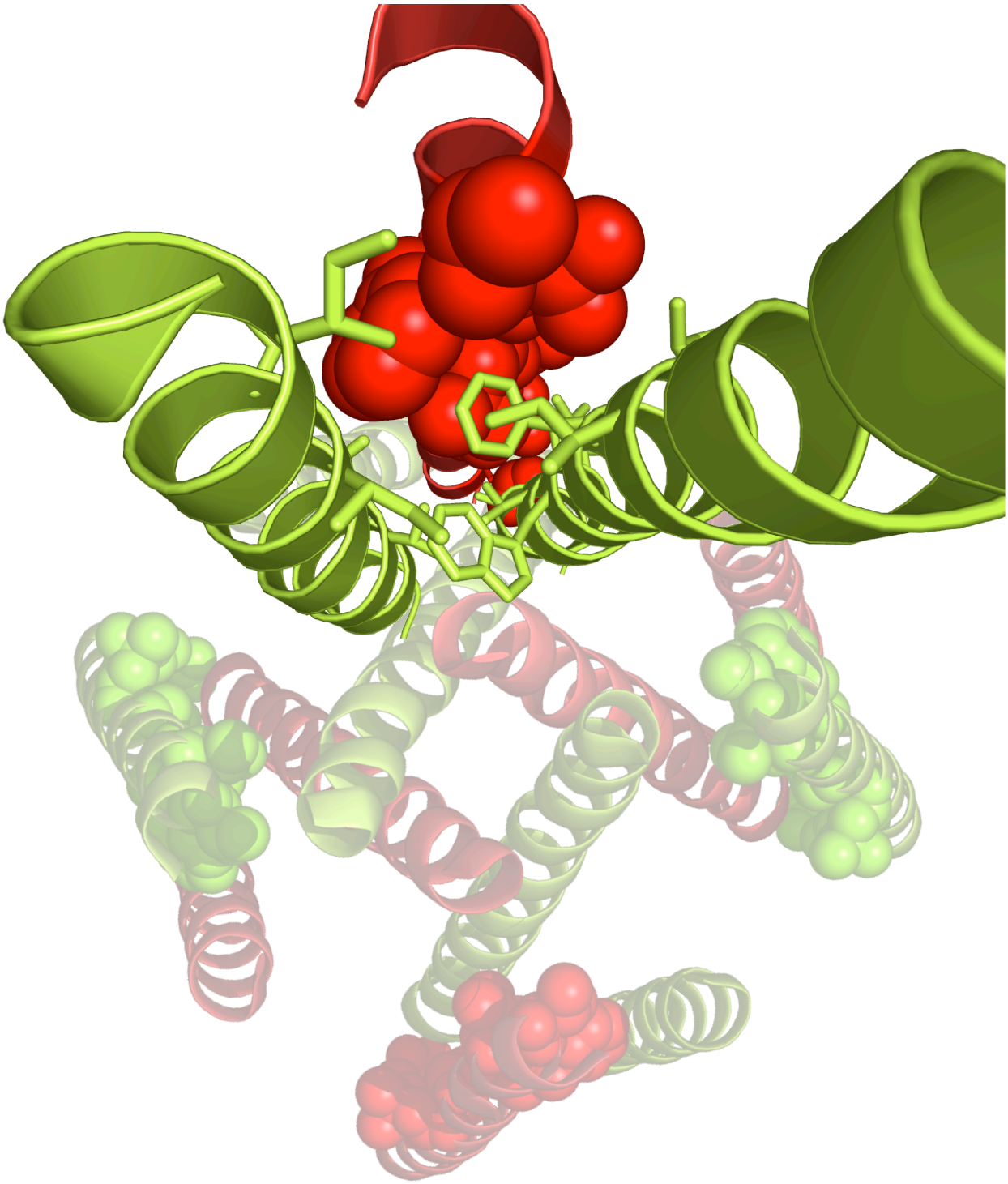

TABLE OF CONTENTS

LIST OF FIGURES

LIST OF TABLES

LIST OF ABBREVIATIONS

iGluRs:	Ionotropic glutamate receptors
NTD:	amino-terminal domain
LBD:	ligand-binding domain
CTD:	carboxyl-terminal domain
PSD:	postsynaptic density
AMPAR:	α-amino-3-hydroxy-5-methyl-4-isoxazolepropionic acid receptor
NMDAR:	N-methyl-D-aspartate receptor
KAR:	kainate receptor
LTP:	long-term potentiation
LTD:	long-term depression
ER:	endoplasmic reticulum
FSEC:	fluorescence-detection size exclusion chromatography
BN-PAGE:	blue native-PAGE
DTT:	dithiothreitol
GABA:	γ-aminobutyric acid
MAGUK:	membrane-associated guanylate kinase
TARP:	transmembrane AMPA receptor regulatory proteins
CNQX:	6-cyano-7-nitroquinoxaline-2,3-dione
MTS:	methanethiosulfonate
MTSET:	2-(trimethylammonium)ethyl methanethiosulfonate
GAPDH:	glyceraldehyde 3-phosphate dehydrogenase
CTZ:	cyclothiazide

ACKNOWLEDGEMENTS

My deepest gratitude to Janet Allopenna for all of the time and effort she put into generating all of the constructs used in my research projects. Janet was instrumental in all aspects of my work, serving as a sounding board and helping me troubleshoot protocols. Additionally, I would like to thank Janet for her support and camaraderie throughout my dissertation research.

I thank my mentor and advisor Dr. Lonnie P. Wollmuth for his tutelage and challenging me to think critically about experimental questions. His comments and feedback – both verbal and via red fine-point pens – have aided my maturation as a scientist.

I would like to thank all the past and current members of the Wollmuth Lab who have aided me in my work including: Dr. Alexandra Corrales, Dr. Iehab Talukder, Dr. Michael Prodromou, Gulcan Akgul, Jessica Helm, Martin Prieto, Rashek Kazi, Quan "Alfred" Gan, Michael Markowitz, and Ashwin Malhotra. I would like to especially thank Gulcan, aka "Swiss", for her friendship and the many songs we shared over the course of the past four years.

I appreciate the support and insight I garnered from my thesis committee – Drs. Maurice Kernan, Hiro Furukawa, Myles Akabas, and David Talmage – over the years. Their input has been indispensible. I would like to thank Drs. Puja Singh and Hiro Furukawa for their assistance in completing my FSEC work. I would also like to thank Dr. Michael Frohman and Carron Kaufman of the Medical Scientist Training Program for their guidance and support throughout the program. Within the Program in

Neuroscience, I would like to thank Dr. Joel Levine, Diane Godden, Catherine Costanzo, and Marlene Vera-Viteri for their assistance with paperwork and answering all of my questions.

To my friends and colleagues – Justin Rodriguez, Gulcan Akgul, Walter Hanel, Mallory Locklear, Drs. Laneah Snyder, Darshan Kothari, Emily Campito, Igor Feinstein, Iehab Talukder, and Tejus Bale – your support and encouragement has been greatly appreciated.

Finally, I would like to thank my family for all of their love and support throughout my education. To my parents, Linda and Nick, for encouraging me to reach for my dreams and to never give up. To my brother, Nicholas, who has been and continues to be my inspiration – his strength and resolve know no bounds. It is because of my brother that I am so deeply committed to pursuing a career in neuroscience. To my grandparents, Leslie and Nick, for their support, love, and home-baked meals and soups! To my extended family, the Salussolia's, the Dooner's, and the Bejarano's, your love and support is greatly appreciated.

MOLECULAR MECHANISMS OF IONOTROPIC GLUTAMATE RECEPTOR ASSEMBLY

Chapter 1: Introduction

The human brain is a complex network comprising on average over 10^{11} neurons. A single pyramidal neuron in the hippocampus receives input from over 7,000 neurons at specialized contact sites known as synapses (Kandel 2000). The plastic nature of the brain allows one to differentiate, analyze, and incorporate all of the diverse and varied inputs one perceives into an appropriate response. By definition, synaptic plasticity refers to the activity-dependent modification of the strength of connections between neurons (Citri and Malenka 2008). This property underlies the neuronal network activity modulating long-term potentiation (LTP) and long-term depression (LTD) – processes critical for early neural development, learning and memory (Martin, Grimwood et al. 2000; Citri and Malenka 2008).

Communication amongst neurons of the central nervous system (CNS) occurs via electrochemical transmission (Figure 1.1). Transient fluxes in the flow of ions across the membrane of a cell alter its membrane potential, driving the cell into a more depolarized or hyperpolarized state, thereby directly modulating the cell's propensity to fire an action potential – regenerative, all or none responses that are propagated along the length of the axon (Kandel 2000). Depolarization of a cell above a certain threshold elicits the generation of a positive electrochemical driving force and the initiation of an action potential. In contrast, hyperpolarization drives the electrical potential of the cell further away (e.g., more negative) from threshold making it harder for the cell to fire, thus preventing the propagation of excitatory signaling to the next neuron in the network (Kandel 2000).

For synaptic transmission to occur, electrical signals in the form of action potentials must be recoded or transduced into a chemical signal (Di Maio 2008; Bito 2010). Chemical signaling at synapses allows for rapid and amplified cell-to-cell communication between neurons. Depolarization of the presynaptic cell results in the opening of voltage-gated Ca^{2+} channels and the subsequent influx of calcium along its concentration gradient into the nerve terminal (Di Maio 2008). The rapid calcium influx facilitates the fusion of synaptic vesicles containing neurotransmitters at specialized regions of the presynaptic plasma membrane known as the active zone (Kandel 2000; Haucke, Neher et al. 2011). The exocytosis of synaptic vesicles at the active zone results in the release of neurotransmitters into the synaptic cleft – the space separating the presynaptic and postsynaptic cells (approximately 20 – 40 nm in width) (Kandel 2000; Haucke, Neher et al. 2011). Newly exocytosed neurotransmitters transverse the synaptic cleft by Brownian diffusion to bind and activate receptors embedded in the postsynaptic membrane of the next neuron in the circuit eliciting a postsynaptic response that either facilitates or inhibits further electrochemical activity (Di Maio 2008). In the brain, glutamate and gamma-aminobutyric acid (GABA) are the major excitatory and inhibitory neurotransmitters, respectively. The close apposition of the active zone with the postsynaptic density – a dense network of scaffolding proteins that anchor and cluster iGluRs in the postsynaptic membrane – aids in the fidelity and speed of synaptic transmission (Sheng and Hoogenraad 2007).

Glutamatergic Signaling

In the central nervous system, most fast excitatory neurotransmission is mediated by the neurotransmitter glutamate. Thus, glutamatergic signaling is fundamental to central nervous system function. In fact over 70% of all synapses in the brain are glutamatergic in nature (Fishell and Rudy 2011). Mediating this fast excitatory neurotransmission are ligand-gated or ionotropic glutamate receptors (iGluRs) (Dingledine, Borges et al. 1999). iGluRs are cation-selective ion channels composed of three major receptor subtypes named with respect to their selective agonists: (i) N-methyl-D-aspartate (NMDA); (ii) α-amino-3-hydroxy-5-methyl-4-isoxazolepropionic acid (Paille, Picconi et al. 2010); and (iii) kainate (KA) receptors (Dingledine, Borges et al. 1999). iGluRs play an important role in many physiological states including the activity-dependent changes observed during long-term potentiation (Citri and Malenka 2008), pain perception (Woolf and Salter 2000; Cull-Candy and Leszkiewicz 2004), neuronal development (Mattson 2008), and most higher-order brain and spinal cord processes.

At a prototypical synapse, fast synaptic transmission is mediated predominantly by the AMPA and NMDA receptor subtypes in concert with auxiliary proteins (Figure 1.1B) (Sheng and Hoogenraad 2007). In the mammalian brain, glutamatergic synapses are preferentially formed at dendritic spines. Dendritic spines are functional compartments or microdomains that are physically separate from the dendritic shaft and contain their own metabolic machinery (Matsuzaki, Ellis-Davies et al. 2001). Present within the dendritic spine is the postsynaptic density (PSD) composed of a dense network of cytoskeletal and scaffolding proteins that cluster and stabilize NMDA and AMPA receptors at the synapse (Sheng and Hoogenraad 2007; Newpher and Ehlers

2008). The highly compartmentalized nature of the dendritic spine allows for and facilitates activity-dependent changes in spine geometry that serve to enhance (enlarged spines) or weaken (decreased spine size) synaptic transmission.

Influencing the shape and magnitude of the postsynaptic response, excitatory postsynaptic potential (EPSP), are three factors: (i) the number of iGluRs embedded in the postsynaptic membrane; (ii) the location of the receptors; and (iii) the biophysical properties of the iGluR complexes present in the postsynaptic membrane. As such, the number and location of iGluRs in the PSD are critical for mediating electrochemical transmission in neuronal networks. On average, there are 10 – 100 iGluR complexes present in the postsynaptic density (Matsuzaki, Ellis-Davies et al. 2001; Oertner, Sabatini et al. 2002); however, the probability that a given receptor will bind glutamate and undergo activation is dependent on the amount of glutamate released from the presynaptic vesicles, as well as, the subcellular distribution of receptors within the postsynaptic membrane (Oertner, Sabatini et al. 2002; Traynelis, Wollmuth et al. 2010).

iGluR complexes are highly mobile, undergoing rapid exchange amongst synaptic, perisynaptic, and extrasynaptic regions of the plasma membrane, as well as, continuously being recycled via endocytosis and exocytosis (Derkach, Oh et al. 2007; Newpher and Ehlers 2008). The advent of single particle tracking has furthered the understanding of the mechanisms governing the trafficking of receptors between different synaptic (i.e., extrasynaptic vs. synaptic) and subsynaptic (i.e., recycling endosomes) compartments (Heine 2012). These advances have provided evidence that the subunit composition of iGluRs is critical in determining the localization of iGluRs within the plasma membrane (i.e., synaptic vs. extrasynaptic), as well as, the initiation of

different cell signaling cascades necessary for glutamatergic signaling (Hardingham and Bading 2010; Kaufman, Milnerwood et al. 2012).

The kinetic properties of individual iGluR subtypes also play a great role in influencing the postsynaptic response. Stimulus-evoked excitatory postsynaptic currents (EPSCs) from hippocampal cultures in the whole-cell configuration are composed of two distinct components: (i) a fast, transient component mediated by AMPA receptors; and (ii) a slower component that has a delayed onset mediated by NMDARs (Figure 1.1C) (Lester, Clements et al. 1990). In contrast to non-NMDARs which show rapid onset and decay, as well as greater than 90% desensitization in response to agonist application, NMDARs display slow activation (i.e., slow rise-time) and decay (Lester, Clements et al. 1990). The characteristic slow deactivation rate of NMDARs persists even following removal of agonist due to the high-affinity of the agonist for the LBD, thus allowing for long-lasting modulatory effects on synaptic strength (Dingledine, Borges et al. 1999; Furukawa, Singh et al. 2005). Additionally, the differential kinetic properties of NMDARs, such as channel open probability (P_o) and/or desenstization, are determined by the specific isoform of the GluN2 subunit, therefore modulating NMDAR signaling (Hansen, Furukawa et al. 2010). Thus, the subunit composition, as well as the density and location of iGluR complexes in the postsynaptic membrane are critical determinants of the shape and magnitude of the EPSP that drive synaptic transmission.

Ionotropic Glutamate Receptors

In the past three decades, the structure/function of iGluRs have been elucidated as a result of the identification and cloning of eighteen iGluR genes [for review see (Dingledine, Borges et al. 1999; Traynelis, Wollmuth et al. 2010)]. These eighteen iGluR genes are grouped into four subtypes or families (AMPA, kainate, NMDA, and δ) according to sequence homology and ligand-selectivity. Each subtype demonstrates distinct functional and pharmacological properties that influence receptor function, thus generating great molecular and functional diversity that contributes to the flexibility and dynamics of glutamatergic signaling.

The NMDA receptor family comprises of eight genes: GluN1, GluN2(A-D), and GluN3(A-B). NMDARs are obligate heteromers typically composed of two glycine-binding GluN1 subunits and two glutamate-binding GluN2 subunits (Table 1.1) (Dingledine, Borges et al. 1999). However, NMDARs can also form excitatory, glycine-gated diheteromeric receptors formed by GluN1 and GluN3 (Chatterton, Awobuluyi et al. 2002), as well as triheteromeric receptors composed of either GluN1/GluN2/GluN3 or GluN1/GluN2A/GluN2B (Traynelis, Wollmuth et al. 2010). The significance of these non-traditional NMDARs to glutamatergic signaling is currently not well understood.

Non-NMDA receptors – AMPA and kainate – are often grouped together based on sequence similarity and receptor activation by both kainate and AMPA (Armstrong and Gouaux 2000). In contrast to NMDARs, AMPA and kainate receptors form preferential heteromers (Table 1.1). AMPA receptor (GluA1, GluA3, or GluA4) subunits can form homomeric receptors, but native receptors are largely thought to be heteromeric

complexes containing the GluA2(R) subunit (Table 1.1) (Jonas, Racca et al. 1994; Geiger, Melcher et al. 1995). GluA2 is the "functionally dominant" subunit governing the calcium permeability, single channel conductance, rectification index and expression of AMPARs in the brain (Sommer, Kohler et al. 1991; Greger, Khatri et al. 2002).

Unlike NMDA and AMPA receptors which are predominantly localized in or near the postsynaptic density of glutamatergic synapses, kainate receptors are typically localized on the presynaptic cell (Figure 1.1B). Kainate receptors (KARs) modulate synaptic transmision via signaling by both metabotrophic and ionotropic mechanisms to facilitate the induction of synaptic plasticity in the hippocampus by increasing neurotransmitter release probability (Contractor, Mulle et al. 2011). Kainate receptors represent a third class of organization in which certain subunits, specifically the low-affinity subunits (GluK1, GluK2, and GluK3) can form functional homomeric receptors, whereas other subunits, the high-affinity subunits (GluK4 and GluK5), form functional receptors only when in complex with low affinity subunits (Swanson, Green et al. 2002) (Table 1.1).

The delta (δ) subunits (GluD1-GluD2) or orphan-subtype of glutamate receptor subunits do not form functional receptors or modify the function of the other iGluR subytpes (Dingledine, Borges et al. 1999). Although these orphan receptors only share weak sequence similarity with the three major iGluR subtypes, δ subunits share the same overall subunit architecture.

All iGluR subunits possess a modular structure comprising a large extracellular domain, a transmembrane domain (TMD), and an intracellular carboxyl-terminal domain

(CTD) (Figure 1.2) (Wo and Oswald 1995). The extracellular domain can be further subdivided into two semi-autonomous domains: (i) the distal portion or amino-terminal domain (NTD) – comprising approximately the first 400 amino acids – which shares homology with the bacterial leucine-isolecuine-valine binding protein (LIVBP) and ligand-binding region of mGluR1 (Stern-Bach, Bettler et al. 1994; Hansen, Furukawa et al. 2010); and (ii) the ligand-binding domain formed by two discontinuous polypeptides, S1 (the ~150 amino acids preceding the M1 transmembrane segment) and S2 (the region between the M3 and M4 transmembrane segments), organized in a clamshell-like fashion with the cleft between the two lobes representing the agonist binding site (Armstrong, Sun et al. 1998). The transmembrane domain, which forms the ion channel, is composed of three, full-pass transmembrane segments (M1, M3, M4) and a re-entrant cytoplasmic pore loop (M2) (Wo and Oswald 1995). The ion channel core – formed by the M1-M3 segments – shares structural similarities, albeit an inverted membrane topology with that of two-transmembrane voltage-gated K^+ channels (Arinaminpathy, Biggin et al. 2003). The intracellular C-terminal domain – whose length varies amongst iGluR subunits – is pivotal in the clustering and trafficking of iGluRs at the synapse (Traynelis, Wollmuth et al. 2010).

Synaptic Plasticity

Activity-dependent alterations in the synaptic strength or efficacy are defined as synaptic plasticity. The phrase “fire together, wire together” describes the ability of neurons to strengthen or weaken their connectivity in response to activity, which forms the cellular basis for learning and memory (Anggono and Huganir 2012). Short-periods of synaptic activity – either high- or low-frequency stimulation – can elicit long-lasting changes in synaptic transmission known as long-term potentiation (LTP) or long-term depression (LTD), respectively (Malinow and Malenka 2002). Although synaptic plasticity exists in regions throughout the brain including the amygdala, striatum, and dopaminergic neurons in the midbrain, perhaps the most studied and best-characterized form of plasticity is LTP in the CA1 region of the hippocampus (Malinow and Malenka 2002; Citri and Malenka 2008; Hunt and Castillo 2012).

Long-term plasticity generates rapid, changes in synaptic efficacy lasting for hours to days via an NMDA-dependent mechanism (NMDA-dependent LTP) (Citri and Malenka 2008). During basal synaptic activity when the resting membrane potential is at negative potentials (approximately -80 mV), NMDARs contribute little to the postsynaptic potential due to the voltage-dependent magnesium blockade of the channel pore (Monyer, Burnashev et al. 1994). In contrast, AMPA receptors can be activated at resting membrane potentials to allow the passage of ions across the membrane (Dingledine, Borges et al. 1999). The integration of AMPAR-mediated signaling at multiple synapses results in the rapid depolarization of the cell membrane and subsequent dissociation of magnesium from the NMDAR pore. Upon the coincident activation of NMDARs by agonist binding (typically both glutamate and

glycine) (Johnson and Ascher 1987) and depolarization-induced relief of the Mg^{2+} block, the ion channel opens allowing the passage of ions, including the critical divalent cation, calcium, into the postsynaptic cell (Nowak, Bregestovski et al. 1984).

NMDAR-mediated increases in intracellular Ca^{2+} concentration activate several signaling cascades that not only initiate, but also facilitate a persistent increase in synaptic efficacy. One molecule that has garnered particular interest in mediating the molecular changes associated with LTP is calcium/calmodulin (CaM)-dependent protein kinase II (CaMKII). Previous studies have shown that CaMKII phosphorylates AMPA receptor subunits and potentiates AMPAR synaptic currents by increasing single-channel conductance (Benke, Luthi et al. 1998). Further, it has been shown that loss of CaMKII function by either genetic knockout or inhibition of CaMKII activity by pharmacological manipulation prevents induction of LTP (Citri and Malenka 2008). However, it should be noted that during early neural development, CaMKII expression is relatively low; yet, in young (4-5 week old) ∝CaMKII knockout mice, LTP and LTD induction is still present, suggesting that at least in young animals, synaptic plasticity can occur independent of CaMKII activity (Kirkwood, Silva et al. 1997).

Activation of CaMKII as well as other intracellular signaling cascades by the increased influx of calcium is necessary to induce gene transcription and protein synthesis – processes necessary to ensure the maintenance of LTP in the CA1 region of the hippocampus (Malenka and Bear 2004). Recent evidence suggests that new protein synthesis occurs both at the soma, as well as locally within the dendrites (Sheng and Hoogenraad 2007; Cui-Wang, Hanus et al. 2012). Local protein synthesis at dendritic spines facilitates the structural remodeling of the size and shape of the PSD

(Matsuzaki, Ellis-Davies et al. 2001). Underlying these changes are the incorporation and/or recruitment of additional AMPARs and scaffolding proteins at the synapse (Malenka and Bear 2004; Citri and Malenka 2008).

Until recently, there was much controversy concerning the origin of LTP expression – either presynaptically, due to changes in the probability of neurotransmitter release, or postsynaptically, resulting from changes in the expression and composition of AMPARs in the postsynaptic membrane. The identification of "silent synapses" aided in the resolution of this controversy. Silent synapses are composed solely of NMDA receptors (Liao, Hessler et al. 1995). Thus, during basal synaptic transmission, a silent synapse does not exhibit any detectable postsynaptic currents due to the presence of the voltage-dependent Mg^{2+} block. Induction of LTP "un-silences" these synapses by facilitating the lateral diffusion and activity-dependent incorporation of AMPA receptors from perisynaptic pools into the PSD (Shi, Hayashi et al. 2001; Malenka and Bear 2004; Heine 2012).

Within the hippocampus, two major heteromeric forms of AMPARS exist: GluA1/GluA2 and GluA2/GluA3 (Wenthold, Petralia et al. 1996). Recent evidence has suggested that not only does synaptic activity regulate AMPAR incorporation into the plasma membrane, but alterations in synaptic plasticity can also affect the subunit-composition of iGluR complexes in a cell- and synapse-specific manner (Malinow and Malenka 2002; Liu and Zukin 2007). AMPA receptor subtypes are differentially inserted into the plasma membrane with regards to the length of their C-terminal tails (Shi, Hayashi et al. 2001). During basal synaptic activity, the subcellular localization of AMPA receptor subunits with long C-terminal tails (i.e., GluA1, GluA4) is restricted to

extrasynaptic populations along the dendritic shaft (Shi, Hayashi et al. 2001). In contrast, AMPAR subunits containing a short C-terminal tail (i.e., GluA2, GluA3) are readily incorporated into the synaptic membranes within dendritic spines (Passafaro, Piech et al. 2001). Synaptic activity – LTP induction or CaMKII activity – facilitates the lateral diffusion of calcium-permeable GluA1-containing receptors into the synapse; whereas GluA2-containing receptors show no change in expression levels following alterations in synaptic activity, suggesting that AMPAR subunits containing short carboxy-termini are constitutively expressed at the plasma membrane (Shi, Hayashi et al. 2001). Further, GluA2-containing receptors are restricted to synaptic sites that previously contained GluA2 receptors and that GluA1-, but not GluA2-containing receptors can be inserted into the plasma membrane at silent synapses (Shi, Hayashi et al. 2001). Thus, these studies suggest that the differential trafficking of specific AMPAR subunits directly modulates synaptic activity and that activity-dependent expression of GluA1-containing receptors at the synapse is critical for stable LTP.

NMDA-mediated calcium influx can also result in the weakening of synaptic connections in the form of long-term depression (LTD). Modest levels of calcium influx (that are not high enough to elicit LTP) activate Ca^{2+}-dependent phosphatases (i.e., calcineurin) resulting in subsequent dephosphorylation of AMPAR subunits and the dissociation of AMPARs from the scaffolding proteins in the PSD (Derkach, Oh et al. 2007). This rapid destabilization of iGluRs within the synapse results in the lateral diffusion of AMPARs to endocytic zones positioned at the edge of the PSD, the internalization and possible degradation of receptors, and a structural remodeling and/or shrinkage of the size of the dendritic spine (Derkach, Oh et al. 2007; Citri and Malenka

2008). As with LTP, it has been suggested that specific subunit-composition – specifically GluA2 due to its direct interaction with AP2, a protein involved in clathrin-dependent endocytosis (Blanpied, Scott et al. 2002) – may also play a role in mediating LTD. However, the mechanisms underlying subunit-specific contributions to LTD are not simple. Studies in hippocampal slices from mice lacking GluA2 and/or GluA3 have demonstrated the presence of LTD suggesting that additional experiments must be completed to delineate the mechanisms mediating subunit-specific contributions to LTD (Citri and Malenka 2008).

Thus, what is the significance of the subunit-composition of the NMDARs in the hippocampus in mediating the calcium influx presumably responsible for the induction of LTP and LTD? As mentioned previously, NMDARs are obligate heteromers whose kinetic and pharmacological properties are determined by the GluN2 (GluN2A-GluN2D) subunit (Traynelis, Wollmuth et al. 2010). Through the use of GluN2-specific antagonists, the role of specific NMDAR subunits in synaptic plasticity has begun to be elucidated. Some studies suggest that GluN2A – which is enriched at synapses (Steigerwald, Schulz et al. 2000) and possesses both a higher channel open probability, as well as a higher peak current density than that of GluN2B subunits – is necessary for LTP induction (Chen, Luo et al. 1999; Massey, Johnson et al. 2004). Yet other studies report contradicting results [for review see (Yashiro and Philpot 2008)]. As a result, further studies, including those that account for developmental and spatial alterations in both subunit- and signaling-protein expression profiles, must be performed to delineate the subunit-specific mechanisms underlying synaptic plasticity. Hopefully, with a better understanding of the differential contribution NMDAR subunits have during the induction

of synaptic plasticity, we will gain insight into the mechanisms underlying changes in synaptic efficacy associated with neurological disorders such as schizophrenia and Parkinson's disease.

iGluRs in Neurological Disease States

Perturbations in glutamatergic signaling have been implicated in many neurological diseases including developmental (autism spectrum disorders) (Pardo and Eberhart 2007), psychiatric (bipolar disorder, mood disorders, schizophrenia) (Lau and Zukin 2007; Mony, Kew et al. 2009), acute excitotoxic (epilepsy, stroke) (Hazell 2007; Kalia, Kalia et al. 2008), and chronic neurodegenerative (Huntington's, Parkinson's and Alzheimer's disease) disorders (Lau and Zukin 2007; Kalia, Kalia et al. 2008; Okamoto, Pouladi et al. 2009). Disruption in early neural development due to genetic and/or environmental insults often results in alterations in the neuronal circuitry of the brain. NMDA receptor-mediated signaling is particularly critical during neural development influencing corticogenesis, synaptogenesis, and neuronal migration (Loftis and Janowsky 2003), as well as, neuronal survival and apoptosis (Zhang, Steijaert et al. 2007; Hardingham and Bading 2010; Kaufman, Milnerwood et al. 2012). Dysregulation of glutamatergic signaling contributes to the cognitive and social deficits observed in disorders of neurodevelopmental origins (i.e., autism spectrum disorders and schizophrenia) (Waxman and Lynch 2005; du Bois and Huang 2007).

Physiologically, NMDA receptors display many characteristics that are distinct from that of other iGluRs: (i) strong voltage dependence due to magnesium blockade of the channel pore at negative membrane potentials (Dingledine, Borges et al. 1999; Traynelis, Wollmuth et al. 2010); (ii) high permeability to calcium ions, which plays an important role in both physiological and pathological states (Dingledine, Borges et al. 1999; Citri and Malenka 2008; Kalia, Kalia et al. 2008); and (iii) obligate heteromeric composition.

Glutamate excitotoxicity, a pathological process that results in neuronal injury and death, is often a result of excessive NMDAR activation (Kalia, Kalia et al. 2008). Acute glutamate excitotoxicity has been implicated in neuronal trauma following epileptic seizures, stroke, and traumatic brain injury. Injured neurons release their vesicular contents resulting in a large efflux of glutamate into the synaptic cleft that diffuses along its concentration gradient resulting in the activation of both synaptic and extrasynaptic iGluRs in the postsynaptic cell. Activation of extrasynaptic NMDARs following neuronal injury (i.e., ischemic stroke) results in mitochondrial dysfunction, the generation of reactive-oxygen species that further propagate the neuronal insult, and the activation of pro-death or apoptotic signaling cascades (Kalia, Kalia et al. 2008; Hardingham and Bading 2010). Chronic glutamate excitotoxicity plays a role in many neurodegenerative conditions including Alzheimer's, Parkinson's, and Huntington's diseases, as well as, amyotrophic lateral sclerosis and multiple sclerosis (Paoletti and Neyton 2007; Kalia, Kalia et al. 2008). Additionally, it has been postulated that glutamate excitotoxicity may mediate and enhance the growth of malignant brain tumors (e.g., glioblastoma multiforme) (Nicoletti, Arcella et al. 2007), as well as underlie sensitization disorders such as dyskinesias (Brotchie 2000) and neuropathic pain states (Woolf and Salter 2000).

Hypoactivation of NMDARs has been implicated in many psychiatric diseases including schizophrenia (Gaspar, Bustamante et al. 2009) and mood disorders (Bitanihirwe, Lim et al.). Studies have shown that hypoactivation of the glutamatergic corticostriatal and thalamocortical inputs onto inhibitory GABAergic neurons results in reproducible neuroanatomic and behavioral alterations observed in schizophrenia

(Gaspar, Bustamante et al. 2009). Further support for the glutamatergic hypothesis of schizophrenia has come from the use of pharmacological agents. Administration of NMDA antagonists, such as MK-801, phencyclidine, and ketamine, in human and animal models have been shown to induce both the positive (e.g., disorganized thought, hallucinations, and delusions) and negative symptoms (e.g., flattened affect and social withdrawal) characteristic in schizophrenic patients (Krystal, Karper et al. 1994; Malhotra, Pinals et al. 1996). Thus, it would seem that the use of NMDAR agonists or modulators would be an ideal treatment for patients suffering from diseases stemming from NMDA hypofunction; however, one must be careful not to achieve excitotoxic levels of glutamatergic activation and elicit the adverse side-effects observed with NMDA hyperactivation.

Thus, the challenge in treating aberrant glutamatergic transmission is one of specificity. Many previous attempts to develop pharmacological agents that target glutamatergic transmission have resulted in poor tolerance and/or efficacy due to adverse side effects (e.g., drowsiness, hallucinations, coma, and even death) (Lipton 2004; Kalia, Kalia et al. 2008) resulting from indiscriminate inhibition of iGluRs throughout the CNS. Effective treatments must selectively target dysfunctional glutamatergic signaling without adversely affecting normal neuronal function and the neuroprotective effects of synaptic glutamatergic transmission (Hardingham 2009; Hardingham and Bading 2010). Clinical therapeutics currently used to treat glutamatergic-based diseases modulate aspects of glutamate receptor function in both a subunit-specific and activity-dependent manner (Lipton 2004; Kalia, Kalia et al. 2008). Thus, further understanding of the altered composition and differential distribution of

iGluR complexes in neurological diseases will allow for the advent of therapeutic treatments that target glutamatergic signaling in a subtype- and subunit-specific manner.

Subunit Composition and its Role in Parkinson's Disease

Differential expression– both developmentally and with regards to the subcellular localization – of NMDAR subunits suggests that the subunit composition of the obligate heteromeric NMDARs is critical to physiological and pathological states. During embryonic development, GluN2B-containing receptors are predominantly expressed throughout the cortex of mice; however, at early postnatal ages (~21 days of age), GluN2A expression increases yielding a greater GluN2A/GluN2B ratio that remains relatively stable throughout adulthood (Loftis and Janowsky 2003; Yashiro and Philpot 2008). A developmental shift also exists with respect to the subcellular localization of NMDARs both in a general and subunit-specific manner. In the immature hippocampus, approximately 75% of all NMDARS are localized extrasynaptically (Hardingham and Bading 2010); however, with increasing neural development, there is an increased incorporation of NMDARs at the synapse. Further, evidence suggests that GluN2B is critical to the formation of new synapses, whereas the delayed onset of GluN2A expression is thought to play a role in stabilizing synapses (Gambrill and Barria 2011). Therefore, given the increase in GluN2A expression and synaptic NMDAR localization throughout development, it is not surprising that GluN2A is preferentially enriched at the synapse, while GluN2B is predominantly localized to extrasynaptic sites (Steigerwald, Schulz et al. 2000; Groc, Heine et al. 2006).

Parkinson's disease (PD) – a neurodegenerative disorder associated with motor function deficits due to widespread degeneration of dopaminergic neurons in the substantia nigra – is noted for its alterations in NMDAR trafficking and/or subunit composition. In experimental models of PD, the composition of NMDAR complexes is

markedly altered in striatal spiny neurons (Gardoni, Picconi et al. 2006; Picconi, Piccoli et al. 2012). Rat models of advanced PD show significant decreases in GluN2B expression, but no change in GluN2A expression compared to sham-lesioned controls. Additionally, alterations in the trafficking and clustering of GluN2A- and GluN2B-containing NMDARs within the synaptic membrane due to a decrease in association with PSD95 and SAP97 have been observed in parkinsonian animals (Nash, Johnston et al. 2005; Gardoni, Picconi et al. 2006). Further, it has been shown that the decrease in GluN2B expression in the striatum results in the loss of long-term potentiation (LTP) in animals with advanced PD (Gardoni, Picconi et al. 2006). In contrast, rat models of early PD (incomplete dopamine denervation of the striatum) exhibit some LTP and show an increase in the expression of GluN2A-containing receptors in striatal spiny neurons (Paille, Picconi et al. 2010) suggesting that the GluN2A subunit may offer a potential therapeutic target in Parkinson's disease.

iGluR Origins

The evolution of mammalian iGluRs from its bacterial ancestor is not well understood. In iGluRs, the core of the ion channel – formed by the M1 and M3 transmembrane segments and an intracellular M2 loop – is structurally and evolutionarily related to inverted two-transmembrane K^+ channels (Figure 1.3) (Arinaminpathy, Biggin et al. 2003). However, all known eukaryotic iGluR subunits contain an additional transmembrane segment, the M4 segment, C-terminal to the ion channel core that is presumed to be critical to iGluR function and/or trafficking (Schorge and Colquhoun 2003; Horak, Al-Hallaq et al. 2008; Horak, Chang et al. 2008). Prokaryotic iGluR subunits, such as GluR0 from *Synechocystis*, share similar features of both eukaryotic glutamate and potassium channels. Despite lacking a NTD and containing only two transmembrane segments, GluR0 forms functional glutamate-activated receptors expressed at the plasma membrane (Chen, Cui et al. 1999). In contrast to eukaryotic iGluRs, which are non-selective cation channels permeable to Na^+, K^+, Ca^{+2} ions (Dingledine, Borges et al. 1999), GluR0 forms potassium-selective ion channels due to the presence of the signature K^+ selectivity filter (the 'TXVGYG' motif) in the M2 pore loop (Chen, Cui et al. 1999). Thus, while GluR0 is structurally similar to the ion channel core of eukaryotic iGluRs, it is functionally very different.

Recently the identification of an iGluR from an early divergent eukaryote, *Adineta vaga* (AvGluR1), has bridged the evolutionary gap between prokaryotic and mammalian iGluRs. AvGluR1 possesses the modular domain architecture of eukaryotic iGluRs – that is a NTD, LBD, TMD, and an intracellular C-terminus – while also retaining certain structural characteristics (i.e., 'TXVGYG' motif) of GluR0 (Janovjak, Sandoz et al. 2011).

Further, AvGluR1, like mammalian iGluRs, contains the highly conserved 'SYTAXLA' motif in the M3 segment, as well as an additional transmembrane segment C-terminal to the ion channel core (Janovjak, Sandoz et al. 2011). Unlike GluR0, AvGluR1 is activated by traditional iGluR agonists (i.e., AMPA and kainate) and permeable to both K^+ and Na^+ (Janovjak, Sandoz et al. 2011). This evidence suggests that AvGluR1 is a structural and functional intermediate between prokaryotic and mammalian iGluRs.

Domain/Subunit Organization in the Full-Length Receptor

A recent advance – the elucidation of the first crystal structure of a largely intact AMPA (GluA2) receptor comprising four identical subunits – has furthered the understanding iGluR structure/function (Sobolevsky, Rosconi et al. 2009). Consistent with the previous crystal structures of the isolated GluA2 amino-terminal (Jin, Singh et al. 2009) and ligand-binding domains (Armstrong, Sun et al. 1998; Armstrong and Gouaux 2000), the GluA2 crystal structure revealed that the extracellular domain was organized as a dimer of dimers with an overall two-fold symmetry. In contrast, the transmembrane domain showed a four-fold rotational symmetry, thus creating a symmetry mismatch between the extracellular and transmembrane domains (Figure 1.2A) (Sobolevsky, Rosconi et al. 2009).

Surprisingly, the GluA2 structure revealed that subunit pairs forming the NTD and LBD dimer assemblies were not equivalent. Sobolevsky et al. (2009) showed that the subunits forming the dimer pairs at the level of the NTD (A:B and C:D) and the LBD (A:D and C:B) were not aligned, but rather angled approximately ~24° and ~19° away from the overall two-fold axis of symmetry, respectively, forming a “Y” like structure (Figure 1.2A). At the level of the NTD, the dimer of dimers interface is formed by weak contacts between the lower lobes of the B and D subunits; whereas, in the LBD, the dimer of dimers interface is mediated by residues in the upper lobes of the A and C subunits (Mayer 2011). Thus, this subunit mismatch or domain swapping amongst dimer pairs at the level of the NTD and LBD may have significant implications on the assembly, oligomeric stability, and/or activation of iGluRs (see **iGluR Biogenesis**).

Short peptide linkers (S1-M1, M3-S2, and S2-M4) mediate the symmetry mismatch amongst the two-fold extracellular amino-terminal and ligand-binding domains with that of the four-fold ion channel. Interestingly, at the level of the linkers, individual subunits in the homomeric receptor adopted two distinct conformations – termed A/C and B/D – with subunits in the same conformation positioned opposite one another (Figure 1.2B, C) (Sobolevsky, Rosconi et al. 2009). The linkers of the B/D subunits, which form the NTD dimer interface, adopt an extended conformation perhaps facilitating the subunit crossover amongst the dimer pairs between the NTD and the LBD. Additionally, at the level of the TMD, the three, short peptide linkers joining the LBD with the ion channel (S1-M1, M3-S2, S2-M4) also adopt two distinct conformers (Sobolevsky, Rosconi et al. 2009); however, due to the surprising configuration of the ion channel transmembrane segments, not all of linkers adopt the same relative orientation (Figure 1.2C).

Prior to the crystal structure, it was well accepted that the iGluR ion channel comprises three full-pass transmembrane segments (M1, M3, and M4) and a re-entrant pore loop (M2) (Wo and Oswald 1994; Wo and Oswald 1995; Dingledine, Borges et al. 1999); however, the crystal structure revealed novel features regarding the organization and packing of the TMD. The M3 transmembrane helix lines the ion channel pore and forms a bundle crossing at the top of the transmembrane segment that serves as a barrier to ion permeation (Chang and Kuo 2008; Mayer 2011). The M1 segment is positioned on the exterior of the ion channel core; whereas the M2 helix containing the critical Q/R editing site that determines Ca^{2+} permeability is positioned within the pore (Sommer, Kohler et al. 1991; Greger, Khatri et al. 2002). With regards to the

eukaryotic-specific M4 segment, the structure revealed that it was positioned on the exterior of the ion channel domain, however, it unexpectedly showed that the M4 segment of one subunit did not interact with the ion channel core of its own subunit, but rather with the ion channel core of an adjacent subunit (Figure 1.4) (Sobolevsky, Rosconi et al. 2009). Thus, the M4 segment presumably wraps around to join dimer pairs within the transmembrane domain to facilitate the four-fold rotational symmetry. In light of this novel and unexpected revelation, it is not surprising that the relative orientation of the S2-M4 linker that couples the LBD to the M4 transmembrane segment adopts a different conformation relative to the overall two-fold axis of symmetry than that of the pore-lining M3-S2 linker. Although the predicted distances between homologous atoms in the A/C and B/D subunits are equivalent (Mayer 2011), the S2-M4 linker of the B/D subunits adopts a more proximal positioning, whereas in the M3-S2 linker, the B/D conformer is positioned more distal to the ion channel pore (Figure 1.2C) (Sobolevsky, Rosconi et al. 2009).

From a functional perspective, the presence of two distinct conformations may influence the mechanistic basis that couples agonist-induced conformational changes in the LBD to ion channel permeation and allow for conformer-specific (e.g., 'A/C' vs. 'B/D') contributions to ion channel activation. Sobolevsky et al. (2009) proposed that in the obligate heteromeric NMDAR, the GluN1 subunit adopts the 'A/C' conformation, whereas the GluN2 subunit adopts the 'B/D' conformation. The existence of two distinct subunit conformations coupled with evidence that the two NMDAR subunits gate differently (Banke and Traynelis 2003; Sobolevsky, Prodromou et al. 2007; Blanke and VanDongen 2008; Blanke and VanDongen 2008) supports a relationship between

specific subunits and the ‘A/C’ or ‘B/D’ conformations. Thus, the presence of two unique subunit conformations may be an essential element of the obligate arrangement of NMDARs (though the significance and basis for this is unknown).

iGluR Biogenesis

Biogenesis of iGluRs – biosynthesis, folding, oligomerization, and trafficking of receptors to the membrane – is a complex process that requires many synchronized interactions to yield functional tetrameric complexes. Native synaptic iGluRs assemble predominantly as heterotetramers (Monyer, Burnashev et al. 1994; Wenthold, Petralia et al. 1996; Mansour, Nagarajan et al. 2001; Swanson, Green et al. 2002). Thus, the subunit composition of the receptors has critical implications for iGluR signaling, conferring distinct pharmacological and kinetic profiles on the receptor [for review see (Traynelis, Wollmuth et al. 2010)], as well as, mediating the trafficking and synaptic localization of receptors (i.e., extrasynaptic vs. synaptic) in the plasma membrane (Steigerwald, Schulz et al. 2000; Shi, Hayashi et al. 2001). However the mechanisms governing the assembly and preferential stoichiometry of iGluRs are only starting to be delineated.

Membrane proteins, such as iGluRs, undergo synthesis (i.e., translation) and maturation (i.e., folding, assembly, oligomerization) in the endoplasmic reticulum (ER) to form native receptors that can be inserted into the plasma membrane (Figure 1.5B) (Ellgaard and Helenius 2003). The lumen of the ER – which is topologically equivalent to the extracellular space – facilitates the maturation and assembly of energetically stable proteins via disulfide bond formation, signal-peptide cleavage, N-linked glycosylation, and chaperone-mediated folding (Ellgaard and Helenius 2003). Further, the stringent quality control system of the ER ensures that only mature proteins that have achieved proper oligomerization are exported from the ER (Deutsch, 2003), since expression of improperly- or incompletely-folded receptors could be toxic to the cell

(Kriegenburg, Ellgaard et al. 2012). Thus, export of iGluR complexes from the ER is the rate-limiting step determining the surface expression of functional receptors.

The differential expression of iGluR subunits both developmentally and regionally results in a diverse, combinatorial pool of receptors that shape synaptic transmission. Thus, alterations in the expression of heteromeric iGluRs at the synapse can drastically affect physiological and/or pathological conditions. Previous studies of glutamate (Fleck 2006), potassium (Tu and Deutsch 1999; Deutsch 2002), and other voltage-gated ion channels (Schwappach 2008) suggest that ion channel tetramerization occurs in a two-step process: (i) dimer formation; and (ii) dimerization of dimers to form a tetramer (Figure 1.5A). Crystal structures of isolated amino-terminal and ligand-binding domains revealed that the extracellular domains possess a two-fold symmetry (Furukawa, Singh et al. 2005; Clayton, Siebold et al. 2009; Jin, Singh et al. 2009; Kumar, Schuck et al. 2011; Yao, Zong et al. 2011). Further, Ayalon and Stern-Bach (2001) have shown that the ligand-binding – specifically S2 – and the transmembrane domains (M1, M3, and M4) facilitate iGluR tetramerization and adoption of the four-fold rotational symmetry. Thus, these studies coupled with the recent full-length structure of a homomeric AMPAR (Sobolevsky, Rosconi et al. 2009) support the model that iGluR oligomerization occurs via the assembly of a dimer of dimers to form a tetrameric complex.

Many studies have shown that the amino-terminal domain is pivotal in mediating dimer formation amongst iGluR subunits (Leuschner and Hoch 1999; Madry, Mesic et al. 2007; Schuler, Mesic et al. 2008; Rossmann, Sukumaran et al. 2011). Despite sharing a similar overall NTD structure, only those subunits belonging to the same pharmacological subfamily (i.e., AMPA) assemble as dimers (Ayalon and Stern-Bach

2001; Rossmann, Sukumaran et al. 2011). Compatibility at the level of the NTD is not only important during the initial dimerization of two monomeric subunits, but it is also critical to the formation of hetero-tetrameric receptors (Ayalon and Stern-Bach 2001). Additional studies have identified structural determinants (i.e., conserved polar residues) in the dimer interface of the upper-lobes of the non-NMDAR NTDs that favor the formation of heteromeric dimer pairs that can then come together to form a heterotetramer (Ayalon, Segev et al. 2005; Rossmann, Sukumaran et al. 2011). In contrast, the mechanisms underlying assembly of the obligate heteromeric NMDAR remain controversial. Some studies suggest that assembly of NMDARs requires the formation of GluN1 homodimers that then subsequently dissociate to allow incorporation of GluN2 and/or GluN3 subunits to form a heterotetramers (Papadakis, Hawkins et al. 2004; Farina, Blain et al. 2011), whereas others suggest that NMDAR assembly, like non-NMDARs, requires the association of two heterodimers to achieve functional receptors (Madry, Mesic et al. 2007; Schuler, Mesic et al. 2008; Lee and Gouaux 2011). Thus, further work must be performed to determine the role of the NTD in iGluR heteromerization.

The ligand-binding domain, like the NTD, is organized as a “clamshell” and possesses a two-fold symmetry (Armstrong, Sun et al. 1998), but its role in iGluR assembly is vastly different. Unlike the NTD, which has extensive contacts both within dimers (lobe 1 and lobe 2) and between dimers (across the dimer interface) (Sobolevsky, Rosconi et al. 2009), the LBD only forms a dimer interface upon tetramerization (Shanks, Maruo et al. 2010). In fact, recent evidence from single-particle electron microscopy studies suggests that the LBDs within an individual dimer

pair are spatially separated, leading the authors to propose that dimerization of the NTD and TMD precedes the formation of tetrameric complexes (Shanks, Maruo et al. 2010). This novel structural insight coupled with the prediction that the two subunits composing the dimer pair at the level of the NTD (i.e., A/B) do not constitute the dimer pair at the level of the LBD (i.e., A/D) (Sobolevsky, Rosconi et al. 2009; Rossmann, Sukumaran et al. 2011) has important implications on both LBD function and its role in iGluR biogenesis.

From a functional standpoint, the ligand-binding and transmembrane domains form the heart and soul of the receptor, respectively. Agonist-induced conformational changes in the LBD are transduced into channel opening/closing via the linkers that connect the LBD to the ion channel pore (Sobolevsky, Beck et al. 2002; Schmid, Korber et al. 2007). However, the energy generated from agonist-induced conformational changes in the LBD does not only influence channel activation, rather it serves also as a regulatory checkpoint for the export of receptors from the ER. Multiple lines of evidence suggest that iGluRs must be able to bind agonist and undergo structural rearrangements typically associated with agonist-binding prior to export from the ER (Valluru, Xu et al. 2005; Gill, Vivithanaporn et al. 2009; Coleman, Moykkynen et al. 2010). Additionally, single-point mutations that alter the desensitization kinetics (i.e. L489Y in GluA2) through stabilization of the LBD dimer interface result in decreased iGluR surface expression due to alterations in tetramerization and subsequent retention in the ER (Sun, Olson et al. 2002; Priel, Selak et al. 2006; Chaudhry, Weston et al. 2009; Shanks, Maruo et al. 2010).

Post-transcriptional mRNA editing and/or alternative splicing events, which result in the generation of a functionally diverse pool of iGluR subunits, also affect the assembly and export of iGluRs from the ER (Figure 1.5C). Two such sites are present in the S2 region of the LBD and influence the biogenesis of iGluRs: (i) editing of the endogenously encoded arginine (R) residue to glycine (G) at the R/G site in GluA2-GluA4 subunits; and (ii) as well as alternative splicing of the flip/flop exons in all AMPAR subunits (Sukumaran, Penn et al. 2012). RNA editing at the R/G site, which results in more rapid recovery from desensitization, occurs gradually during development with both edited and unedited forms present in the adult (Dingledine, Borges et al. 1999); however, editing at the R/G site also results in decreased surface expression (Greger, Akamine et al. 2006). Alternative splicing of the flip/flop region alters desensitization kinetics with flip variants showing less profound desensitization than that of flop isoforms (Dingledine, Borges et al. 1999). Flip/flop variants exhibit differential expression with flip variants showing approximately a 10-fold increase in surface expression compared to flop variants perhaps due to alterations in ER export amongst the splice variants (Coleman, Moykkynen et al. 2006; Penn, Williams et al. 2008); however, recent work suggests that correlations drawn between the extent of desensitization and protein maturation/assembly may not be the best indicator of iGluR biogenesis (Coleman, Moykkynen et al. 2010). Thus, perhaps the molecular determinant governing ER export is the overall structure of the LBD rather than structural rearrangements associated with gating.

The transmembrane domain (TMD), with its extensive packing interfaces amongst the transmembrane segments, is integral in the formation of hetero-tetrameric

assemblies. Many studies have suggested that the packing of the transmembrane segments – specifically the M4 segment interacting with the ion channel core of an adjacent subunit (Figure 1.4) – is necessary to mask ER-retention signals (Horak, Al-Hallaq et al. 2008; Horak, Chang et al. 2008). Additionally, the M4 segment of AMPAR subunits contains a GXXXG-like motif that facilitates helix-helix interactions that may aid in the formation and/or stabilization of tetrameric AMPAR assemblies (Senes, Engel et al. 2004). Further, Q/R editing of the M2 pore loop in GluA2, GluK1, and GluK2 subunits results in increased dwell time in the ER and decreased surface expression due to the close approximation of unfavorable electrostatic interactions contributed by the four arginine residues during receptor formation (Greger, Khatri et al. 2002). With regards to AMPARs, GluA2 subunits undergo nearly complete editing at the Q/R site resulting in increased pools of GluA2(R) subunits in the ER that can then associate with GluA subunits to form heteromeric assemblies.

The intracellular C-terminal domain (CTD) is a highly regulated domain integral in the trafficking, clustering and anchoring of iGluRs at the postsynaptic membrane. Numerous proteins have been identified that modulate the surface expression of iGluRs, however the transmembrane AMPA regulatory protein (TARP) and membrane-associated guanylate kinase (MAGUK) families have been the most characterized. In contrast to other auxiliary proteins (i.e., NSF or PICK1) that interact with specific subunits, stargazin – the prototypical TARP – directly interacts with all AMPAR subunits to modulate functional expression (Opazo, Sainlos et al. 2011). Co-expression of stargazin with AMPAR subunits results in increased surface expression of receptors, presumably due to increased trafficking (Tomita, Adesnik et al. 2005). Indeed stargazin,

as well as other auxiliary proteins have been shown to interact with iGluR complexes in the ER and Golgi apparatus to facilitate the maturation of proteins (Opazo, Sainlos et al. 2011). Stargazin also aids in the stabilization and clustering of AMPARs at the synapse via its C-terminal PDZ binding site that interacts with PSD-95, the prototypical MAGUK protein enriched in the postsynaptic density (Chen, Chetkovich et al. 2000; Sheng and Hoogenraad 2007). Thus, C-terminal mediated interactions of iGluRs with auxiliary proteins critically regulate glutamatergic signaling by modulating and/or regulating receptor expression, localization and/or function.

.

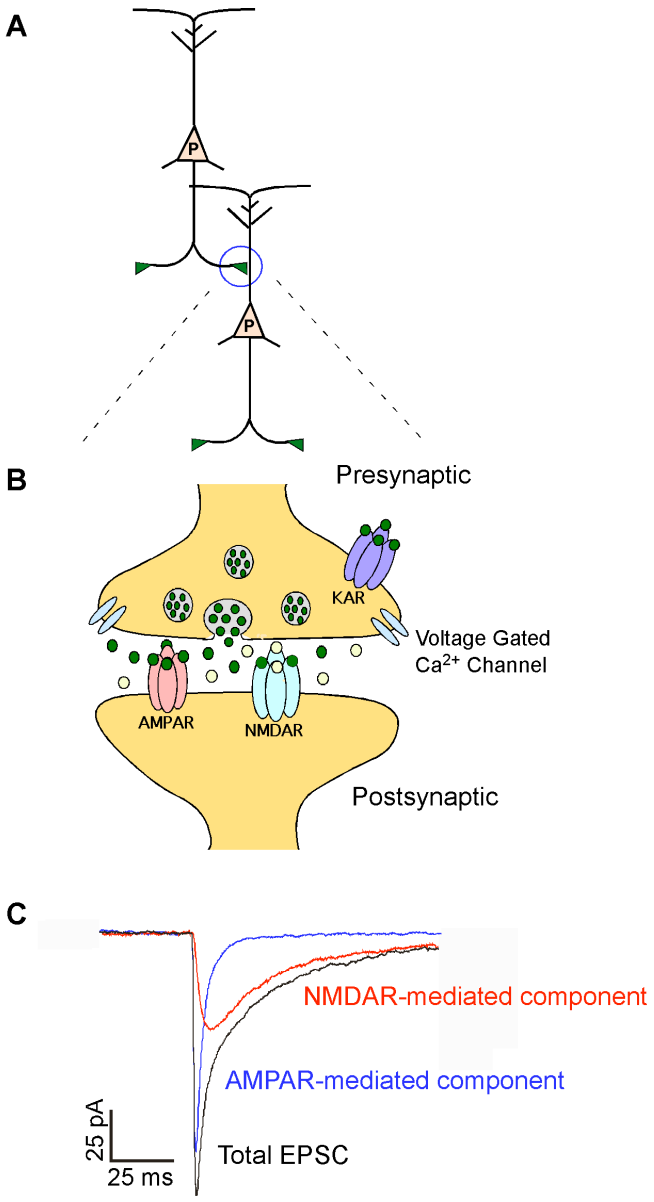

Figure 1.1. Glutamatergic signaling.

(A) Schematic representation of the connections between two pyramidal (P) neurons in the brain. The axon of the presynaptic cell (left) forms a synapse on the dendrite of the postsynaptic cell (right).

(B) Enlarged view of the synapse depicted in (A) showing the presynaptic localization of vesicles and voltage-gated Ca^{2+} channels at the active zone. Kainate receptors are predominantly localized in the presynaptic terminal, although KARs are also found in the postsynaptic membrane (not-pictured). NMDA and AMPA receptors are clustered at the postsynaptic density (PSD) localized in the spines of postsynaptic cells. The close apposition of the active zone with the PSD aids in the fidelity and speed of synaptic transmission.

(C) AMPA and NMDA receptor-mediated excitatory postsynaptic current (EPSC) traces elicited at a synapse in the visual cortex between a pyramidal and multipolar interneuron (L.P. Wollmuth, *unpublished data*). The total EPSC was broken down into the fast (AMPA) and slow (NMDA) components with the use of the AMPAR-specific antagonist CNQX that allowed for visualization of the NMDA-mediated current.

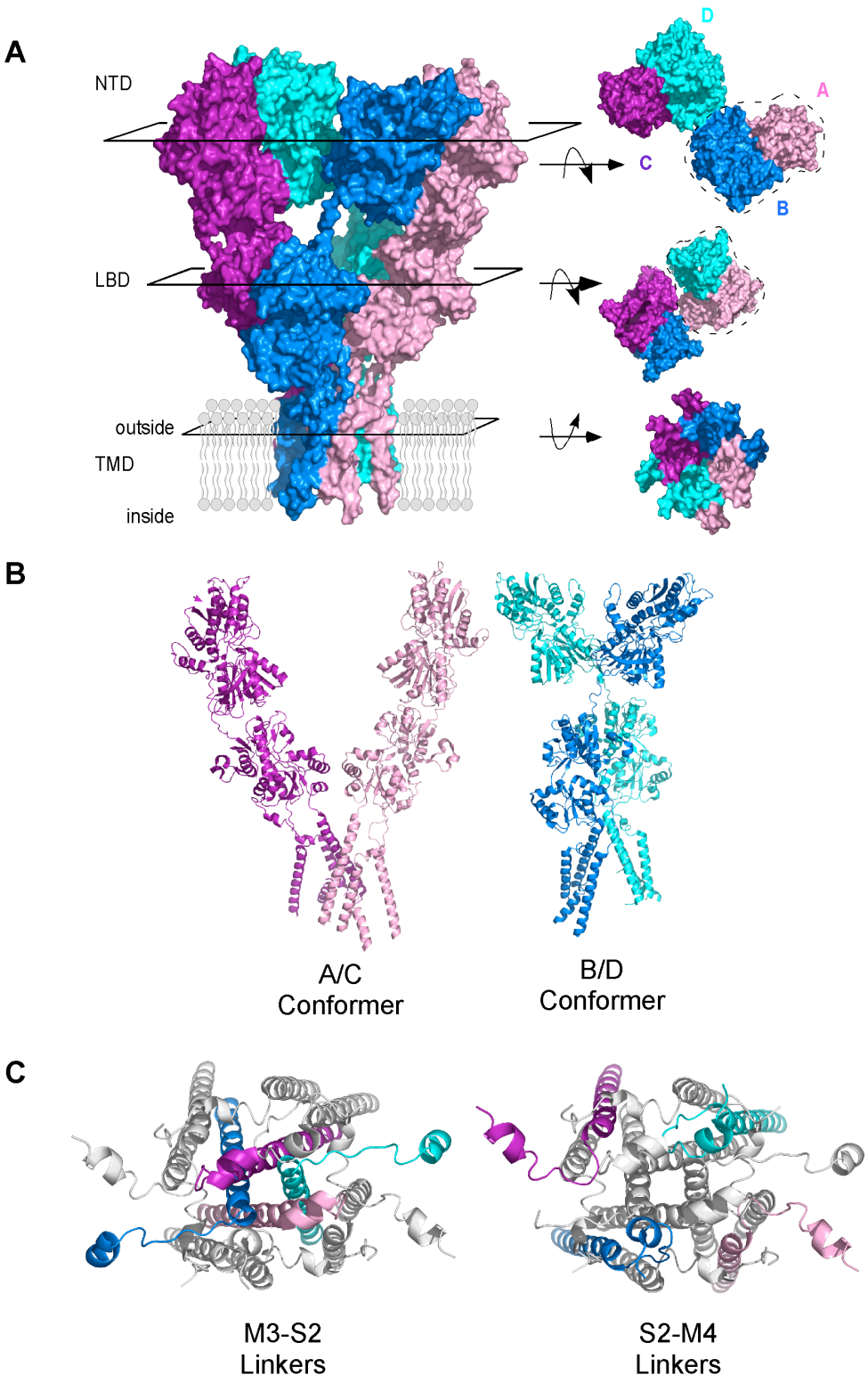

Figure 1.2. iGluR subunits display two unique conformational states.

(A) Crystal structure of the homomeric GluA2 receptor. The schematics represent the arrangement of the subunits at the levels of the NTD, LBD, and transmembrane domain (TMD), as well as, illustrate the domain swapping between the dimers at each level of the receptor. The isolated TMD is viewed from the intracellular side of the receptor to illustrate the four-fold rotational symmetry as well as, interaction of the transmembrane segments in which the M4 segment of one subunit interacts with the ion channel core of the adjacent subunit. This figure was adapted from (Wollmuth and Traynelis 2009).

(B) Ribbon diagrams of two distinct conformational states 'A/C' (left) and 'B/D' (right).

(C) Ribbon diagrams of the M3-S2 (left) and the S2-M4 (right) linkers viewed from the top of the receptor (right). With regards to the M3/S2 linkers, A/C and B/D subunits are proximal and distal to the vertical axis of the ion channel, respectively. The arrangement of the S2/M4 linkers varies from that of M3/S2 with subunits adopting the B/D and A/C conformers positioned proximal and distal to the ion channel pore, respectively. Crystal structure images were composed using PyMol software with the publicly distributed PDB file 3KG2.

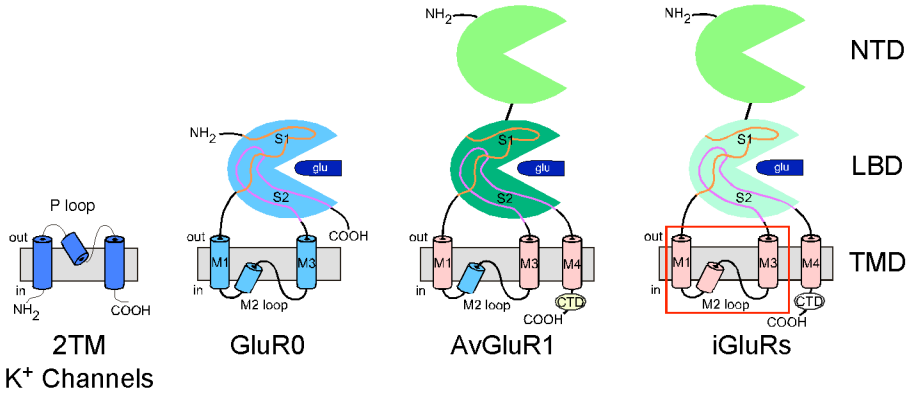

Figure 1.3. Evolution of iGluRs.

Mammalian iGluRs (far right) have a modular domain architecture composed of an extracellular amino-terminal (NTD) and ligand-binding (LBD) domain, a transmembrane domain (TMD) containing the ion channel, and an intracellular carboxyl-terminal domain (CTD). The ion channel core (red box) of mammalian iGluRs is structurally similar to that of prokaryotic iGluRs (GluR0) and two-transmembrane voltage-gated K^+ channels (albeit inverted orientation in the membrane). The recent identification of an early divergent eukaryotic iGluR, AvGluR1, shares the modular architecture of mammalian iGluRs (i.e., AMPAR, NMDAR, and KARs), but retains the signature 'TXVGYG' motif (blue) present in the M2 pore loop of GluR0 and K^+ channels, suggesting that AvGluR1 serves as an evolutionary intermediate between prokaryotic and mammalian iGluRs. This figure was adapted from (Janovjak, Sandoz et al. 2011).

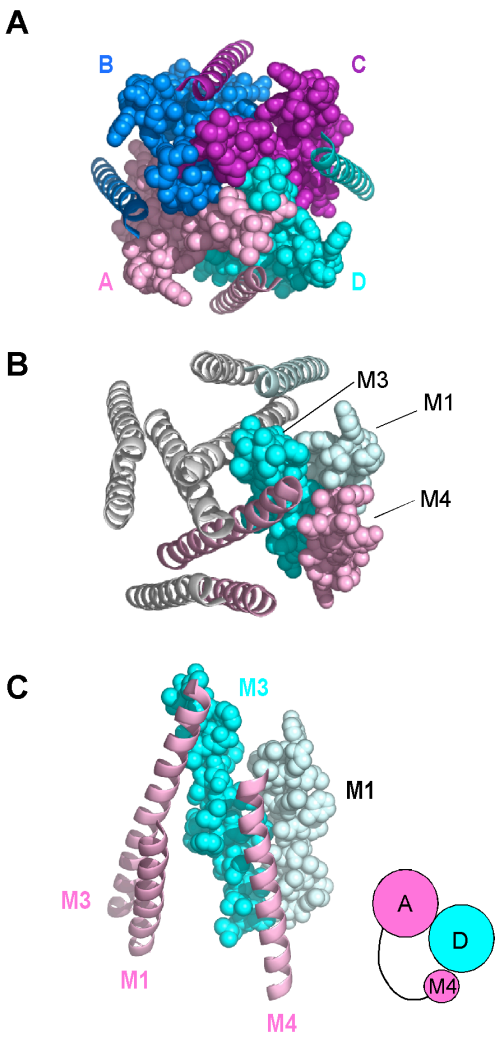

Figure 1.4. Arrangement of the transmembrane segments forming the ion channel.

(A) Crystal structure of TMD of the homomeric GluA2 receptor with the ion channel core (M1-M3) shown as spheres and the M4 segment shown as ribbons. The M3 segments line the ion channel pore with the M1 and M4 segments positioned more externally. The M4 segment of one subunit associates with the ion channel core of the adjacent subunit.

(B), (C) Top down (B) and side (C) views of the M4 – ion channel core interaction of the transmembrane segments in Subunits A and D. The M4 segment of Subunit A (pink) interacts with the ion channel core – M1 (pale blue) & M3 (cyan) segments – of Subunit D. Crystal structure images were composed using PyMol software with the publicly distributed PDB file 3KG2.

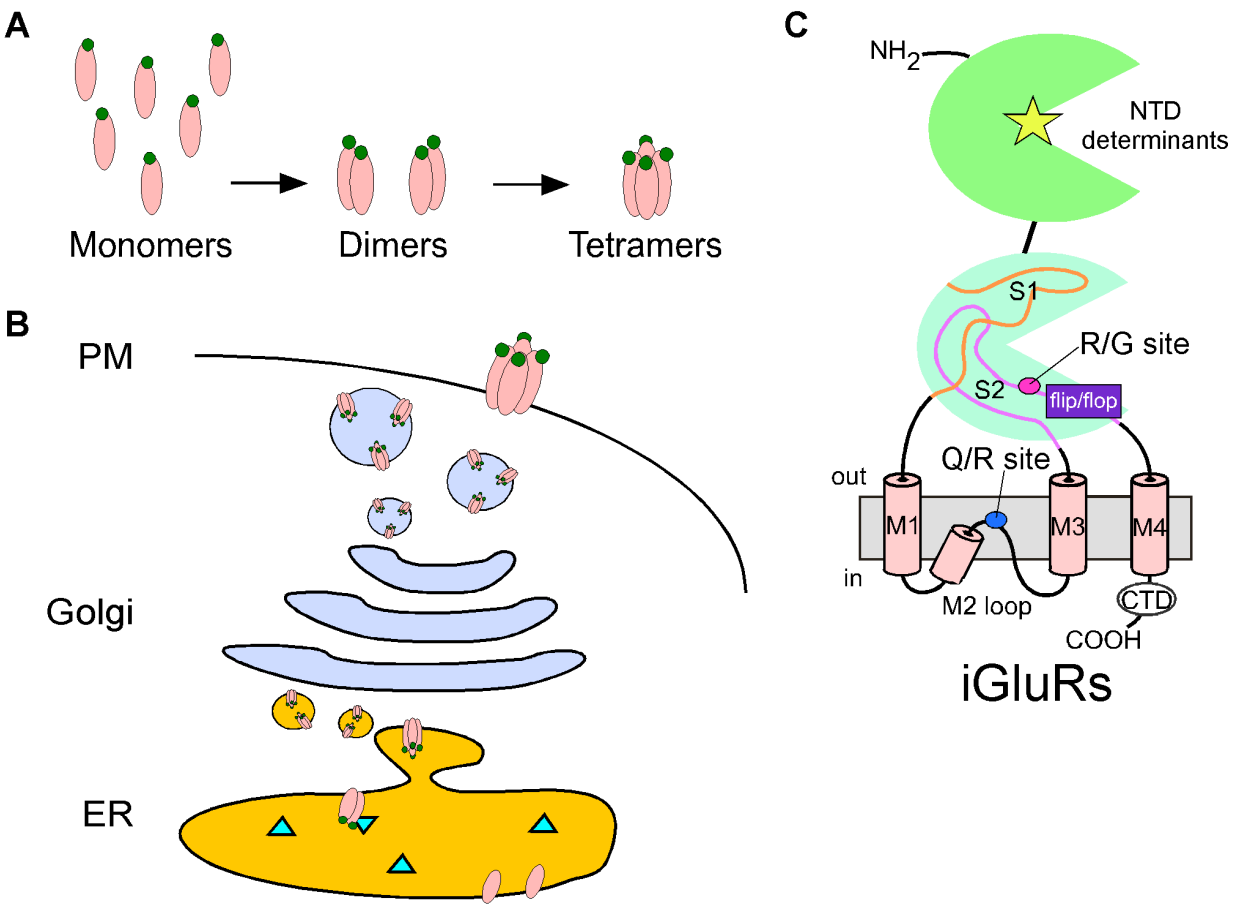

Figure 1.5. Biogenesis of iGluRs.

(A) Proposed two step process of iGluR oligomerization: (i) monomeric subunits co-assemble to form dimers; and (ii) dimerization of dimers to form a tetramer.

(B) Schematic representation of iGluR biogenesis. Newly synthesized proteins fold, assemble, and oligomerize to form iGluR complexes in the endoplasmic reticulum (ER). iGluRs that achieved proper oligomeric assembly – formed tetramers – are then exported from the ER and undergo further post-translational modifications in the Golgi before being incorporated into vesicles and inserted into the plasma membrane (PM). The lumen of the ER is topologically equivalent to the extracellular space. Thus, the extracellular domains (NTD and LBD) are "intracellular" or facing the lumen of organelles in the secretory pathway until they are inserted into the plasma membrane.

(C) Schematic of an iGluR subunit illustrating the molecular determinants that affect iGluR biogenesis.

iGluR Subtype	Subunits	Functional Conformers	Major Native Combination	Presumed Arrangement
NMDARs	N1 N2(A-D) N3(A-B)	- obligate heteromers	N1/N2 (Monyer, Sprengel et al. 1992; Sobolevsky, Rosconi et al. 2009)	N1/N2/N1/N2
AMPARs	A1 A2(R) A3 A4	- homomers - heteromers	A1/A2(R) (Mansour, Nagarajan et al. 2001) A2(R)/A3 (Wenthold, Petralia et al. 1996)	A1/A2(R)/A1/A2(R) (Mansour, Nagarajan et al. 2001)
KARs	Low Affinity K1 K2 K3 High Affinity K4 K5	- homomers - heteromers - obligate heteromers with low affinity subunits	K2/K5 (Swanson, Green et al. 2002)	K2/K5/K2/K5

Table 1.1. iGluR subtypes have different requirements for forming heteromeric receptors.

A list of the three iGluR subtypes and the functional conformers formed by the individual subunits for each iGluR subtype. The major native heteromeric combination of NMDARs is presumed to be N1/N2 and organized in a N1/N2/N1/N2 manner analogous to the A1/A2(R)/A1/A2(R) arrangement of AMPARs (Mansour, Nagarajan et al. 2001). GluA2(R), the edited form of the GluA2, is the “functionally dominant” AMPAR subunit rendering AMPARs impermeable to Ca^{2+} and altering single channel kinetics and rectification index. All GluA2-containing receptors in the brain are edited to GluA2(R).

Chapter 2: Arrangement of Subunits in Functional NMDA Receptors

ABSTRACT

Ionotropic glutamate receptors (iGluRs), including the NMDA receptor subtype, are ligand-gated ion channels critical to fast signaling in the central nervous system. NMDA receptors are obligate heterotetramers composed of two GluN1 and typically two GluN2 subunits. However, the arrangement of GluN subunits in functional receptors – whether like subunits are adjacent to (N1/N1/N2/N2) or diagonal to (N1/N2/N1/N2) one another – remains unclear. Recently, a crystal structure of a homomeric AMPA receptor revealed that the four identical subunits adopt two distinct and subunit-specific conformations termed A/C and B/D with subunits of like conformations (e.g., A/C) diagonal to one another. In the structure, the two conformers were notable at the level of the linkers (S1-M1, M3-S2, and S2-M4) that join the ligand-binding domain to the transmembrane ion channel with the M3-S2 linker positioned more proximal to the central axis of the channel pore in the A/C conformation and S2-M4 more proximal in the B/D conformation. Using immunoblots and functional assays, we show that introduced cysteines in the M3/M3-S2 linker of GluN1, but not GluN2, show dimer formation and oxidation-induced changes in current amplitudes predictive of the A/C conformation. Conversely, introduced cysteines in the S2-M4 linker of GluN2, but not GluN1, showed similar functional effects suggesting that the GluN2 subunit adopts the B/D conformation. Thus, we show that NMDA receptors, like AMPA receptors, possess distinct subunit-specific conformations with GluN1 approximating the A/C and GluN2 the B/D conformation. GluN subunits are therefore positioned in a N1/N2/N1/N2 arrangement in functional NMDA receptors.

INTRODUCTION

Glutamate-activated NMDA receptors are integral in the transduction and modulation of synaptic activity underlying neurodevelopment (Mattson 2008) and higher-order cognitive functions (Lau and Zukin 2007; Citri and Malenka 2008). Perturbations in glutamatergic transmission exacerbate numerous brain diseases including psychiatric, neurodegenerative, and excitotoxic disorders (Kalia, Kalia et al. 2008). NMDA receptors are obligate heterotetramers typically composed of the ubiquitous GluN1 subunit and either GluN2(A-D) and/or GluN3(A & B) subunits (Cull-Candy and Leszkiewicz 2004; Paoletti and Neyton 2007). The resulting diversity in receptor composition contributes to differences in NMDA receptor biogenesis, trafficking, posttranslational modifications, cellular distribution, and biophysical properties (Cull-Candy and Leszkiewicz 2004; Paoletti and Neyton 2007; Pina-Crespo, Talantova et al. 2010; Traynelis, Wollmuth et al. 2010).

At most synapses, functional NMDA receptors are formed by two GluN1 and two GluN2 subunits arranged as a dimer of dimers. Although the dimer pair is almost certainly GluN1/GluN2 (Furukawa, Singh et al. 2005; Gielen, Le Goff et al. 2008; Lee and Gouaux 2011), the arrangement of subunits in functional tetrameric complexes—whether identical subunits are positioned adjacent to (N1/N1/N2/N2) (Schorge and Colquhoun 2003) or diagonal to (N1/N2/N1/N2) (Sobolevsky, Rosconi et al. 2009) one another—remains uncertain. Surprisingly, in a crystal structure of a homomeric AMPA receptor, four identical GluA2 subunits adopted two distinct conformations, termed A/C and B/D, with like conformers diagonal to one another (Figure 2.1) (Sobolevsky, Rosconi et al. 2009). These two distinct conformations were notable at the level of the

linkers (S1-M1, M3-S2, and S2-M4) that couple the ligand-binding domain (LBD) to the ion channel formed by the transmembrane domain (TMD). These linkers accommodate the symmetry mismatch between the LBD (2-fold symmetry) and the TMD (4-fold symmetry) (Figure 2.1) with those linkers in diagonal subunits adopting a common spatial relationship.

For obligate heteromeric NMDARs, if like subunits (i.e., GluN1) are diagonal to one another (N1/N2/N1/N2), then they must adopt either an A/C or a B/D conformation (Sobolevsky, Rosconi et al. 2009). In contrast, if like subunits are adjacent to one another (N1/N1/N2/N2), then the adjacent subunits (e.g., GluN1 and GluN1) must adopt different conformations, one A/C and the other B/D. Sobolevsky et al. (2009) proposed that like subunits in NMDA receptors are diagonal to one another with GluN1 adopting the A/C and GluN2 the B/D conformation. However, these experiments are limited in scope. Only a small number of introduced cysteines were tested for cross-linking (as an index of proximity). Further, the identified receptors, assayed solely by immunoblots, do not necessarily represent functional receptors. During biogenesis, many positions can transiently exist in close proximity to one another (e.g., Clarke and Fersht 1993), thus forming disulfide bonds independent of their positioning in a mature, functional receptor. Finally, the results provided no positive evidence for the predicted B/D conformation of the GluN2 subunit.

Taking advantage of substituted cysteines in the LBD-TMD linkers, we find strong subunit-specific patterns of cross-linking in functional NMDA receptor subunits. The patterns of cross-linking are consistent with GluN1 and GluN2 approximating the

A/C and B/D conformations, respectively, therefore positioning like subunits diagonal to one another in functional tetrameric complexes.

MATERIALS AND METHODS

Materials

The GluN1 glycine-site antagonist, 5, 7-dichlorokynurenic acid (DCKA), was purchased from ToCris Bioscience. All other reagents including the GluN2 glutamate-site antagonist, DL-2-amino-phosphonopentanoic acid (APV), $CuSO_4$, phenanthroline, and dithiothreitol (DTT), were purchased from Sigma Chemicals.

Mutagenesis and expression

Cysteine substitutions in the rat $GluN1_a$ (Accession # P35439), GluN2A (Q00959) and GluN2C (Q00961) subunits were generated as described previously [(see Talukder, Borker et al. 2010) (and references therein)]. All numbering is for the mature protein using signal peptides of lengths of 18 (GluN1), 19 (GluN2A) and 19 (GluN2C) amino acids. The GluN2A background we used in oocytes had an endogenous cysteine replaced with alanine (C399A) (Choi, Tenneti et al. 2000). Although this mutation has been used previously to prevent MTS reagents from reacting with the GluN2A subunit (e.g., Talukder, Borker et al. 2010), it does not alter the effects of reducing or oxidizing agents on NMDA receptors. Wild-type and mutant GluN1 and GluN2A or GluN2C mRNA (0.01-0.1 μg/ml with 50 to 75 nl injected per oocyte) were co-expressed in *Xenopus laevis* oocytes (Sobolevsky, Beck et al. 2002). Wild-type and mutant GluN1 and GluN2A DNA (4 μg) were transfected into HEK 293 cells using Fugene 6 (Roche Molecular Biochemicals).

The α-helical extent of the M3 segment at its C-terminal end depends on the specific conformer with M3 in the A/C conformer extended by about one turn of an α-

helix (Figure 2.2A, *right panel*, dashed box) compared to the B/D conformer (Figure 2.2A, *right panel*, solid box). Correspondingly, the M3-S2 linker (from the C-terminal end of M3 to Helix E in the S2 segment) also varies in length between conformers. Our experiments in this region encompass positions in the C-terminal portion of the M3 segment as well as the M3-S2 linker. Thus, to encompass all positions tested in the present study, we refer to them as the M3/M3-S2 linker.

Whole-cell current recordings and data analysis

Whole-cell currents of *Xenopus* oocytes were recorded at room temperature (20º C) using two microelectrode voltage clamp (TEVC) (DAGAN TEV-200A, DAGAN Corp.) with Cell Works software (*npi* electronic) (Sobolevsky, Beck et al. 2002). When recording GluN1/GluN2C, the external solution consisted of (in mM): 115 NaCl, 2.5 KCl, 0.18 $CaCl_2$ and 5 HEPES (pH 7.2, NaOH). When recording GluN1/GluN2A, the same solution was used except $BaCl_2$ substituted for $CaCl_2$ (to prevent Ca^{2+}-dependent desensitization) and 100 μM EDTA (to minimize Zn^{2+}-mediated modification) was added to the external solution. All reagents, including glutamate (200 μM), glycine (20 μM), APV (100 μM), DCKA (10 μM), Copper(II):phenanthroline (Cu:Phen) (2:50 μM), and DTT (either 1 or 4 mM), were applied with the bath solution.

Experimental protocols

NMDAR wild-type and cysteine-substituted mutant channels were probed from the extracellular side with oxidizing (Cu:Phen) and reducing (DTT) reagents. Stock solutions of phenanthroline (0.5 M) and $CuSO_4$ (0.1 M) were diluted to the experimental concentrations in the external solution immediately before the experiment.

Steady-state reactions were quantified at a holding potential of -60 mV (see Figures 2.3B, 2.3C, 2.3E). Baseline glutamate-activated current amplitudes (I_{pre}) were established by three to five 15-s applications of glutamate and glycine. All agonist or any other reagent applications were separated by 30 to 120 sec washes in glutamate-free solution. Cu:Phen (or DTT) was applied for 60 secs either in the presence of agonists or in their absence (but in the presence of the competitive antagonists APV and DCKA). After exposure to redox reagent, current amplitudes (I_{post}) were determined again using three to five agonist applications. The change in glutamate-activated current amplitude, expressed as a percentage (*% change*), was calculated as: = 100 x (I_{post} - I_{pre})/I_{pre}. In certain instances, we corrected for observed current amplitude rundown by fitting a single exponential function to a minimum of three pre-redox reagent glutamate-activated current amplitudes.

Protein chemistry

Fractionation of membrane proteins. Ten to twelve healthy oocytes were injected with 1-2 ng of mRNA. Two-three days after transfection (HEK 293 cells)/injection (oocytes) cells were washed in phosphate buffer solution (PBS), fixed in PBS containing 0.58 mM N-ethylmalemide (NEM, Pierce), homogenized in lysis buffer (20 mM Tris, 0.58 mM NEM) and centrifuged at 3k RPM (Eppendorf Centrifuge 5417R) for 3 min at 4°C. The supernatant was recovered and centrifuged at 40k RPM (Beckman TLA 120.2 rotor) for 10 min at 4°C. The pellet was rinsed in PBS and recentrifuged at 40k RPM. The resulting pellet was resuspended and first sonicated in solubilization buffer (20 mM Tris, 50 mM NaCl, 1/1000 proteases inhibitor cocktail (Sigma), 0.58 mM NEM) without detergent and then incubated with detergent (0.03% Na-Deoxycholate, 1%Triton-X100)

for 1 hour at 4°C. Solubilized proteins were centrifuged at 40k RPM for 20 min at 4°C and membrane proteins contained in the supernatant were separated by SDS-PAGE under non-reducing or reducing (100 mM DTT) conditions.

Oocytes treated with Cu:Phen were harvested in the same manner as NEM-treated oocytes except for two differences. First, oocytes were washed in PBS and then fixed in PBS containing only Cu:Phen (1:50 μM) and the competitive antagonists APV (100 μM) and DCKA (10 μM). Additionally, Cu:Phen/APV/DCKA and NEM were present in the lysis and solubilization solutions.

Immunoblotting. Proteins were transferred from the gel to 0.45 mm nitrocellulose membranes by semi-dry transfer (BioRad, Hercules, CA) using Bjerrum-Schaffer-Nielsen Buffer. Blots were blocked and incubated with primary antibody, either anti-GluN1 (1:500, Millipore MAB363) or anti-GluN2A (1:500, Millipore AB1555P), overnight. Blots were washed prior to incubation with HRP-conjugated goat anti-mouse (sc-2302) or HRP-conjugated goat anti-rabbit (sc-2030) and developed using WB luminol reagent (sc-2048, all reagents Santa Cruz Biotechnologies) before exposure to chemiluminescence Biomax Film (Kodak, Cedex, France).

Quantification of Immunoblots. Immunoblot films were scanned using an EPSON flat scanner (Epson Perfection V700 Photo) in an 8 bit gray scale mode, 1200 dpi, reflective and quantified using NIH image J (1.38x) on a Windows XP platform. To quantify band densities, we defined a box encompassing the size of the largest monomer band. For each lane in the gel, this box was placed in the presumed location of the monomer and dimer bands as well as in a region in the leading edge (no protein sample) to define background. The measured density of the background was subtracted out from the

density for the monomer and dimer bands, and a ratio of the background-subtracted dimer and monomer densities (dimer/monomer ratio) was expressed in arbitrary units (AU).

To minimize differences in saturation levels in monomer/dimer band densities, we tried to make the monomer band densities approximately equal between groups (i.e., NEM- and Cu:Phen-treated samples). To accomplish this, we typically ran an initial gel where every sample was loaded at 10 μl, and would subsequently run a second gel where loading volumes were varied to generate comparable monomer band densities (typically 5 μL for NEM-treated samples and 15 μL for Cu:Phen-treated samples). Even with this correction, the monomer bands tended to have higher density for the NEM-treated condition (average density was around 550,000 arbitrary units for NEM-treated compared to around 450,000 for Cu:Phen-treated). A higher monomer band density tended to favor the dimer/monomer ratio, further validating the statistical outcomes in Figure 2.4F (where dimer/monomer ratios were higher for certain constructs in Cu:Phen-treated condition).

Data analysis

Data analysis was done using Igor Pro (Wavemetrics, Inc.) and Microsoft Excel. For analysis and illustration, leak currents were subtracted from total currents. An ANOVA or Student's *t*-test was used to define statistical differences. The Tukey or Dunnet's test was used for multiple comparisons. Significance was assumed at $P < 0.05$.

RESULTS

NMDA receptors with introduced cysteines in the M3/M3-S2 linker of GluN1 but not GluN2A yield dimers.

In the closed state for AMPA receptors, the C-terminal end of the M3 segment and the M3-S2 linker, referred to as the M3/M3-S2 linker (see Methods), are proximal in the A/C conformer (Figure 2.2A, *left panel*) with the closest approach in the C-terminal end occurring at M629 (distance between α-carbons 12 Å; Figure 2.2A, *right panel*, arrowhead). The M3/M3-S2 linkers of the B/D conformer (Figure 2.2A, *left panel*) are more distal (M629 separated by 30.2 Å) (Table 2.1) (Sobolevsky, Rosconi et al. 2009). Introduced cysteines at the homologous position in the NMDA receptor GluN1 subunit (P642, position +15, Figure 2.2A), but not in the GluN2A subunit (F639), yielded dimers on immunoblots suggesting that the M3/M3-S2 linkers are proximal in GluN1 (Sobolevsky, Rosconi et al. 2009). However, distal to the highly conserved SYTANLAAF motif (positions +1 to +9) in the M3 transmembrane segment, there is divergence in the identity and nature of the residues in the M3/M3-S2 linkers between AMPA and NMDA receptor subunits, as well as amongst NMDA receptor subunits (Figure 2.2A, *right panel*). Hence, the detailed arrangement of the linkers may differ between subunits. We therefore introduced cysteines over a wider range of positions in NMDA receptor subunits (Figure 2.2A, *right panel*) and characterized these constructs by immunoblots (Figures 2.2B, 2.2D-E).

For GluN1 (Figure 2.2B) and consistent with previous results (Sobolevsky, Rosconi et al. 2009), a dimer band (filled arrowhead) was prominent for P642C. In

addition, D640C also showed a prominent dimer, whereas dimers of decreased and inconsistent intensity were observed for V638C, L639C, R641C, E643C, and E644C (Figures 2.2B, 2.2C). No dimers were detected for wild-type (GluN1/GluN2A), A635C or R645C (Figures 2.2B, 2.2C). Observed dimers for D640 and P642 were not dependent on expression system, were absent under reducing conditions, and were specific to GluN1 with no dimers detected when probed with anti-GluN2A (Figure 2.2E). In contrast, no dimer bands were identified for the tested M3/M3-S2 GluN2A positions (Figure 2.2D).

These results are consistent with the M3/M3-S2 linkers of GluN1 being positioned proximal to one another as in the A/C conformer. Also notable is that positions presumably located even more proximal to one another (e.g., A635 in GluN1 corresponding to A622 in A/C or B/D conformer of GluA2, app. 10.6 Å; Table 2.1) do not yield dimers, indicating that other factors (e.g., membrane, local environment, and backbone rigidity) also affect cross-linking. Still, the present results do not address functional receptors.

Functional assays of proximity.

To test the general arrangement of the linkers in functional NMDA receptor subunits, we introduced individual cysteines in the M3/M3-S2 linker of either GluN1 or GluN2C (Figure 2.3A) and tested the effects of dithiothreitol (DTT), a reducing agent, or Copper(II):phenanthroline (Cu:Phen), an oxidizing agent, on current amplitudes. For these experiments, we preferentially used GluN2C since it shows limited desensitization compared to GluN2A (Krupp, Vissel et al. 1996).

For wild-type GluN1/GluN2C, DTT applied in the presence of agonists produced about a 46% potentiation of current amplitudes (46 ± 3%, n = 7; mean *%change* ± SEM, number of recordings) (Table 2.2). For all cysteine-substituted M3/M3-S2 positions in GluN1 and GluN2C, DTT applied in the presence of agonists did not produce a significant effect on glutamate-activated currents compared to wild-type (Table 2.2) including GluN1(D640C) and GluN1(P642C).

An oxidizing agent produces current inhibition of receptors containing substituted cysteines in the M3/M3-S2 linker in GluN1 but not GluN2.

To test the effects of the oxidizing agent Cu:Phen on functional receptors (Figures 2.3B, 2.3C), we compared glycine- and glutamate-activated (referred to as glutamate-activated) current amplitudes before (I_{pre}) and after (I_{post}) exposure to extracellular Cu:Phen (2:50 μM, thick lines) applied in the presence of agonists, where the channel exists both in the open and closed states. For wild-type GluN1/GluN2C (Figure 2.3B), Cu:Phen had no significant effect on glutamate-activated current amplitudes (-2 ± 2%, n = 9). In contrast, for GluN1(D640C)/GluN2C (Fig. 3C), Cu:Phen induced a strong and persistent inhibition of current amplitudes (-83 ± 9%, n = 5).

Figure 2.3D summarizes the effect of Cu:Phen applied in the presence of agonists (Cu:Phen + Glu) on glutamate-activated current amplitudes. For GluN1, numerous (9) M3/M3-S2 positions (F636 to E644) showed significant effects, either current inhibition (leftward pointing bars) or potentiation (rightward pointing). On the other hand, for homologous positions in GluN2C, only a limited number of positions (3) showed significant effects. Of these, positions N627 and D639 showed significant

current potentiation that rapidly reversed over time (data not shown) and may reflect a transient effect of Cu:Phen on glutamate-activated current amplitudes.

The AMPA receptor crystal structure, where the M3/M3-S2 linker is proximal in the A/C conformation, was generated in the presence of a competitive antagonist (Sobolevsky, Rosconi et al. 2009). We therefore tested the reactivity of Cu:Phen in the absence of agonists, but in the presence of the GluN1 and GluN2 competitive antagonists (DCKA and APV, respectively) (Figure 2.3E) (closed state), focusing on those positions that showed a significant effect in the presence of agonists (Figure 2.3D). As summarized in Figure 2.3F, a subset of GluN1 positions (V638, L639, & D640) showed significant reactivity to Cu:Phen in the closed state. In contrast, GluN2C(Q636C), the single GluN2C position showing persistent effects (and inhibition) in the presence of agonists did not show a significant effect in the closed state (-10 ± 3%, n = 6, data not shown), compared to the observed effect in wild-type (-5 ± 2%, n = 8).

Cu:Phen-induced current inhibition reflects cross-linking of introduced cysteines.

Persistent changes in current amplitudes induced by Cu:Phen in GluN1 are presumably due to cross-linking of introduced cysteines. To test this assumption, we carried out a number of control experiments. Initially, we characterized the effect of the reducing agent DTT on Cu:Phen-induced inhibited currents. If the observed current inhibition following treatment with Cu:Phen is the result of cross-linking of introduced cysteines in the M3/M3-S2 linker of GluN1, then DTT should potentiate current amplitudes more strongly than in wild-type receptors. As illustrated for GluN1(D640C)/GluN2C (Figures

2.4A, 2.4B), an initial application of Cu:Phen in the presence of agonists strongly reduced currents amplitudes (Figure 2.4B, *solid circles*), as shown previously (Figure 2.3D). Subsequent application of DTT dramatically potentiated these Cu:Phen-inhibited current amplitudes (Figures 2.4A, 2.4B, *open squares*) (516 ± 170%, n = 8).

Figure 2.4C summarizes the effect of DTT on wild-type and the three GluN1 cysteine-substituted positions (V638, L639, & D640) that showed significant effects following Cu:Phen in the absence of agonists (Figure 2.3F). For wild-type receptors, DTT applied in the presence of agonists without any Cu:Phen pretreatment (labeled 'DTT' in Figure 2.4C) potentiated current amplitudes by about 46% (46 ± 3%, n = 7), an effect also seen for all three GluN1 cysteine-substituted positions (Table 2.2; open bars, Fig. 4C, *DTT*). For wild-type receptors, application of DTT following Cu:Phen treatment (as for GluN1(D640C)/GluN2C in Figure 2.4A) potentiated current amplitudes by about 8% (7.7 ± 6%, n = 4) (Figure 2.4C, *Cu:Phen/DTT*). For the three GluN1 cysteine-substituted positions, DTT significantly potentiated the Cu:Phen-inhibited current amplitudes compared to wild-type recorded under the same conditions (solid bars, Figure 2.4C, *Cu:Phen/DTT*) and compared to the same position measured with DTT alone (asterisks). These results strongly support the idea that current inhibition reflects cross-linking of substituted cysteines.

We also tested whether the introduced cysteine at D640 interacted with endogenous cysteines in GluN1 or GluN2C. In NMDA receptor subunits, four endogenous cysteines are located in the linkers and/or proximal face of the ligand-binding domain (Furukawa, Singh et al. 2005): GluN1(C726), GluN1(C780), GluN2C(C724) and GluN2C(C779). Replacing these cysteines with serine (S) did not

significantly alter current inhibition for D640C consistent with Cu:Phen inducing cross-linking between introduced cysteines (Figure 2.4D).

As an additional test that Cu:Phen treatment induced disulfide cross-linking amongst GluN1 subunits, we analyzed immunoblots of proteins purified in the absence (NEM) or presence (Cu:Phen) of Cu:Phen for V638, L639, D640, as well as a control position that did not show a significant effect of Cu:Phen, R645 (Figures 2.4E, 2.4F). As summarized in Figure 2.4F, when treated with NEM, position D640C showed a significant dimer/monomer ratio (solid bar) compared to wild-type, as was found for GluN1/GluN2A (Figure 2.2C). Further, when treated with Cu:Phen, introduced cysteines at positions V638, L639, and D640 showed significant increases in the dimer/monomer ratio compared to both wild-type treated with Cu:Phen (solid bars) and to the same positions treated with NEM (asterisks).

In summary, these results indicate that current inhibition induced by Cu:Phen is due to cross-linking of introduced cysteines in the M3/M3-S2 linker of the GluN1 subunits. Since this cross-linking occurs only for the GluN1 and not the GluN2C subunit (Figures 2.3D, 2.3F), the present results strongly support a more proximal positioning of the M3/M3-S2 linker in GluN1 than in the GluN2C subunit. This proximal positioning of the M3-S2 in GluN1 is consistent with it adopting the A/C conformation.

Cross-linking of introduced cysteines in the GluN1 M3/M3-S2 linker is not dependent on the GluN2 subunit.

To verify that the observed cross-linking of the M3/M3-S2 linker in GluN1 was independent of the nature of the GluN2 subunit, we co-expressed GluN1 cysteine

substituted receptors with GluN2A and tested for the effect of Cu:Phen (Figure 2.5). Wild-type GluN1/GluN2A (Figures 2.5A, 2.C), in contrast to wild-type GluN1/GluN2C (Figures 2.3B, 2.3D), showed a significant potentiation (46 ± 5%, n = 7) following Cu:Phen treatment in the presence of agonists. Nevertheless, although the degree of potentiation or inhibition may differ, all tested cysteine-substituted GluN1 positions when co-expressed with GluN2A showed a similar functional profile (Figure 2.5C) as that of GluN1(cys)/GluN2C (Figure 2.3D). These findings support the conclusion that the observed effects of Cu:Phen on introduced cysteines in the M3/M3-S2 linker of GluN1 are a result of cross-linking amongst the GluN1 subunits and that this behavior is not dependent on the specific GluN2 subtype.

Cross-linking of substituted cysteines in GluN2C but not GluN1 S2-M4 linker.

The proximal positioning of the M3/M3-S2 linker in GluN1 relative to GluN2C is consistent with GluN1 subunits adopting the A/C conformation. However, the M3/M3-S2 results do not provide positive evidence for the positioning of the GluN2 subunits. In the AMPA receptor crystal structure, the S2-M4 linkers are considerably more proximal in the B/D conformation (19.3 Å) (from K776 to K783) than in the A/C conformation (54.6 Å) (Figure 2.6A, *left panel*, Table 2.3). Note however, that the specific arrangement of S2-M4 linkers in NMDA receptor subunits is different from that of AMPA receptor subunits due to gaps in the NMDA receptor sequence (Figure 2.6A, *right panel*). If the GluN2 subunits approximate the B/D conformation, we would then anticipate that introduced cysteines in the S2-M4 linker of GluN2, but not GluN1, might cross-link and affect current amplitudes. We therefore tested a range of substituted cysteines in the S2-M4 linkers of GluN1 and GluN2C (Figure 2.6A).

Consistent with the predicted outcome, substituted cysteines in the S2-M4 linker of GluN2C, but not GluN1, showed significant, albeit small, effects of Cu:Phen applied in the presence of agonists (Figures 2.6B-2.6D). A subset of these GluN2C positions also showed current inhibition when Cu:Phen was applied in the absence of agonists (Figures 2.7A, 2.7B) replicating the proximal positioning of the S2-M4 linker as observed in the AMPA receptor crystal structure (Sobolevsky, Rosconi et al. 2009).

To verify that the current inhibition was due to disulfide cross-linking, we tested the effect of the reducing agent DTT on those S2-M4 GluN2C positions that were reactive in the absence of agonists (N781, E782, K783) (Figure 2.7B) either without initial Cu:Phen treatment (Figure 2.7C, *DTT*) or following Cu:Phen treatment (Figure 2.7C, *Cu:Phen/DTT*). Compared to the potentiation in wild-type, application of DTT without Cu:Phen treatment did not elicit any significant changes in the current amplitudes for the cysteine-substituted receptors (Figure 2.7C, *DTT*), though potentiation was largely absent in K783. In contrast, following Cu:Phen-induced current inhibition, DTT significantly potentiated current amplitudes for both N781C and E782C compared to wild-type when recorded under the same conditions (solid bars, Figure 2.7C, *Cu:Phen/DTT*) and for each N781C, E782C, and K783C compared to the same position measured with DTT alone (asterisks). Interestingly, K783C did not show a significant effect when compared to wild-type (open bar, Figure 2.7C, *Cu:Phen/DTT*), but did show a significant effect when compared to DTT alone (asterisk) suggesting that the mutation itself might alter the redox state of the receptor. Nevertheless, the fact that the DTT potentiation of Cu:Phen-inhibited currents is significantly greater than DTT

alone for K783C as well as N781C and E782C supports the idea that current inhibition is due to cross-linking of substituted cysteines.

The reduced magnitude of current inhibition for GluN2C S2-M4 positions reactive in the absence of agonists (Figure 2.7B) relative to those for GluN1 M3/M3-S2 (Figure 2.3F) may reflect a generally more remote relative positioning: average distance for GluN2C S2-M4 positions (assuming B/D conformation) is 22.9 Å (Table 2.3) whereas it is 16.3 Å for GluN1 M3/M3-S2 positions (assuming A/C conformation) (Table 2.1).

In summary, these experiments suggest that the S2-M4 linker in GluN2C is more proximal than that of GluN1. In the context of the AMPAR structure, these results are consistent with the GluN2 subunit approximating the B/D conformation. In combination with the results for the M3/M3-S2 linker, which suggest that GluN1 approximates the A/C conformation, like subunits in the functional tetrameric complex are diagonal to one another in a N1/N2/N1/N2 arrangement.

DISCUSSION

Defining the subunit arrangement in functional ionotropic glutamate receptors (iGluR) is an important advance in understanding mechanisms of iGluR biogenesis, trafficking and gating. Activation of iGluRs occurs when agonist-induced conformational changes in the ligand-binding domain (LBD) are propagated to the transmembrane domain (TMD) resulting in ion channel opening (Sun, Olson et al. 2002; Erreger, Chen et al. 2004). Three polypeptide linkers (S1-M1, M3-S2, S2-M4) that join the LBD to the ion channel mediate these agonist-induced effects on ion channel opening/closure. The recent crystal structure of a homomeric AMPA receptor (GluA2) showed that identical subunits adopted two distinct conformations, termed A/C and B/D, which were notable at the level of the LBD-TMD linkers because they took on subunit specific conformations (Sobolevsky, Rosconi et al. 2009). Using immunoblots and whole-cell electrophysiology, we show that functional obligate heteromeric NMDA receptors take on distinct, subunit-specific conformations with GluN1 approximately the A/C conformer and GluN2 approximating the B/D conformer with subunits therefore arranged as N1/N2/N1/N2 (Rambhadran, Gonzalez et al. 2010).

Conformers of NMDA receptor subunits.

Given the overall sequence homology amongst the iGluR subtypes and subunits (Traynelis, Wollmuth et al. 2010), it is likely that iGluRs (e.g., NMDA and AMPA) share a common LBD-TMD linker structure. Compared to AMPA receptors, the linkers in NMDA receptors vary in their primary sequence and/or length (e.g., S2-M4) (Figures 2.3A, 2.6A), but these differences probably result in small local structural differences rather

than changing the overall general arrangement of the linkers. Nevertheless, because of these small differences and the absence of a full length NMDA receptor structure, NMDA receptor subunits can only be considered to approximate rather than adopt the A/C and B/D conformations.

In this study, introduced cysteines in the M3/M3-S2 linker of GluN1, but not GluN2, showed both dimer formation (Figures 2.2B, 2.2D, 2.4E) and oxidation-induced alteration of current amplitudes (Figure 2.3D) consistent with a more proximal positioning of the M3/M3-S2 linker in the GluN1 subunit. Spontaneous disulfide bond formation only occurs when sulfhydryl moieties are within 2 Å of one another (Careaga and Falke 1992; Clarke and Fersht 1993). Hence, assuming proper orientation for a rigid structure, the α-carbons of introduced cysteines must be positioned within 6-8 Å of one another in order to cross-link. If either the backbone is flexible or one utilizes a strong oxidation agent (e.g., Cu:Phen), then cross-linking can occur amongst cysteines over a greater range of separation ($\approx$20 Å) (Careaga and Falke 1992; Clarke and Fersht 1993). On average in the crystal structure, the distance between M3/M3-S2 positions (A622 to P632) of the A/C and B/D conformations is 16.3 Å and 24.3 Å, respectively (Table 2.1). Based on these considerations, there are positions in the GluN2 M3/M3-S2 linker whose analogous position in the crystal structure is quite proximal in the B/D conformer (e.g., GluN2A(Q636)) (Table 2.1) that do not show dimer formation (Figure 2.2D) nor significant oxidized-induced current inhibition (Figure 2.3D). Additionally, the observed oxidation-induced inhibition in the S2-M4 linker of the GluN2 but not GluN1 subunit (Figure 2.6D) is consistent with a more proximal positioning of the GluN2 S2-M4 linker. It is important to note that the local S2-M4 structure of NMDA receptor subunits

is almost certainly different than that in AMPA receptor subunits due to gaps in the sequence alignments (Figure 2.6A, *right panel*). Still, we do not believe these differences greatly alter the relative spatial positioning of the conformers—especially given the dramatic difference in typical distances in the A/C (46.7 Å) compared to the B/D (22.9 Å) conformations (Table 2.3). Further, we concede that Cu:Phen likely induces rarely visited conformations, however, this point is not critical here since we are only interested in proximity rather than gating states.

An alternative interpretation of the present results is that the GluN1 and GluN2 subunits are positioned adjacent to each other in a N1/N1/N2/N2 arrangement. Although we cannot completely rule out this alternative, it is highly unlikely if one accepts that the general arrangement of NMDA receptor subunits including at the LBD-TMD linkers is comparable to that of AMPA receptors. Specifically, if like subunits (e.g., GluN1 and GluN1) are adjacent to one another, then one subunit must adopt the A/C conformation and the other the B/D conformation. Thus, a N1/N1/N2/N2 arrangement would result in GluN1/GluN1 and GluN2/GluN2 dimers at the level of the linkers having identical conformational symmetry. With regards to our experimental protocol, if like subunits adopted a N1/N1/N2/N2 arrangement, then we would expect cross-linking for GluN1 and GluN2 to show identical patterns functionally—that is, introduced cysteines in the M3/M3-S2 linkers of both GluN1 and GluN2 should show cross-linking due to their identical conformations. However, we find that the pattern of cross-linking is highly subunit-specific showing cross-linking either in M3/M3-S2 (GluN1) (Figures 2.2, 2.3) or S2-M4 (GluN2) (Figure 2.6). As such, our results suggest that like subunits, sharing a

common conformer, are positioned diagonal to one another, which we interpret as A/C (GluN1) and B/D (GluN2) leading to a N1/N2/N1/N2 arrangement.

The present study does not address the subunit-specific conformations of external iGluR elements, specifically the amino-terminal domain (NTD). Indeed, the NTD in NMDA receptor subunits may take on a twisted closed-cleft conformation (Karakas, Simorowski et al. 2009; Stroebel, Carvalho et al. 2010; Karakas, Simorowski et al. 2011) that is distinct to the conformation of the same domain in AMPA (Clayton, Siebold et al. 2009; Sobolevsky, Rosconi et al. 2009) and kainate (Kumar, Schuck et al. 2009) receptors, possibly resulting in differences in the pattern of domain swapping. However, additional work is required to determine the arrangement of subunit domains at the level of the NTD, as well as the functional relationship between the NTDs and the A/C and B/D conformations at the level of the LBD-TMD linkers (Gielen, Siegler Retchless et al. 2009; Yuan, Hansen et al. 2009).

Subunit-specific effects on gating and biogenesis.

Because cross-linking occurred only for specific subunits, it appears that the conformation approximated by NMDA receptor subunits in the tetrameric complex is invariant, either A/C (GluN1) or B/D (GluN2). Nevertheless, the functional significance of the different conformers and how they might arise and be constrained during biosynthesis is unknown. In terms of functional properties, subunit-specific differences in the LBD-TMD linker structure may underlie subunit-specific contributions to ion permeation (Watanabe, Beck et al. 2002) and channel gating (Banke and Traynelis 2003; Sobolevsky, Prodromou et al. 2007; Blanke and VanDongen 2008; Blanke and

VanDongen 2008) (Kussius and Popescu 2009). Recent work from our laboratory suggests that despite subunit-specific differences in the structure of the LBD-TMD linkers, NMDA receptors undergo concerted gating that appears tightly coupled at the level of these linkers (Talukder and Wollmuth 2011). Still, how these different LBD-TMD linker arrangements couple the LBD to pore opening remain unknown.

NMDA receptors can form di-heteromeric (e.g., GluN1/GluN2 and/or GluN1/GluN3) or tri-heteromeric (e.g., GluN1/GluN2/GluN3) receptors that differ widely in their biophysical and pharmacological properties (Traynelis, Wollmuth et al. 2010). The initial step mediating the formation of these iGluR heteromers is dimer formation. However, much controversy exists regarding the nature of this initial dimer—whether it is a homodimer (e.g., GluN1) (Papadakis, Hawkins et al. 2004; Farina, Blain et al. 2011) or a heterodimer (e.g., GluN1/GluN2) (Schuler, Mesic et al. 2008)—and the order in which the dimers assemble to form a functional tetrameric receptor. The amino-terminal domain in iGluRs is critical for initial dimer formation (Paoletti and Neyton 2007; Shanks, Maruo et al. 2010; Farina, Blain et al. 2011). Interestingly, heteromeric AMPA receptors (e.g., GluA1/GluA2), like NMDA receptors, are arranged in an alternating subunit-specific manner (A1/A2/A1/A2) (Mansour, Nagarajan et al. 2001). Therefore, the presence of subunit-specific conformations in heteromeric assemblies may be a necessary component not only of dimer formation, but also for tetramerization and/or for stabilization of the tetrameric assembly. Thus, the existence of two distinct conformations may serve a role in ensuring the proper biosynthesis and trafficking of iGluRs to the membrane but the role of the specific conformations in these processes remain unknown.

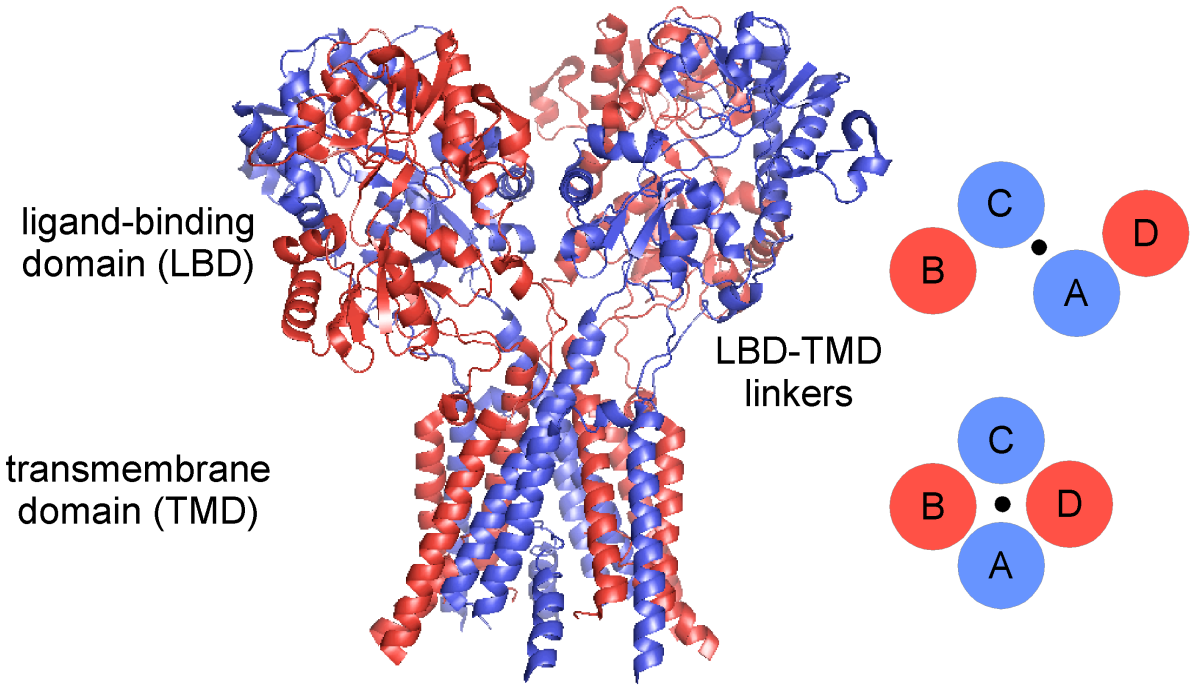

FIGURE 2.1. Individual subunits within tetrameric ionotropic glutamate receptors adopt two distinct subunit conformations.

Structure of a homomeric glutamate receptor ($GluA2_{cryst}$, PDB accession code 3KG2) (Sobolevsky, Rosconi et al. 2009) depicting the organization of individual subunits at the level of the ligand-binding domain (LBD) and the transmembrane domain (TMD). The LBD is organized as a dimer of dimers composed of individual dimer pairs A/D and B/C, whereas the ion channel within the TMD is organized as a tetramer displaying four-fold symmetry (schematics on the right). Four identical subunits showed two distinct subunit conformations termed A/C (blue) and B/D (red) with like conformers diagonal to one another. The two distinct subunit conformations are notable at the level of the LBD-TMD linkers that mediate the transition from the two-fold symmetry of the LBD to the four-fold symmetry of the TMD.

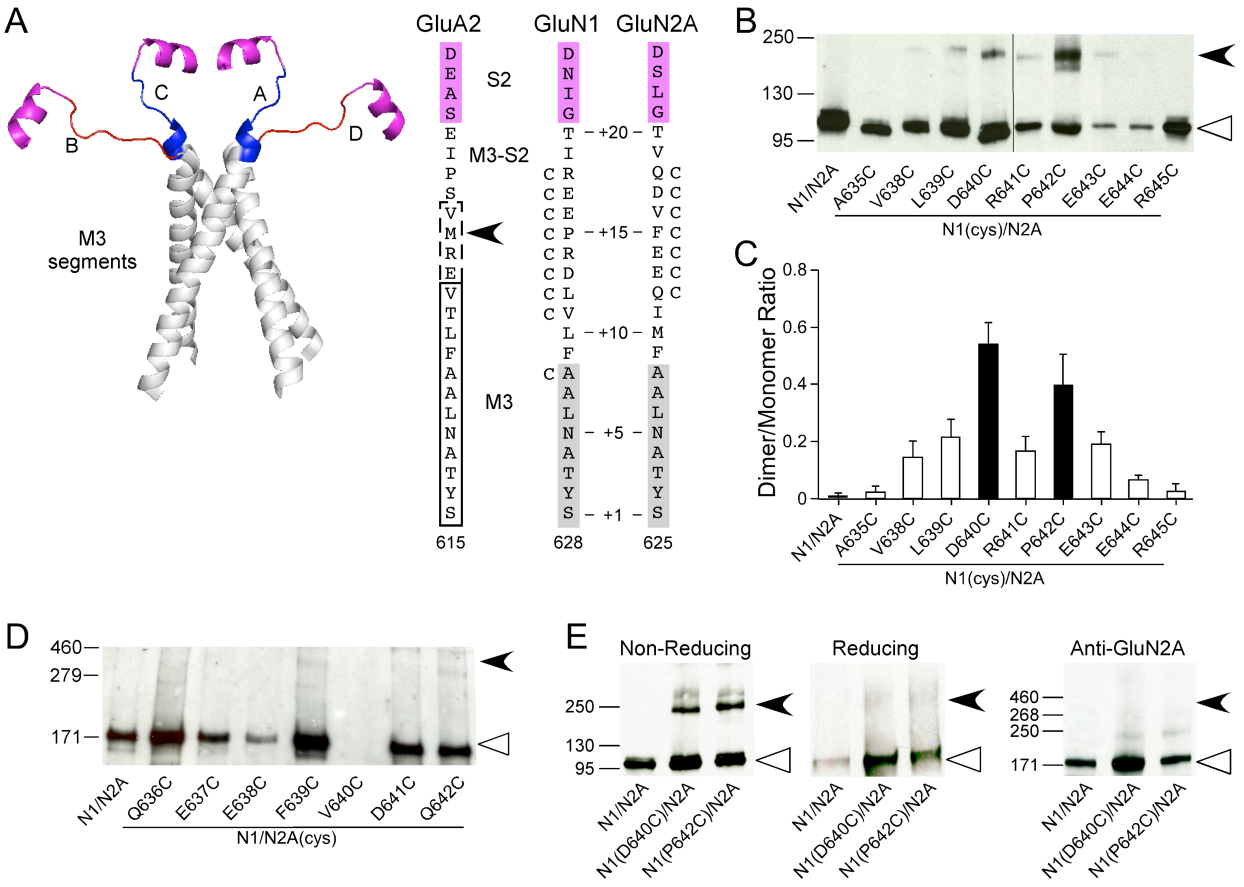

FIGURE 2.2. Receptors with cysteines substituted in the GluN1 but not in the GluN2A M3/M3-S2 linker yield dimers.

(A) Backbone structure (left) of the M3 transmembrane segment (gray)—the major pore-forming domain—and the M3/M3-S2 linkers (A/C, blue; B/D, red) that connect the M3 transmembrane segment to helix E of the LBD (magenta) ($GluA2_{cryst}$, PDB accession code 3KG2). Sequence alignment (right) of residues in and around the M3/M3-S2 linker in AMPA GluA2 and NMDA GluN1 and GluN2A. Proximal S2 (helix E) is shown in magenta. For GluA2, the boxed regions indicate the α-helical extent of the A/C (dashed lines) or B/D (solid lines) conformation of M3 (Sobolevsky, Rosconi et al. 2009). For NMDA receptor subunits, M3, as defined by hydrophobicity (Biology Workbench, San Diego), is highlighted in gray. Substitution of M629 with cysteine in GluA2 (arrowhead) yielded dimers in immunoblots (Sobolevsky, Rosconi et al. 2009). Positions substituted with cysteine are indicated by a 'C' adjacent to the native residue. Numbering is for the mature protein (see Materials & Methods). We also used a relative numbering system, referencing the initial serine (S) in the highly conserved SYTANLAAF motif as +1 (Jones, VanDongen et al. 2002).

(B) & (D) Immunoblots of membrane-purified proteins isolated from *Xenopus* oocytes injected with wild-type or cysteine-substituted GluN1 (B) or GluN2A (D) subunits. Protein expression was assayed using antibodies against the N-terminal domain of GluN1 (B) or GluN2A (D). Open triangles and arrowheads indicate approximate location of monomer (GluN1, 114 kDa; GluN2A, 173 kDa) and dimer (GluN1, 228 kDa; GluN2A, 346 kDa) bands, respectively. The GluN2A gel was overexposed to illustrate the lack of subunit-specific dimers. Note receptors containing GluN2A(V640C) (D) showed functional currents and positive monomer signal when probed with the anti-GluN1, but we could not detect a monomer band using the anti-GluN2A antibody.

(C) Quantification of band intensity (see Materials & Methods) for wild-type and GluN1 cysteine-substituted mutants ($n > 4$ for each). Filled bars indicate values statistically different from GluN1/GluN2A ($P < 0.05$).

(E) Immunoblots of membrane-purified proteins isolated from HEK 293 cells probed for anti-GluN1 under non-reducing (*left*) or reducing (100 mM DTT, *middle*) conditions or for anti-GluN2A (*right*) demonstrating subunit-specific dimer formation. Open triangles and arrowheads indicate approximate location of monomer (GluN1, 114 kDa; GluN2A, 173 kDa) and dimer (GluN1, 228 kDa; GluN2A, 346 kDa) bands, respectively.

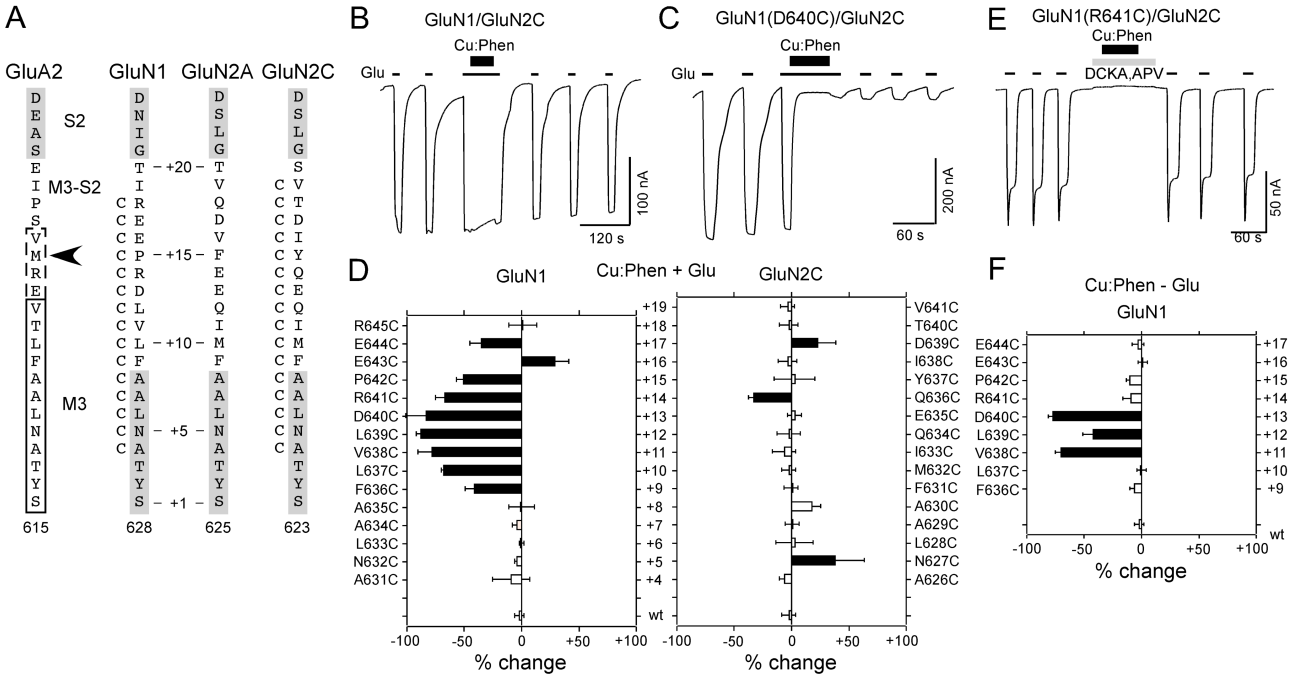

FIGURE 2.3. Receptors with substituted cysteines in the M3/M3-S2 linker of GluN1 but not GluN2C show widespread current inhibition following oxidation.

(A) Same as Figure 2.2A (right) but including GluN2C. Proximal portion of Helix E is indicated in gray.

(B & C) Example current recordings from oocytes showing the effect of Copper(II):phenanthroline (Cu:Phen) (2:50 μM, thick lines, 60 sec) in the presence of agonists (open & closed states) on GluN1/GluN2C (B) or GluN1(D640C)/GluN2C (C). Currents were elicited by glycine (20 μM) and glutamate (200 μM) (thin lines labeled with 'Glu') at a holding potential of -60 mV.

(D) Mean percent change (% change) (± 2SEM) (n ≥ 3 for each) of glutamate-activated current amplitudes measured before (*Ipre*) and after (*Ipost*) exposure of wild-type and cysteine-substituted GluN1 (left) or GluN2C (right) to Cu:Phen in the presence of agonists (*% change* = 100 x (I_{post} - I_{pre})/I_{pre}). Left and right pointing bars indicate inhibition and potentiation, respectively. Filled bars indicate values significantly different from wild-type GluN1/GluN2C ($P < 0.05$). The small current potentiation seen for GluN2C(N627C) & GluN2C(A630C) is transient and reflects the effect of Cu:Phen in the presence of agonists.

(E) Example recording of the effect of Cu:Phen (60 sec) applied in the absence of agonists, but in the presence of the competitive antagonists DCKA (10 μM) and APV (100 μM) (gray box) (closed state) on glutamate-activated currents in oocytes injected with GluN1(R641C)/GluN2C.

(F) Mean percent change (% change) (± 2SEM) (n > 3) of glutamate-activated current amplitudes, measured in the absence of agonists, for GluN1 cysteine-substituted positions that showed significant effects in the presence of agonists. Results are shown as in (D).

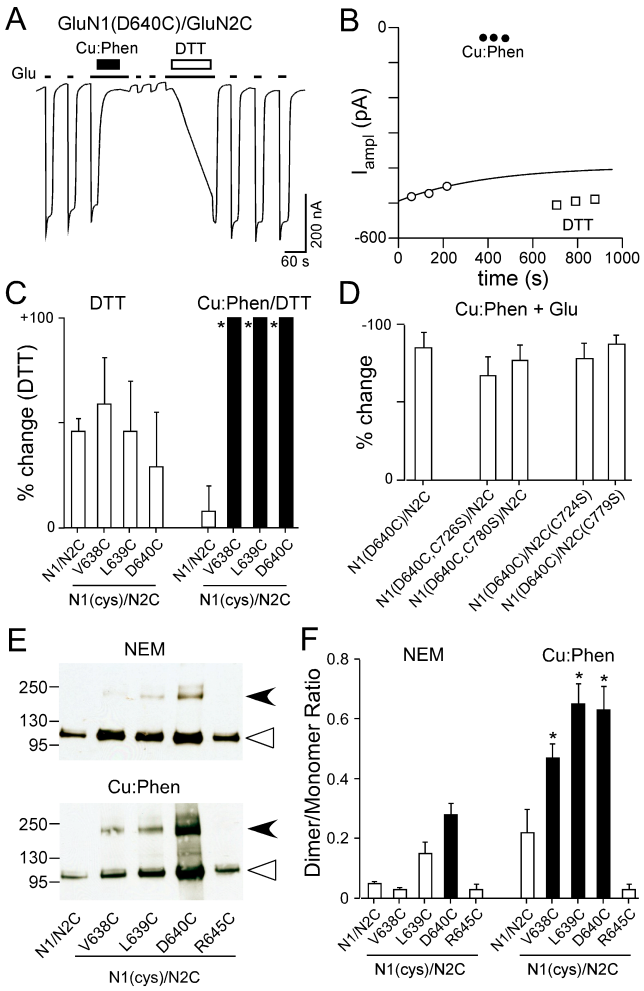

FIGURE 2.4. Current inhibition reflects cross-linking of substituted cysteines.

(A) Effect of dithiothreitol (DTT, 1 mM), applied in the presence of agonists, on Cu:Phen-induced inhibited currents in GluN1(D640C)/GluN2C.

(B) Glu-activated current amplitudes for GluN1(D640C)/GluN2C recorded before (*open circles*) and after Cu:Phen (*filled circles*) or DTT (*open squares*) (amplitudes are from trace shown in (A).

(C) Mean percent change (% change) (± 2SEM) (n > 3) of glutamate-activated current amplitudes for wild-type and GluN1 cysteine-substituted positions that showed significant effects of Cu:Phen in the absence of agonists (Figure 2.3F). % change is measured following DTT (I_{post}) either relative to currents before any treatment (*DTT*) (Table 2.2) or to currents following Cu:Phen (*Cu:Phen/DTT*) (as in Figures 2.4A, 2.4B). Filled bars indicate values significantly different from GluN1/GluN2C within treatment groups ($P < 0.05$). Asterisks indicate values statistically different between treatment groups for equivalent positions ($P < 0.05$). The mean %change for DTT in the Cu:Phen/DTT condition was 540 ± 100%, n = 5 (V638C), 150 ± 15%, n = 4 (L639C), and 520 ± 170%, n = 8 (D640C).

(D) Mean percent change (% change) (± 2SEM) (n > 4) of glutamate-activated current amplitudes for GluN1(D640C)/GluN2C or the same constructs with endogenous cysteines neutralized to serine (S) measured before or after Cu:Phen treatment in the presence of agonists. None of the values were significantly different from that for GluN1(D640C)/GluN2C indicating that the effect of Cu:Phen arises from introduced cysteines.

(E) Immunoblots of membrane-purified proteins isolated from *Xenopus* oocytes injected with wild-type or cysteine-substituted GluN1 subunits co-expressed with GluN2C treated without (NEM, *top*) or with (Cu:Phen, *bottom*) Cu:Phen. Protein expression was assayed using antibodies against the N-terminal domain of GluN1. Open triangles and arrowheads indicate approximate location of monomer (114 kDa) and dimer (228 kDa) bands, respectively.

(F) Quantification of band intensity (see Materials & Methods) for wild-type and GluN1 cysteine-substituted receptors (n > 4 for each) either without (*left*) or with (*right*) Cu:Phen treatment. Filled bars indicate values statistically different than GluN1/GluN2C within treatment groups ($P < 0.05$). Asterisks indicate values statistically different between treatment groups for equivalent positions ($P < 0.05$).

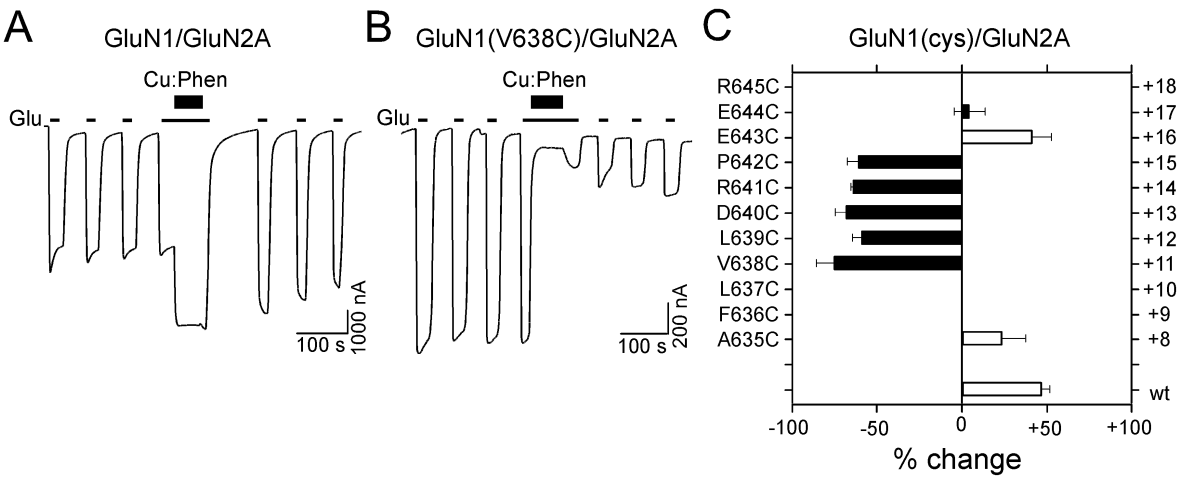

Figure 2.5. Cu:Phen has comparable effects on receptors with substituted cysteines in the GluN1 M3/M3-S2 linker when co-expressed with GluN2A.

(A) & (B) Example current recordings from *Xenopus* oocytes injected with GluN1/GluN2A (A) or GluN1(V638C)/GluN2A (B) mRNA. Cu:Phen was applied in the presence of agonists (e.g., Figures 2.3B, 2.3C).

(C) Mean percent change (% change) (± 2SEM) (n > 4) in glutamate-activated current amplitudes measured before (*Ipre*) and after (*Ipost*) exposure of wild-type and cysteine-substituted GluN1 co-expressed with GluN2A in the presence of agonists. Left and right pointing bars indicate inhibition and potentiation, respectively. Filled bars indicate values significantly different from wild-type GluN1/GluN2A ($P < 0.05$). Note that with respect to wild-type GluN1/GluN2C (Figure 2.3D) and GluN1/GluN2A, treatment with Cu:Phen produces a persistent potentiation in GluN1/GluN2A, however, the effect of Cu:Phen on the positions tested (except for E643) in both GluN2C (Figure 2.3D) and GluN2A were identical.

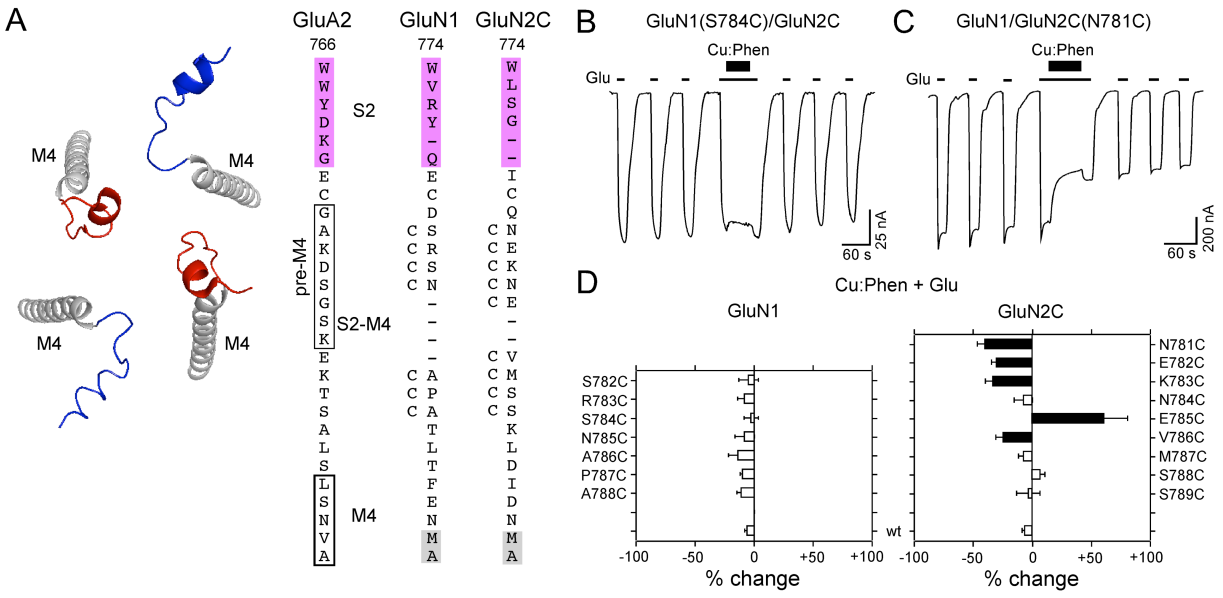

FIGURE 2.6. Receptors with substituted cysteines in the S2-M4 linker of GluN2C but not GluN1 show current inhibition following oxidation.

(A) Backbone structure (left) of the M4 transmembrane segment (gray) and the S2-M4 linkers of the A/C (blue) and B/D (red) subunits ($GluA2_{cryst}$, PDB accession code 3KG2). Sequence alignment (right) of residues in and around the S2-M4 linker in AMPA GluA2 and NMDA GluN1 and GluN2C with introduced cysteines indicated by a 'C' adjacent to the native residue. The pre-M4 helix in GluA2 is boxed (Sobolevsky, Rosconi et al. 2009). Dashes indicate gaps in aligned sequence. Other features are displayed as in Figure 2.2A with M4, as defined by hydrophobicity (Biology Workbench, San Diego), highlighted in gray and helix K of the S2 domain highlighted in magenta.

(B & C) Example recordings of Cu:Phen applied in the presence of agonists for S2-M4 cysteine substitutions either GluN1(S784C)/GluN2C (B) or GluN1/GluN2C(N781C) (C).

(D) Mean percent change (% change) (± 2SEM) (n > 3) of glutamate-activated current amplitudes measured before (*Ipre*) and after (*Ipost*) exposure of wild-type and cysteine-substituted GluN1 (left) or GluN2C (right) subunits to Cu:Phen in the continuous presence of agonists. Results are shown as in Figure 2.3D.

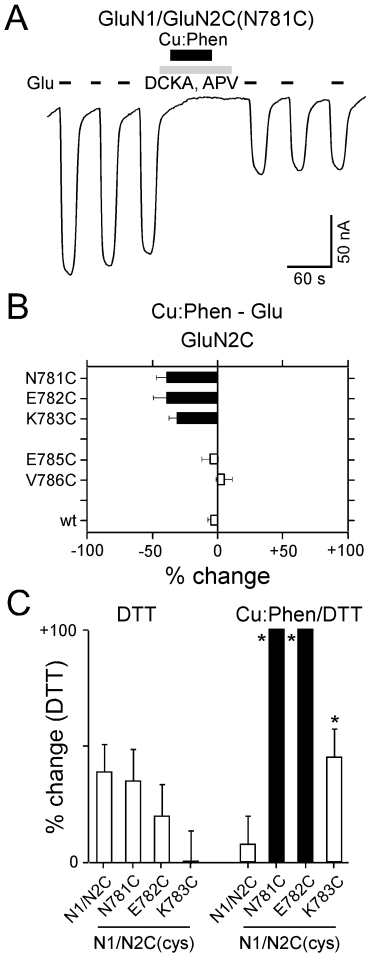

FIGURE 2.7. A subset of positions in the GluN2C S2-M4 linker are reactive in the absence of agonists.

(A) Example recording of the effect of Cu:Phen (60 sec) applied in the absence of agonists, but in the presence of the competitive antagonists DCKA (10 μM) and APV (100 μM) (gray box) (closed state) on glutamate-activated currents in oocytes injected with GluN1/GluN2C(N781C).

(B) Mean percent change (% change) (± 2SEM) of glutamate-activated current amplitudes, measured in the absence of agonists, for GluN2C S2-M4 cysteine-substituted positions that showed significant effects in the presence of agonists (Figure 2.6D).

(C) Mean percent change (% change) (± 2SEM) (n > 3) of glutamate-activated current amplitudes for wild-type and GluN2 cysteine-substituted positions that showed significant effects of Cu:Phen in the absence of agonists (Figure 2.7B). %change is measured following DTT (I_{post}) relative to currents before any treatment (*DTT*) (raw data not shown) or to currents following Cu:Phen (*Cu:Phen/DTT*). Filled bars indicate values significantly different from GluN1/GluN2C within treatment groups ($P < 0.05$). Asterisks indicate values statistically different between treatment groups for equivalent positions ($P < 0.05$). The mean % change for DTT in the Cu:Phen/DTT condition was 100 ± 30%, n = 6 (N781C), 110 ± 25%, n = 9 (E782C), and 45 ± 12%, n = 5 (K783C).

Table 2.1. Distance between α-carbons for homologous positions in the M3 segment and M3-S2 linker in the A/C and B/D subunits in $GluA2_{cryst}$

GluA2	αCs		GluN1	GluN2A	GluN2C
	A/C	B/D			
	Å	*Å*			
P632	26.6	49.6	R	Q	T
S631	19.7	42.7	E	D	D
V630	18.2	35.8	E	V	I
M629	12.0	30.2	P	F	Y
R628	16.9	22.7	R	E	Q
E627	19.1	19.6	D	E	E
V626	12.7	12.2	L	Q	Q
T625	11.3	10.2	V	I	I
L624	14.9	15.9	L	M	M
F623	17.0	17.2	F	F	F
A622	10.4	10.8	A	A	A

Shown are residues in $GluA2_{cryst}$ (Sobolevsky, Rosconi et al. 2009) (PDB ID 3KG2) and homologous positions in GluN1, GluN2A or GluN2C. Underlined residues for $GluA2_{cryst}$ are part of the M3 helix for the A/C and B/D subunits. Bolded residues are the additional helical component of the A/C subunit. Average distances for positions shown are 16.3 Å (A/C) and 24.3 Å (B/D).

Table 2.2. Effect of DTT on current amplitudes in wild-type and cysteine-substituted GluN1 and GluN2C subunits

construct	% change	n	Relative Position	construct	% change	n
N1/N2C	46 ± 3	7				
N1(R645C)/N2C	61 ± 6	8	+18	N1/N2C(T640C)	60 ± 9	5
N1(E644C)/N2C	68 ± 3	8	+17	N1/N2C(D639C)	36 ± 4	7
N1(E643C)/N2C	67 ± 8	5	+16	N1/N2C(I638C)	41 ± 9	10
N1(P642C)/N2C	35 ± 1	5	+15	N1/N2C(Y637C)	41 ± 12	5
N1(R641C)/N2C	31 ± 8	8	+14	N1/N2C(Q636C)	47 ± 17	6
N1(D640C)/N2C	29 ± 4	10	+13	N1/N2C(E635C)	42 ± 8	5
N1(L639C)/N2C	46 ± 4	9	+12	N1/N2C(Q634C)	47 ± 10	4
N1(V638C)/N2C	59 ± 12	11	+11	N1/N2C(I633C)	36 ± 11	5
N1(L637C)/N2C	46 ± 3	7	+10	N1/N2C(M632C)	41 ± 11	5
N1(F636C)/N2C	57 ± 7	6	+9	N1/N2C(F631C)	38 ± 12	5
N1(A635C)/N2C	42 ± 10	6	+8	N1/N2C(A630C)	17 ± 5	7

Values shown are mean ± SEM. %change was obtained in the presence of agonist as in Figure 2.3B (with DTT replacing Cu:Phen) and with DTT applied at 1 or 4 mM. None of the values are significantly different from that seen in wild-type (ANOVA, $P < 0.05$). Relative position references the initial serine (S) in the highly conserved SYTANLAAF motif as +1 (Figure 2.3A).

Table 2.3. Distance between α-carbons for homologous positions in the S2-M4 linker in the A/C and B/D subunits in $GluA2_{cryst}$

GluA2	αCs		GluN1	GluN2A	GluN2C
	A/C	B/D			
	Å	*Å*			
K776	61.1	18.8	D	H	Q
D777	59.5	18.5	S	N	N
S778	61.8	23.5	R	E	E
G779	56.6	22.3	S	K	K
S780	51.4	13.4	N	N	N
K781	52.9	18.8	A	E	E
E782	47.2	18.4	P	V	V
K783	45.9	21.2	A	M	M
T784	40.7	24.4	T	S	S
S785	34	25.2	L	S	S
A786	31	29.6	T	Q	K
L787	29.9	28.9	F	L	L
S788	35.6	34.6	E	D	D

Shown are residues in $GluA2_{cryst}$ and homologous positions in GluN1, GluN2A or GluN2C. Positions highlighted in bold are part of the pre-M4 helix. Based on sequence alignment there are gaps in the vicinity of the pre-M4 helix in NMDA receptor subunits (See Figure 2.6A for additional details). Average distances for positions shown are 46.7 Å (A/C) and 22.9 Å (B/D).

Chapter 3 : Interaction of the M4 segment with other Transmembrane Segments is Required for Surface Expression of Mammalian AMPA Receptors

ABSTRACT

Ionotropic glutamate receptors (iGluRs) are ligand-gated ion channels with a modular structure. The ion channel itself shares structural similarity, albeit an inverted membrane topology, with P-loop channels. Like P-loop channels, prokaryotic iGluR subunits (e.g., GluR0) have two transmembrane segments. In contrast, eukaryotic iGluRs have an additional transmembrane segment (M4), located C-terminal to the ion channel core. However, the structural/functional significance of this additional transmembrane segment is poorly defined. Although topologically similar to GluR0, mammalian AMPA receptor (GluA1) subunits lacking the M4 segment do not display surface expression. This lack of expression is not due to the M4 segment serving as an anchor to the ligand-binding domain since insertion of an artificial polyleucine transmembrane segment does not rescue surface expression. Specific interactions between M4 and the ligand-binding domain are also unlikely since insertion of polyglycines into the linker connecting them has no deleterious effects on function or surface expression. On the other hand, tryptophan and cysteine scanning mutagenesis of the M4 segment, as well as recovery of function in the polyleucine background, defined a unique face of the M4 helix that is required for iGluR surface expression. In the AMPA receptor structure, this face forms intersubunit contacts with the transmembrane helices of the ion channel core (M1 and M3) from another subunit within the homotetramer. Thus, our experiments show that a highly specific interaction of the M4 segment with an adjacent subunit is required for surface expression of AMPA

receptors. This interaction may represent a mechanism for regulating AMPA receptor biogenesis.

INTRODUCTION

Fast excitatory neurotransmission in the central nervous system is primarily mediated by ionotropic glutamate receptors (iGluRs), specifically NMDA, AMPA, and kainate receptor subtypes (Dingledine, Borges et al. 1999). iGluRs are tetramers formed by four identical (homo-) or similar (hetero-) subunits. Each iGluR subunit is modular (Mayer 2006; Oswald, Ahmed et al. 2007) containing four discrete domains: an amino-terminal (NTD), a ligand-binding (LBD), a transmembrane (hydrophobic segments M1–M4) (TMD), and a carboxy-terminal (CTD) domain (Figure 3.1A, lower panel). Functionally, iGluRs also display modularity. The NTD plays a critical role in iGluR biogenesis along with modulation of receptor gating (Ayalon and Stern-Bach 2001; Gielen, Siegler Retchless et al. 2009; Yuan, Hansen et al. 2009; Hansen, Furukawa et al. 2010; Rossmann, Sukumaran et al. 2011). However, its removal has only minor effects on expression and receptor function (Pasternack, Coleman et al. 2002). Similarly, the CTD is critical for regulation of the expression, distribution and function of iGluRs (e.g., Derkach, Oh et al. 2007), but can also largely be removed while leaving basic properties intact (Suzuki, Kessler et al. 2005). The LBD (S1S2 construct) also binds glutamate independent of other domains (Arvola and Keinanen 1996). Finally, the NTD (Jin, Singh et al. 2009; Karakas, Simorowski et al. 2009; Kumar, Schuck et al. 2009) and the LBD (Armstrong, Sun et al. 1998; Sun, Olson et al. 2002; Furukawa, Singh et al. 2005; Mayer 2005) have been crystallized as soluble independent entities.

The core of the ion channel – transmembrane helix M1, the reentrant M2 loop, and transmembrane helix M3 – shares a similar membrane topology to pore loop

channels such as K^+ channels, albeit being inverted 180° in the plane of the membrane (Wo and Oswald 1995; Wood, VanDongen et al. 1995; Sobolevsky, Rosconi et al. 2009). The two-transmembrane prokaryotic iGluR subunit, GluR0, is functional and supports an evolutionary link between the K^+ and iGluR ion channels (Chen, Cui et al. 1999). In contrast, despite retaining the other modular components, truncated NMDA receptor subunits lacking the M4 segment lose functionality (Schorge and Colquhoun 2003; Horak, Chang et al. 2008). Nevertheless, the specific role of the M4 transmembrane segment remains poorly understood.

In the present study, we find that AMPA GluA1 subunits lacking the M4 segment do not express on the membrane surface, an effect not due to the absence of the CTD. Replacement of M4 in GluA1 with an artificial polyleucine transmembrane helix, as well as polyglycine-mediated decoupling of M4 from the LBD, suggests that the lack of surface expression is not due to the interaction of M4 with the LBD. Rather, tryptophan and cysteine mutagenesis scans identified residues, lining a single face of the M4 segment, that interacts specifically with the M1 and M3 transmembrane segments of an adjacent subunit (Sobolevsky, Rosconi et al. 2009). We conclude that the interaction of the M4 segment with the other transmembrane segments – rather than with the LBD – is required for receptor biogenesis in mammalian iGluRs.

MATERIALS AND METHODS

Mutagenesis and expression – Truncated AMPA receptor subunits, polyleucine substitutions, site-directed mutations, and polyglycine insertions were made in and around the M4 segment of the rat GluA1 (old GluR1) (Accession#P19490) subunit in the 'flip' form (Collingridge, Olsen et al. 2009). For expression in oocytes, we used a construct where a leucine in the ligand-binding domain was substituted with a tyrosine [GluA1(L479Y) or GluA1'] as a reference and as a background for all subsequent mutagenesis. For wild-type channels, this construct is essentially non-desensitizing (Stern-Bach, Russo et al. 1998) (see also Schmid, Korber et al. 2007). For HEK-293 cells, wild-type GluA1 was used as a background for all mutagenesis. Point mutations and insertions were generated using the QuickChange site-directed mutagenesis kit (Stratagene, La Jolla, CA) (see (Talukder, Borker et al. 2010) for additional details). Numbering of amino acids is for the mature protein (signal peptide, 18 amino acids).

The M4 segment was initially defined by hydrophobicity encompassing Val788 to Ile808 (Boulter, Hollmann et al. 1990; Keinanen, Wisden et al. 1990). However, the recent crystal structure of a GluA2 homotetramer in a closed state (bound to a competitive antagonist) identified that the M4 segment is extended by about one turn of an α-helix on each end (for GluA1, Leu785 to Asn813) (Sobolevsky, Rosconi et al. 2009). Nevertheless, our conclusions based on the core of the M4 segment (Val788 to Ile808) are valid for the entire segment.

We generated deletions of the M4 segment (and the CTD) by replacing Val788 with a stop codon (TGA) (GluA1(V788stop) referred to as GluA1-ΔM4 (or GluA1'-ΔM4 when in the non-desensitizing background). The S2-M4 linker, from the C-terminal end of S2

to the N-terminal end of M4, is present in the ΔM4 constructs. The C-terminal domain (CTD) deletion (GluA1-ΔCTD) was made by introducing a stop codon (TAA) at Ser814 (GluA1(S814stop)).

Wild-type and mutant AMPA receptor subunits were expressed in *Xenopus laevis* oocytes and/or human embryonic kidney 293 (HEK 293) cells (Sobolevsky, Beck et al. 2002; Yelshansky, Sobolevsky et al. 2004). Oocytes were treated as previously described (Sobolevsky, Beck et al. 2002) and were maintained in a nutrient OR-3 medium containing 50% L-15, 50 mg/ml penicillin-streptomycin, 5 mM glutamine, and 15 mM NaHEPES (all Gibco BRL, Grand Island, NY) (pH 7.2, NaOH) as well as in CNQX (25 mM). Unless otherwise noted, wild-type constructs including GluA1' were injected at 0.01 μg/μl with 50 to 75 nl injected per oocyte (0.5 to 0.75 ng mRNA per oocyte), whereas all mutant constructs were tested at 0.1 μg/μl (5 to 7.5 ng mRNA per oocyte) unless otherwise noted. Recordings were performed two to five days after injections. Protein harvests for immunoblots were performed two to three days after injection.

HEK 293 cells were transfected with iGluR subunits (4 μg total) using FuGene 6 (Roche, Indianapolis, IN). A vector for enhanced green fluorescent protein (pEGFP-C1, Clontech, Palo Alto, CA) was typically co-transfected at a ratio of 1:9 (pEGFP-C1:iGluR subunits). Recordings were typically made one to three days after transfection. Immunocytochemistry (ICC) and biotinylation experiments were performed two days after transfection.

Current recordings Xenopus laevis – Membrane currents in *Xenopus laevis* oocytes were recorded at room temperature (20-23°C) using a two-electrode voltage-clamp

(DAGAN TEV-200A, DAGAN Corp., Minneapolis, MN) with Cell Works software (*npi* electronic, Tamm, Germany). Microelectrodes were filled with 3 M KCl, and had resistances of 1-4 MΩ. The external solution consisted of (mM): 115 NaCl, 2.5 KCl, 0.18 $CaCl_2$, and 5 HEPES (pH 7.2, NaOH). All reagents, including glutamate (typically 1 mM), were bath applied.

Concentration-response curves were measured in *Xenopus* oocytes using GluA1' as a reference. Solutions containing various concentrations of glutamate (1.3 mM to 3 mM) were applied to cells held at –60 mV. Current amplitudes normalized to the maximal response were plotted as a function of concentration and fitted with the Hill equation, $I/I_{max} = 1/(1 + (EC_{50}/[conc])^{n})$ (Ma, Tsai et al.), where EC_{50} is the concentration to achieve half-maximal response and *n* is the Hill coefficient.

Substituted Cysteine Accessibility Method (SCAM) – AMPAR cysteine-substituted mutant channels were probed from the extracellular side of the membrane with the positively-charged methanethiosulfonate (MTS) reagent 2-(trimethylammonium)ethyl MTS (MTSET). MTSET was purchased from Toronto Research Chemicals, Inc. (Ontario, Canada) and was prepared, stored, and applied as described.

Steady-state reactions were quantified at –60 mV. Baseline agonist-activated current amplitudes (I_{pre}) were established by three to five consecutive 15 to 20 s applications of glutamate separated by 60 to 120 s washes in glutamate free solution. Subsequent to the last wash, MTSET (2 mM) was applied for 60 s in the presence of agonists. After the MTSET exposure, current amplitudes (I_{post}) were determined again using three to five agonist applications. The change in the agonist-activated current

amplitude, expressed as a percentage (*% change*), was calculated as: = (I_{post} - I_{pre}) /I_{pre} × 100.

Current recordings HEK 293 – Currents in the whole-cell mode or outside-out patches, isolated from HEK 293 cells, were recorded at room temperature (20-23°C) using an EPC-9 amplifier with Patchmaster software (HEKA Elektronik, Lambrecht, Germany), digitized at 10 kHz and low-pass filtered at 2.9 kHz (-3 dB) using an 8 pole low pass Bessel filter. Pipettes had resistances of 2-5 MΩ when filled with the pipette solution and measured in the standard Na^+ external solution. We did not use series resistance compensation nor did we correct for junction potentials.

For HEK 293 cell recordings, external solutions were applied using a piezo-driven double barrel application system. One barrel contained the external solution while the other barrel contained the same solution with added glutamate (5 mM). To optimize solution exchange for fast agonist application, we briefly treated the tips of the theta glass with hydrofluoric acid to reduce the thickness of the septum.

Our standard internal (pipette) solution consisted of (mM): 105 K-gluconate, 30 KCl, 10 HEPES, 10 phosphocreatine, 4 Mg-ATP and 0.3 GTP, pH 7.3 (KOH). The standard external solution consisted of (mM): 140 NaCl, 10 HEPES, 1.8 $CaCl_2$, and 1 $MgCl_2$, pH 7.2 (NaOH). When measuring current amplitudes, cyclothiazide (CTZ, 15 to 30 μM, stock solution in 100 mM NaOH) was added to the external solutions to minimize AMPA receptor desensitization. Unless otherwise noted, all chemicals were obtained from Sigma (St. Louis, MO) or J.T. Baker (Phillipsburg, NJ).

To determine the rate and extent of desensitization, we rapidly (< 300 msecs) applied glutamate for 100 ms at -60 mV to outside-out patches excised from HEK 293 cells. Time constants of desensitization (τ_{des}) were determined by fitting the current decay with a single exponential function. The extent of desensitization was based on the steady-state (I_{ss}) and peak (I_p) current amplitudes and calculated as the percent desensitization (*%des* = 100 × (1 – I_{ss}/I_p)).

Immunocytochemistry – HEK 293 cells were washed twice with PBS 48 hrs after transfection. Non-permeabilized cells were incubated at 37ºC with anti-(NTD)GluA1 (Calbiochem) for 30 mins, rinsed with PBS and fixed in 4% paraformaldehyde. Cells were then rinsed with PBS, blocked in 1% goat serum for 1 hr, and incubated with an Alexa Fluor® 633 goat anti-rabbit secondary antibody (Invitrogen, Carlsbad, CA). Permeabilized cells were fixed in 4% paraformaldehyde, rinsed with PBS, and permeabilized with 0.25% Triton-X 100 for 5 mins at room temperature. Permeabilized cells were then blocked and incubated with primary antibody each for 1 hr at room temperature and 37ºC, respectively. Cells were rinsed with PBS and incubated with Alexa Fluor® 633 goat anti-rabbit secondary antibody (Invitrogen, Carlsbad, CA). HA-tagged constructs were visualized by the same procedures outlined above for both non-permeabilized and permeabilized conditions using an anti-HA antibody (Y-11) (Santa Cruz Biotechnologies). Cells were examined using an upright microscope Axio Imager Z1 with an Axiocam MR3 (Carl Zeiss, Jena, Germany).

Purification of Membrane Proteins – Ten healthy oocytes were injected with 0.1 μg/μl of mRNA. Two to three days after injection, oocytes were washed in PBS containing 0.58 mM N-ethylmalemide (NEM, Pierce), homogenized in lysis buffer (20 mM Tris,

0.58 mM NEM) and centrifuged (Eppendorf Centrifuge 5417R) at 3 k RPM to separate out the yolk. The supernatant was recovered and centrifuged at 40 k RPM (Beckman TLA 120.2 rotor) for 10 mins at 4°C. The pellet was rinsed in PBS and recentrifuged at 40k RPM. The resulting pellet was resuspended and first sonicated in solubilization buffer without detergent (20 mM Tris, 50 mM NaCl, 1/1000 protease inhibitor cocktail (Sigma), 0.58 mM NEM) and then incubated with detergent (0.03% Na-Deoxycholate, 1% Triton-X100) for 1 hr at 4°C. Solubilized proteins were centrifuged at 40k RPM for 20 mins at 4°C and membrane proteins contained in the supernatant were separated by SDS-PAGE under non-reducing conditions.

Biotinylation – Forty-eight hours after transfection, HEK 293 cells were cooled on ice and washed three times with ice-cold PBS containing 0.1 mM $CaCl_2$ and 1 mM $MgCl_2$ (PBS/CM). Cells were treated with either PBS/CM (control, no biotin) or 2-5 mg/mL Sulfo-NHS-SS-Biotin (Thermo) for 45 mins on ice. Cells were then rinsed with ice-cold PBS/CM, quenched in 0.1 M Glycine PBS/CM, and pelleted in PBS/CM. Pellets were resuspended in lysis buffer (40 mM DDM dissolved in PBS containing protease inhibitors) and incubated on ice for 30 mins. The cell lysate was then centrifuged at 10,000 g for 2 mins and the supernatant was incubated with Neutravidin-Plus beads (Thermo) end-over-end for 2 hrs at room temperature. Beads were rinsed three times with PBS/CM and bound proteins were eluted by incubation with 50 mM DTT in 2X loading buffer for 1 hr at room temperature. Eluted proteins, whole-cell lysates, and unbound proteins (flow-through) were separated by SDS-PAGE under reducing conditions.

Immunoblotting – Proteins were transferred from the gel to 0.45 mm nitrocellulose membranes by semi-dry transfer (BioRad, Hercules, CA) using Bjerrum-Schaffer-Nielsen Buffer (Bjerrum and Schafer-Nielsen 1986). Blots were blocked with milk and incubated with primary antibodies overnight. The antibodies used were anti-(NTD)GluA1 [GluR1(E6) which is directed against the N-terminal domain (NTD)] (sc-13152, Santa Cruz Biotechnologies, Santa Cruz, CA), and anti-β-tubulin (Axyll, H8481, Accurate Chemical & Scientific Corporation, Westbury, NY). Blots were washed prior to incubation with HRP-conjugated goat anti-mouse (sc-2302) or HRP conjugated goat anti-rabbit (sc-2030) and were developed using luminol reagent (sc-2048, all reagents Santa Cruz Biotechnologies) before exposure to chemiluminescence Biomax Film (Kodak, Cedex, France). For biotinylation experiments, blots were probed with anti-HA (Covance) and GAPDH (Calbiochem) and visualized using the Odyssey Infrared Imaging System (Licor) with anti-mouse 800CW and 680LT secondary antibodies, respectively.

Quantification of Immunoblots – Immunoblot films were scanned using an EPSON flat scanner (Epson Perfection V700 Photo) in an 8 bit gray scale mode, 1200 dpi, reflective and quantified using NIH Image J (1.38x) on a Windows XP platform. iGluR protein levels were expressed relative to a loading control (β-tubulin). Immunoblots of biotinylated proteins were analyzed using the Odyssey software (Licor).

Statistical analysis – For statistical analysis, we used Igor Pro (WaveMetrics, Inc., Lake Oswego, OR) and Microsoft Excel (Redmond, WA). Results are reported and shown graphically as mean ± SEM. An ANOVA or a Student's t-test was used to define

statistical differences. The Tukey or Dunnet's test was used for multiple comparisons. Significance was assumed if $P < 0.05$.

RESULTS

To investigate the structural and functional significance of the M4 segment in mammalian iGluRs, we used the AMPA receptor subunit GluA1 in the 'flip' form due to its robust expression as a homomultimer in heterologous expression systems. For most functional assays, we used *Xenopus* oocytes since there is no uncertainty whether the oocyte has been injected in contrast to HEK 293 cells where transfection is uncertain even with co-transfected GFP.

AMPA receptors require the M4 transmembrane segment for surface expression – The upper panels of Figures 3.1A and 3.1B show representative membrane current recordings from *Xenopus* oocytes injected with mRNA for the non-desensitizing AMPA receptor subunit GluA1' and GluA1'-ΔM4. The predicted membrane topology of GluA1' and GluA1'-ΔM4 is shown in the lower panels of Figures 3.1A and 3.1B. Oocytes injected with GluA1' mRNA show robust glutamate-activated current amplitudes, typically on the order of several μAs (Table 3.1). Similarly, HEK 293 cells transfected with wild-type GluA1 and recorded in cyclothiazide (CTZ) displayed large glutamate-activated currents (Table 3.1). In contrast, GluA1 subunits lacking the M4 transmembrane segment, as well as the C-terminal domain (CTD), did not show any detectable glutamate-activated currents in *Xenopus* oocytes (non-desensitizing background) (Figure 3.1B) or in HEK 293 cells (wild-type background) (Table 3.1). Stargazin (γ2), the canonical member of transmembrane AMPAR related proteins (TARPs), increases surface expression of AMPA receptors (e.g., Tomita, Adesnik et al. 2005), but co-expression of the GluA1-ΔM4 construct with Stargazin in HEK 293 cells did not rescue glutamate-activated currents (Table 3.1).

Immunoblots of whole cell lysates from oocytes expressing GluA1' or GluA1'-ΔM4 show protein expression at the expected relative sizes (GluA1', 110 kDa; GluA1'-ΔM4, 90 kDa) (Figure 3.1C). Quantification of protein expression (see Experimental Procedures) in *Xenopus* oocytes showed that both GluA1' and GluA1'-ΔM4 are expressed at similar levels, which were significantly greater than background (DEPC-injected oocytes) (Figure 3.1D). Hence, the absence of functional agonist-induced currents for the ΔM4 construct is not a result of lack of translation or ubiquitous protein degradation.

The lack of detectable membrane currents but the presence of protein expression by immunoblots suggests that the ΔM4 constructs are synthesized, however we cannot eliminate the possibility that the ΔM4 construct is expressed at the cell surface, but is not functional. Therefore, we used biotinylation and immunocytochemistry (ICC) to distinguish whether the lack of detectable glutamate-activated currents was a result of a biogenesis versus a gating defect. Although mutants in the non-desensitizing background (L479Y) show functional currents, previous evidence has shown that the L479Y mutation attenuates GluA2 tetramer formation (Shanks, Maruo et al. 2010). We therefore tested for surface expression of wild type GluA1 constructs in HEK 293 cells using biotinylation (Figures 3.1E & 3.1F) and ICC (Figures 3.1G & 3.1H). Biotinylation of cell surface proteins showed that wild-type GluA1, but not GluA1-ΔM4 (Figures 3.1E, lower panel & 3.1F) was expressed at the cell surface. Quantification of the biotinylated signal of GluA1-ΔM4 was not statistically different than that of controls (Figure 3.1F) suggesting that the GluA1-ΔM4 is not trafficked to the membrane. Further, immunocytochemistry of wild-type GluA1 showed prominent surface expression (Non-

Permeabilized images, Figure 3.1G), whereas, the GluA1-ΔM4 construct showed no detectable surface expression (Non-Permeabilized images, Figure 3.1H), though the protein was expressed robustly (Permeabilized images, Figure 3.1H). Identical results were found using HA-tagged GluA1 and GluA1-ΔM4 constructs (data not shown).

The ΔM4 construct lacks not only the M4 segment but also the CTD (Figure 3.1B, lower panel), an element that is critical for regulating iGluR expression (e.g., Derkach, Oh et al. 2007). Partial deletion of the CTD in GluA1 (removal of last 52 amino acids of 77 total), leaving 25 amino acids after M4 including a PKA binding site, has little effect on its expression or function (Suzuki, Kessler et al. 2005). To verify further that the absence of the CTD in the ΔM4 construct does not underlie the lack of surface expression, we generated a construct in which even more of the CTD was deleted, placing a stop codon at position 814 (GluA1'-ΔCTD or GluA1-ΔCTD) (removal of 77 amino acids of CTD) corresponding to the polar clamp of the M4 transmembrane helix (Sobolevsky, Rosconi et al. 2009). The amplitude of glutamate-activated currents for GluA1'-ΔCTD (Figures 3.2A & 3.2B) as well as general gating properties such as concentration-response curves (Figures 3.2C & 3.2D; Table 3.1) and rates of entry into desensitization (Table 3.1) were indistinguishable from wild-type. Thus, while the CTD is critical for modulating iGluR trafficking (Derkach, Oh et al. 2007; Traynelis, Wollmuth et al. 2010), its absence does not underlie the lack of surface expression for the ΔM4 constructs (Figure 3.1).

The interaction of the M4 segment with the LBD does not appear critical to its function – Previous experiments have indicated that the ability of the LBD to bind glutamate is a key component of iGluR biogenesis (Mah, Cornell et al. 2005; Valluru, Xu

et al. 2005; Penn, Williams et al. 2008; Gill, Vivithanaporn et al. 2009). The M4 segment is coupled to helix K in Domain 1 of the LBD via the S2-M4 linker. Helix J, just N-terminal to helix K, is a critical component of the LBD dimer interaction whose stability is key to receptor gating (Sun, Olson et al. 2002; Horning and Mayer 2004). Therefore, one potential role of the M4 segment in iGluRs may be to act simply as a membrane spanning element that serves as an additional anchor (along with M1 and M3) to the LBD permitting agonist binding. To test this idea, we replaced the membrane spanning portion of the M4 segment in GluA1 with polyleucines (21 residues). Such polyleucine (pLeu) stretches are frequently used as model transmembrane helices (e.g., Zhou, Merianos et al. 2001; Caputo and London 2004) since they form spontaneous, stable α-helices and insert naturally into membranes. To avoid any potential helix-helix interactions, we did not use a polyalanine transmembrane segment.

When the M4 segment was replaced with polyleucines (GluA1'-M4^{pLeu}) (Figure 3.3A), we did not observe any detectable glutamate-activated currents in either oocytes (right panel, Figure 3.3B) or HEK 293 cells (data not shown). Like the ΔM4 construct, whole-cell lysates of the pLeu construct showed robust protein expression (Figures 3.3C & 3.3D), but no detectable surface expression as visualized by immunocytochemistry (Figure 3.3E). Thus, a polyleucine transmembrane helix that presumably mimics the membrane spanning property of M4, while lacking any helical interaction motifs, does not yield functional receptors. This suggests that specific residues within the M4 segment are essential to its function.

As an additional test of whether the connection between M4 and the LBD is critical to iGluR function, we inserted up to eight glycine residues in the S2-M4 linker coupling

the M4 segment to the LBD (Figure 3.4A). Glycine, a small amino acid that lacks a side chain, is a strong helix breaker for soluble proteins. Thus, stretches of polyglycines will introduce flexibility and also lengthen the linker, effectively decoupling the LBD from the M4 segment while retaining the native membrane spanning segment. Hence, if specific interactions between M4 and the LBD are important to AMPA receptor function, we anticipate that the addition of these glycines to the S2-M4 linker should produce a phenotype comparable to ΔM4 constructs – either poor or no surface expression and subsequent deficits in agonist-induced current amplitudes.

As shown in Figures 3.4B and 3.4C, receptors containing introduced glycines still showed significant glutamate-activated current amplitudes, considerably different from the non-expressing ΔM4 construct. The additional glycines also had no notable effect on glutamate sensitivity (Figure 3.4D), nor desensitization or activation gating within the time constraints of our exchange system (Figures 3.4E & 3.4F). These results further support the idea that the interaction of the M4 transmembrane segment with the LBD does not play a significant role in the M4-mediated surface expression deficits in AMPA receptors.

One potential complication of these experiments is that introduced polyglycines were inserted N-terminal to a conserved cysteine residue (C769) known to form a disulfide bond that stabilizes the LBD (Armstrong, Sun et al. 1998). Hence if this endogenous disulfide bond is intact in the polyglycine-substituted receptors, then it may prevent the introduced glycines from having their desired effect, namely decoupling the LBD from the M4 segment through lengthening the distance of S2 from the M4 segment. DTT, a reducing agent, significantly potentiates current amplitudes in wild-

type GluA1 (40 ± 1%, n = 3) in the presence of CTZ (data not shown) expressed in *Xenopus* oocytes, consistent with this disulfide bond being intact. In contrast, for GluA1' S2-M4^{8G}, DTT had no effect on current amplitudes (0 ± 2%, n = 3) (data not shown), suggesting that the disulfide bond is no longer intact. These results suggest that since the disulfide bond is not intact, the polyglycines are not simply "looped out" out of the LBD, but rather perturb the linker joining the LBD to the M4 segment and decouple the LBD from the M4 segment.

A tryptophan mutagenesis scan reveals a putative interacting face of the M4 segment – The results presented so far argue that the interaction of M4 with the LBD is not required for surface expression. The recent crystal structure of a homomeric AMPA receptor (Sobolevsky, Rosconi et al. 2009) indicates a strong interaction of M4 with transmembrane segments M1 and M3 in an adjacent subunit. Thus, the interaction of the M4 segment with other transmembrane segments may be critical for surface expression. To test this hypothesis and to identify specific residues integral to surface expression, we carried out a site-directed mutagenesis scan of the GluA1 M4 segment. We substituted each individual position with tryptophan (W) and compared glutamate-activated current amplitudes from these mutant channels to that of wild-type. Tryptophan has a bulky, hydrophobic side chain that is well tolerated in a lipid environment but can disrupt points of helix-helix interactions (Liu, Eilers et al. 2004; Moore, Berger et al. 2008). Hence, we anticipated that if transmembrane helix interactions are important for receptor function, then tryptophan substitutions at positions located at such interfaces should disrupt surface expression.

Figure 3.5A shows representative glutamate-activated currents in *Xenopus* oocytes for GluA1' as well as three tryptophan-substituted receptors (G790W, V805W, or A806W). Figure 3.5B summarizes current amplitudes, normalized to those for GluA1', for the tryptophan-substituted receptors. Many of the mutant receptors showed robust glutamate-activated current amplitudes on the same order of magnitude as wild-type. On the other hand, many positions showed no detectable glutamate-activated current (demarcated by an 'X') like that of the ΔM4 construct (V791W, L795W, G798W, A802W, E809W) or greatly reduced current amplitudes (N787W, V788W, A789W, G790W, F792W, I794W, V805W) (Figure 3.5B; Table 3.2). These tryptophan-substituted receptors that had no detectable or greatly reduced (<0.1 of wild-type) glutamate-activated current amplitudes showed protein expression (Figures 3.5C & 3.5D, respectively).

Figure 3.5E (*left panel*) plots the results for *Xenopus* oocytes from Figure 3.5B onto a helical net. All positions tested are shown in this plot with those showing no detectable glutamate-activated current highlighted in red and those showing greatly reduced current amplitudes (<0.1 of wild-type) highlighted in blue. Notable is that the colored positions – especially those that yield no detectable current – fall on one face of a canonical α-helix, extending from the N-terminal end (N787) to the C-terminal end (E809). Figure 3.5F shows the GluA2 M4 segment from an AMPA receptor structure (Sobolevsky, Rosconi et al. 2009) with only the positions that showed significant reductions in glutamate-activated current amplitudes highlighted in the same color scheme as in Figure 3.5E. Clearly, those positions that showed significant effects on glutamate-activated currents were positioned on one side of the M4 segment.

Because the L479Y mutation attenuates GluA2 tetramer formation (Shanks, Maruo et al. 2010), we performed parallel experiments in HEK 293 cells in which the current amplitudes of tryptophan-substituted receptors in the wild-type GluA1 background were recorded using CTZ. The pattern of functional and non-functional mutants in oocytes (non-desensitizing background) and HEK 293 cells (wild-type background) were nearly identical (Table 3.2; summarized in Figure 3.5E, *right panel*) with the exception being that in HEK 293 cells, A789W showed robust currents and more positions showed no detectable current. This may be an effect of limited sampling or may represent a more restrictive nature of iGluR biogenesis in HEK 293 cells since all of the new positions in HEK 293 cells without detectable currents (V788, G790, I794, V805) had extremely small currents and/or were inconsistently detected in oocytes. Nevertheless, these results strongly support the idea that this interacting face is common in all expression systems and is not dependent on the non-desensitizing background.

In summary, the tryptophan scan of the M4 segment identified a specific face of M4 segment that strongly disrupts receptor expression. As will be discussed in the Discussion, this face – especially those positions that showed no glutamate-activated current (highlighted in red in Figure 3.5E) – interacts specifically with the core of the ion channel (M1 and M3) of adjacent subunits.

Tryptophan-substituted receptors that do not show glutamate-activated currents are not expressed at the membrane – To verify that the absence of membrane currents in cells expressing tryptophan-substituted receptors coincided with a lack of surface expression, we used immunocytochemistry (Figure 3.6) focusing mainly on those tryptophan-substituted receptors that did not show glutamate-activated currents in

Xenopus oocytes (V791W, L795W, G798W, A802W, and E809W) as well as G790W that showed no detectable glutamate-activated current in HEK 293 cells (Table 3.2). Immunocytochemical analysis showed that these non-functional receptors, generated in the wild-type background, could not be detected at the cell surface (Figure 3.6) (*left*, Non-permeabilized), but were present intracellularly (*right*, Permeabilized). Furthermore, tryptophan-substituted mutants that showed similar current amplitudes as wild-type (e.g., G797W) also showed strong surface expression (Figure 3.6, *left*). Thus, these results further support the hypothesis that specific interactions along the interface of the M4 segment with that of the other transmembrane domains are critical for AMPA receptor surface expression.

A cysteine mutagenesis scan highlights the interacting face – The tryptophan scan identified a face of the M4 segment that when substituted with tryptophan showed greatly reduced surface expression. To further verify this point, we carried out a cysteine scan of the GluA1' M4 segment. Since cysteine is a smaller residue than tryptophan, it should have less dramatic effects on receptor surface expression.

Figure 3.7A (left panel) summarizes normalized current amplitudes for wild-type and cysteine-substituted GluA1 subunits. Many of the cysteine-substituted receptors showed current amplitudes comparable to control, but a subset of positions showed either no detectable glutamate-activated current ('X') or greatly reduced current amplitude (<0.3 of control) (Figure 3.7B). These positions that showed significant decreases in current amplitude, with the exception of Y793 that was unaffected in the tryptophan-scan, were a subset of those positions affected in the tryptophan scan.

These results are therefore consistent with the idea that there is a specific interacting face required for surface expression in AMPA receptors.

We also took advantage of the substituted cysteines to look at the water accessibility of the different positions using methanethiolsulfonate (MTS) reagents (Figure 3.7A, right panel). Only one position tested, N787, showed a significant effect of the positively charged MTSET. Although we cannot rule out the possibility of silent reactions (the MTS reagents reacts with a position but has no functional effect), these results argue that there are no water filled cavities around the M4 segment consistent with the idea that it interacts strongly with other transmembrane segments.

Restoration of function in the polyleucine background – Given the observation that certain residues are necessary for receptor surface expression (Figures 3.5, 3.6 & 3.7), we wanted to consider the opposite scenario – the minimum number of these key residues required to restore surface expression in a non-expressing background. Hence, starting with the non-expressing polyleucine construct as a background (Figure 3.3), we systematically re-introduced key residues to identify the minimum number needed to restore surface expression as assayed by glutamate-activated currents (Figure 3.8).

Figure 3.8A aligns the core of the GluA1 M4 segment with sequence alignments of conserved residues within non-NMDA (*upper panel*) and NMDA (*lower panel*) receptor subunits. Across all subtypes, 16 of 23 residues were similar in identity and three positions (G790, F792, and E809) were fully conserved (Figure 3.8A). Of these 16 positions, 14 of them (out of 14 total) when substituted with tryptophan yielded poor or no surface expression (Figure 3.5). When the most conserved positions in the M4

segments, G790 and F792 in GluA1 (demarcated by dark gray boxes in Figure 3.8A) were reintroduced into the M4 polyleucine background (GluA1'-M4$^{pLeu(GF)}$), they did not restore glutamate-activated currents (raw data not shown) (note that E809 was present in GluA1'-M4^{pLeu}). Reintroducing a number of other conserved residues (e.g., G798, A802) in a stepwise fashion also did not yield functional receptors. Function, albeit small in amplitude, was restored only when a cluster of residues were converted back to their native conformation (L790G/L791V/L792F/L798G/L802A/L805V; note a conserved leucine, L795 (red position, Figure 3.5E), is already present in the polyleucine background) (Figures 3.8B & 3.8C). A slightly different combination starting with the addition of V788 (VGVFGAV) yielded a comparable outcome (Figure 3.8C).

Figure 3.8D highlights the distribution of those positions necessary to recover function in the M4 polyleucine background on the M4 segment from the GluA2 structure. These results are consistent with the idea that an interacting face in the M4 transmembrane segment is critical to iGluR surface expression. In addition, they suggest that it is this interacting face, rather than a single side chain, that underlies this functional action.

DISCUSSION

Mammalian iGluRs like their prokaryotic relative (GluR0) share a common ion channel core structure (M1-M3) with two-transmembrane K^+ channels, albeit inverted 180° in the plane of the membrane. Yet what distinguishes mammalian iGluRs and perhaps all eukaryotic iGluRs (Janovjak, Sandoz et al. 2011) from GluR0 is the presence of an additional transmembrane segment, the M4 segment that connects the highly regulated C-terminal domain (CTD) to the core of the ion channel. GluR0 forms fully functional tetrameric receptors without the presence of the additional M4 segment (Chen, Cui et al. 1999) (unpublished data). In the present study, we investigated the role of the M4 transmembrane segment in AMPA receptor function. Using a truncated GluA1 construct, we show that the M4 transmembrane segment is necessary for surface expression. Through the use of single amino-acid tryptophan- and cysteine-substitutions, we find that a specific face along the M4 α-helix is critical for iGluR function. In the AMPA receptor structure, the M4 transmembrane segments are associated with the core of the ion channel (M1-M3) of an adjacent subunit (Sobolevsky, Rosconi et al. 2009), and our functionally-defined interacting face aligns extremely well with the adjacent subunit (Figure 3.9). We conclude that in addition to linking the highly regulated CTD to the core of the ion channel, the M4 segment itself is involved in some way in receptor biogenesis. Our experiments however do not address what specific biogenic process the M4 segment is required for.

Interaction of M4 with other transmembrane segments is required for efficient surface expression – Our results demonstrate the significance of the M4 segment to the function of mammalian iGluRs and delineate, at least at an initial level, the basis for this.

Specifically, we find that an interaction amongst the M4 transmembrane segment and the other transmembrane elements, either M1 and/or M3, is required for iGluR function. Various lines of evidence support this idea. First, both deletion (Figure 3.1) and substitution of the M4 segment with an inert polyleucine membrane-spanning segment (Figure 3.3) results in the loss of surface iGluR expression, an effect not dependent on the CTD (Figure 3.2). A tryptophan mutagenesis scan revealed a distinct pattern of positions (highlighted in Figures 3.5E & 3.5F) that disrupt function. Here red positions – positions that show no glutamate-activated current – line one face of the M4 transmembrane helix. Strategic reintroduction of a series of residues along this face in the non-functioning polyleucine background results in functional/surface expressed channels (Figure 3.8). Finally, our data indicating an interacting face of the M4 segment is required for iGluR function is strengthened by the GluA2 crystal structure (Sobolevsky, Rosconi et al. 2009). Specifically, the functionally-defined interacting face is strongly aligned with portions of the M1 and M3 transmembrane segments of an adjacent subunit with positions showing no effect typically located on the portion of the helix in contact with the lipid interface (Figure 3.9; Table 3.3). However, further experiments are required to identify the specific residues within the M1/M3 transmembrane helices that interact along the face of the M4 segment and are critical to receptor function.

One alternative explanation for the role of the M4 segment is that it is required for the proper functioning of the ligand-binding domain (LBD). We believe that this alternative is unlikely since decoupling of the LBD from M4 has no notable effect on receptor function (Figure 3.4). Similarly, an artificial polyleucine transmembrane

domain, that replicates the membrane spanning aspect of M4 (Figure 3.3), but not specific interactions, does not restore channel function. Presumably, this polyleucine transmembrane domain should function like M4 and anchor the LBD. Coupled together, these data suggest that it is specific residues within the M4 segment that are important for iGluR function, rather than serving as a physical link between M4 and the LBD.

All available evidence indicates that an interaction of the M4 segment with the other transmembrane segments is essential for surface expression. Nevertheless, the M4 segment may also contribute in some form to receptor gating (Ren, Honse et al. 2003; Ren, Salous et al. 2008) and/or interactions with TARPs (Terhag, Gottschling et al. 2010). Indeed, for those tryptophan-substituted receptors that did show reduced, albeit measurable currents, we often saw a small shift in the glutamate EC_{50} (Table 3.2). Presumably, this may reflect an alteration in the positioning and dynamics of M4 with other transmembrane segments such as the M3 transmembrane helix – the major pore-lining gating domain. In fact, the M3 transmembrane segment interacts most strongly with M4 (Table 3.3). Thus, mutations in M4 may not directly influence the LBD by the S2-M4 linker, but rather indirectly alter the LBD dynamics and gating via the associated M3 segment and hence the M3-S2 linker.

Helical interactions – Specific transmembrane packing interactions are critical determinants of the folding, stability, and function of membrane proteins including ion channels (Moore, Berger et al. 2008). These interacting faces often display specific amino acid side chains or even unique sequence motifs that facilitate such interactions. At the core of this interacting face of the M4 segment is a GxxxG-like sequence (G798xxxA802). GxxxG motifs, in which two amino acids with small side chains,

typically glycine but also alanine or serine are separated by 3 amino acids, are well-known to be located at points of transmembrane helix-helix interactions (Russ and Engelman 2000; Senes, Engel et al. 2004; Moore, Berger et al. 2008). Substitution of either G798 or A802 with tryptophan and/or cysteine resulted in loss of function (Figures 3.5B & 3.7A).

Deletion of the M4 segment does not interrupt early stages of iGluR biogenesis – Biogenesis of iGluRs – the biosynthesis, folding, oligomerization, and trafficking of receptors to the membrane – requires many synchronized interactions to yield surface expressed/functional ion channels (Greger, Ziff et al. 2007; Traynelis, Wollmuth et al. 2010; Farina, Blain et al. 2011). Our results suggest that the interaction of the M4 segment with other transmembrane segments affects one or more of these biogenesis steps. Lack of protein biosynthesis is unlikely since immunoblots of whole membrane lysates demonstrate protein production at the expected size (Figures 3.1C & D, 3.5C & D). Further, protein expression was detected in permeabilized conditions for ΔM4 (Figure 3.1H) and for non-functional single amino-acid substitutions (Figure 3.6). On the other hand, these mutations could disrupt protein folding. However, we believe this alternative is unlikely for a variety of reasons. Multi-domain proteins including ion channels are highly modular (e.g., Alabi, Bahamonde et al. 2007). iGluR subunits are also largely modular (see Introduction) and truncation of the M4 segment (ΔM4 construct) yields a subunit with a topology like the functional GluR0. Finally, single tryptophan or cysteine substitutions yield a phenotype like ΔM4 and these substitutions largely line a single side of a helix, one that interacts specifically with other transmembrane segments (Figure 3.9). Although substitution with a large amino acid

like tryptophan might disrupt folding for some of these positions it seems highly unusual that it would occur for a single side of a transmembrane segment and that it would occur also for the smaller cysteine side chain (Figure 3.7B). Nevertheless, specific experiments will be needed to fully address the question of whether membrane folding is disrupted.

One intriguing possibility is that the M4 segment is involved in the oligomerization of iGluR subunits to form tetramers. In the AMPA receptor crystal structure, the M4 of one subunit is associated with the core of the ion channel (M1-M3) of an adjacent subunit (Sobolevsky, Rosconi et al. 2009), and the identified interacting face is strongly aligned with M1 and M3 of an adjacent subunit (Figure 3.9). Thus, it is plausible that the M4 segment might be involved in the assembly and/or oligomerization of iGluRs via either the stabilization of dimers and/or tetramerization of functional receptors. Alternatively, the M4 may function to mask an unidentified retention signal (Horak, Chang et al. 2008), which would provide support for a role in the trafficking of receptors. Further studies must be performed to discern the precise mechanistic role of the M4 segment in iGluR biogenesis.

Perturbations of M4 as a pathway for modulation of receptor trafficking – Modulation of iGluR function is critical in regulating synaptic activity including plasticity (Derkach, Oh et al. 2007) and can occur by a variety of means such as phosphorylation, membrane phospholipid composition, auxiliary subunits and post-synaptic density proteins many of which interact with the CTD. At present, the molecular mechanism by which these agents act remains largely undefined. Although speculative, perturbations in the orientation of M4 relative to other transmembrane segments in the plane of the

membrane possibly driven by modification of the CTD or interactions with TARPs (Terhag, Gottschling et al. 2010) could represent one such mechanism. Nevertheless, specific experiments will be needed to address any potential role for the positioning of M4 as a regulatory mechanism of iGluR biogenesis.

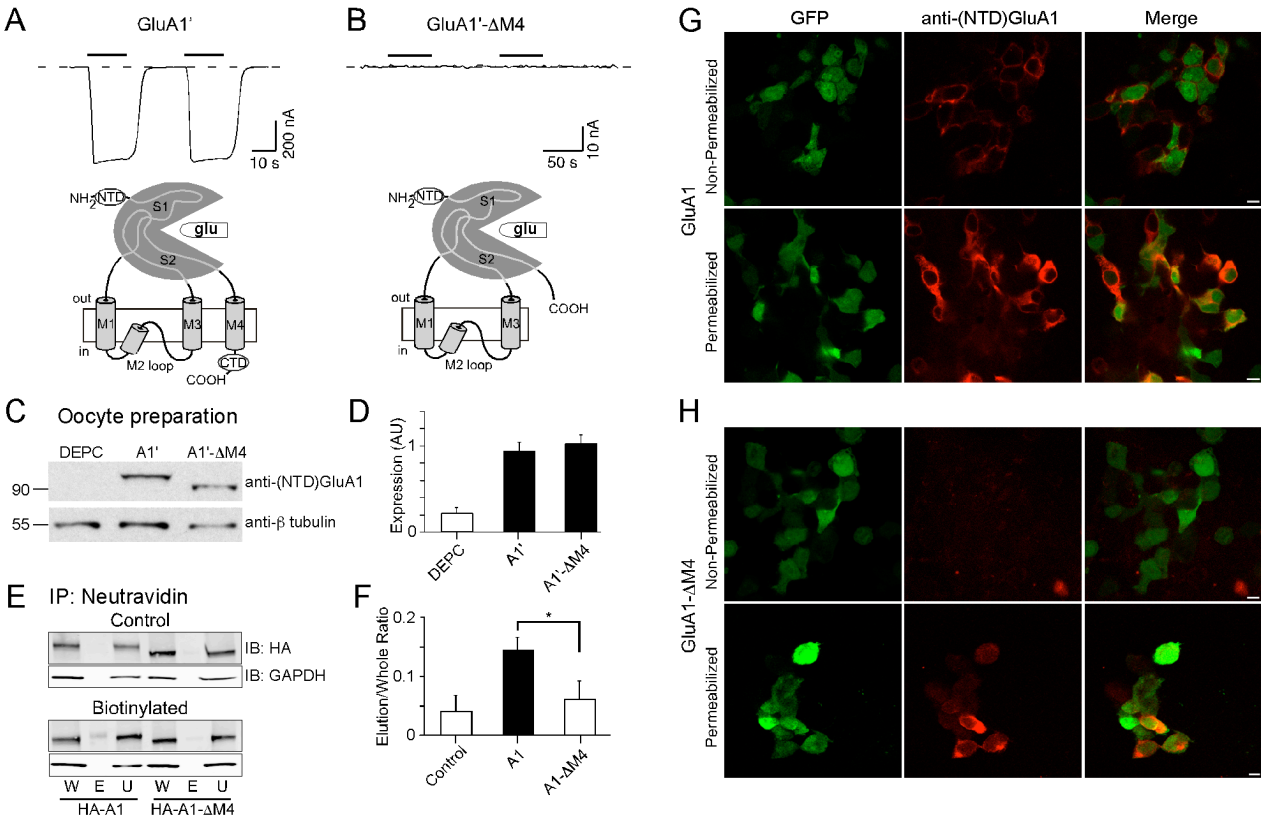

FIGURE 3.1. GluA1 subunits lacking the M4 transmembrane segment are not expressed at the membrane surface.

(A & B) *Upper panels*, Whole-cell currents recorded in *Xenopus* oocytes injected with wild-type or mutant mRNA based on a non-desensitizing form (L479Y) of the $GluA1_{(flip)}$ subunit (GluA1') (see Methods). Dashed lines indicate zero current (thick solid lines, 1 mM glutamate, 15 to 60 secs in duration). Holding potential (V_h) was –60 mV. *Lower panels*, Schematics of presumed membrane topology of individual subunits of injected mRNA: (A) GluA1' and (B) GluA1' with a stop codon introduced near the start of M4 (GluA1'-ΔM4).

(C) Immunoblot of a whole cell lysate preparation from *Xenopus* oocytes injected with either DEPC water (DEPC), GluA1' (A1') or GluA1'-ΔM4 (ΔM4) mRNA. Protein expression was visualized using antibodies against the N-terminus of GluA1 (anti-(NTD)GluA1) (*upper band*) or β-tubulin (*lower band*). Predicted molecular weight of GluA1' and ΔM4 are 110 and 90 kDa, respectively. Slight differences in the observed molecular weights presumably reflect different glycosylation or other post-translational modifications.

(D) Quantification of protein expression of GluA1' subunits in whole-cell oocyte lysates (C) relative to endogenous β-tubulin (see Experimental Procedures). Values shown are mean ± SEM (n > 7 for each). Solid bars indicate values significantly different from DEPC injected control ($P < 0.05$).

(E) Biotinylation of cell surface protein expression of HEK 293 cells transfected with either HA-GluA1 (HA-A1) or HA-GluA1-ΔM4 (HA-A1-ΔM4). Cells were treated with either PBS-CM (control) (*top*) or 2-5 mg/mL Sulfo-NHS-SS-Biotin (Thermo) (*lower*) and immunoprecipitated with Neutravidin-Plus beads. Protein expression was visualized using antibodies against the hemagglutinin (HA) tag (Covance) or the intracellular protein GAPDH for the whole-cell (W), elution (cell surface) (E), and unbound (flow-through) (U) fractions.

(F) Quantification of the biotinylated signal for the elution/whole-cell fractions of control, HA-GluA1 (A1), and HA-GluA1-ΔM4 (A1-ΔM4). Values shown are mean ± SEM (n = 5 for each). Solid bars indicate values significantly different from control ($P < 0.05$). An asterisk indicates values significantly different from wild-type GluA1 ($P < 0.05$).

(G & H) Immunocytochemistry of HEK 293 cells transfected with either GluA1 (G) or GluA1-ΔM4 (H) cDNA, both in the wild-type background. Non-permeabilized (*upper panels*) or permeabilized (*lower panels*) cells were labeled with an Alexa-633 secondary antibody. We could not detect any surface expression (Non-permeabilized condition) for GluA1-ΔM4. Scale bars represent 10 microns.

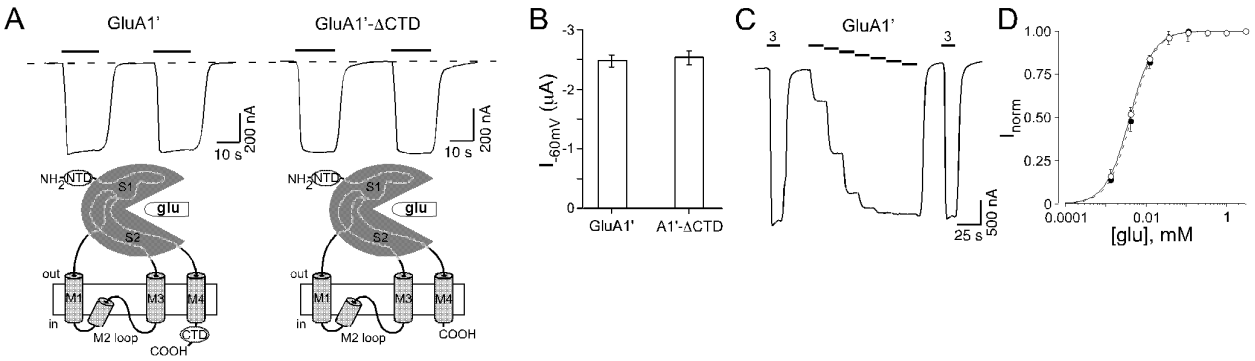

FIGURE 3.2. Removal of the C-terminal domain has no notable effect on AMPA receptor expression or function.

(A) *Upper panels*, Whole-cell currents recorded in *Xenopus* oocytes injected with mRNA for GluA1' or GluA1'-ΔCTD. *Lower panels*, Schematics of presumed membrane topology of individual subunits encoded by injected mRNA: GluA1' and GluA1'-ΔCTD.

(B) Mean current amplitudes (± SEM) for GluA1' or GluA1'-ΔCTD (n > 10).

(C) Whole-cell currents recorded in a *Xenopus* oocyte injected with GluA1'. Glutamate applications (solid bars) were at 3 mM (outer solid lines) or between 0.0013 and 1 mM (staggered lines).

(D) Concentration-response curves for GluA1' (*open circles*) or GluA1'-ΔCTD (*solid circles*). Current amplitudes, as in (C), were normalized to those in 3 mM glutamate. Points were fit with the Hill equation (see Experimental Procedure) yielding EC_{50}s (in mM) and Hill coefficients of 4.5 ± 0.3 & 1.5 ± 0.1 (mean ± SEM) for GluA1' (n = 5) and 4.6 ± 0.3 & 1.5 ± 0.1 for GluA1'-ΔCTD (n = 4).

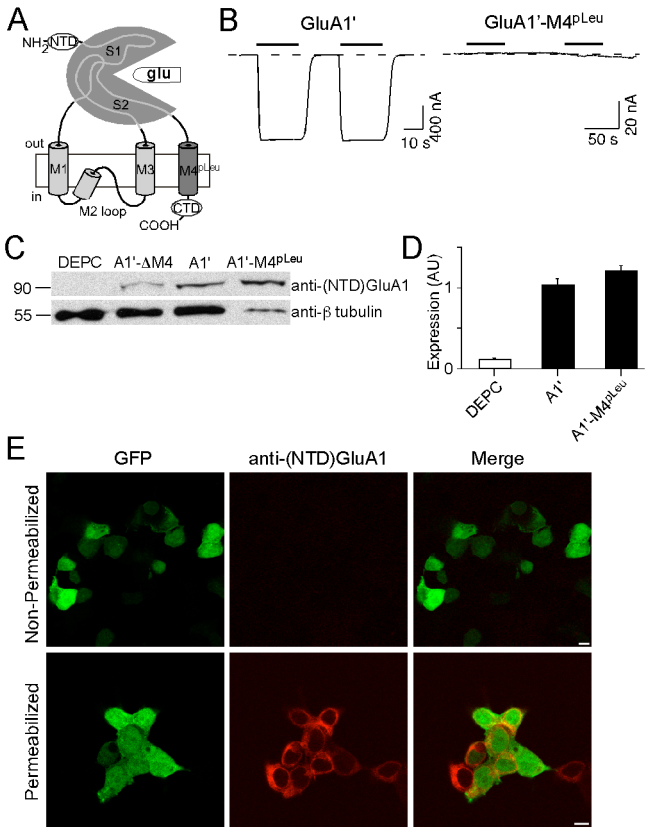

FIGURE 3.3. An artificial transmembrane α-helix substituted for the M4 segment does not restore surface expression.

(A) Presumed membrane topology of a construct where the core of the GluA1' M4 segment (V788 to I808) was replaced with leucines (21 total) (GluA1'-M4^{pLeu}). Stretches of leucine residues (polyleucines) are used as artificial transmembrane α-helices (Zhou, Merianos et al. 2001).

(B) Whole-cell currents recorded in *Xenopus* oocytes injected with GluA1' (*left*) or GluA1'-M4^{pLeu} (*right*). Glutamate-activated current could not be detected in oocytes injected with GluA1'-M4^{pLeu} (n > 20).

(C) Immunoblot of GluA1' or GluA1'-M4^{pLeu} probed with anti-NTD GluA1 (*upper panel*) or anti-β-tubulin (*lower panel*).

(D) Quantification of surface expression, relative to endogenous β-tubulin (*lower panel*), as in Figure 1D. The values for A1' and A1'-M4^{pLeu} were not significantly different ($P < 0.05$).

(E) Immunocytochemistry of HEK 293 cells transfected with GluA1-M4^{pLeu}. No surface expression could be detected for GluA1-M4^{pLeu} (Non-permeabilized condition). See Figures 3.1G & 3.1H for details.

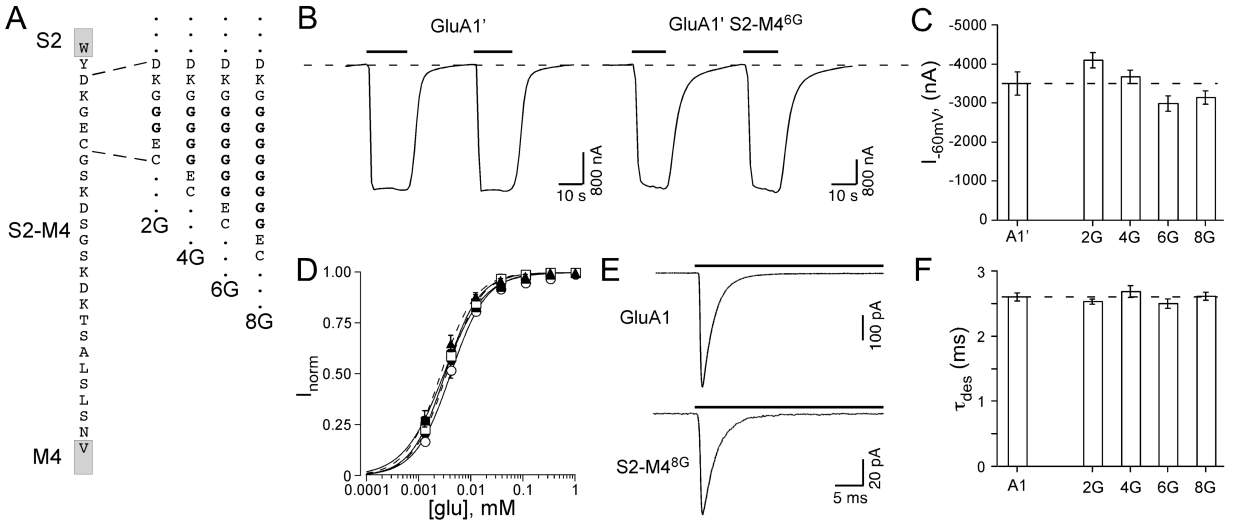

FIGURE 3.4. Addition of polyglycines to the S2-M4 linker has no notable effect on receptor function.

(A) Schematic indicating the sites of glycine (G) insertions (2-8) in the S2-M4 linker in the GluA1' or GluA1 background.

(B) Representative whole-cell currents recorded from *Xenopus* oocytes injected with GluA1' or GluA1' S2-M4^{6G}.

(C) Mean current amplitudes (± SEM) of whole cell glutamate-activated currents recorded in wild-type GluA1' or GluA1' with inserted glycines in S2-M4. All constructs were injected at ~0.5-0.75 ng mRNA. None of the values were significantly different from that for GluA1' ($P < 0.05$)

(D) Concentration-response curves for GluA1' (*open circles*), GluA1' S2-M4^{2G} (*solid circles*), GluA1' S2-M4^{4G} (*solid squares*), GluA1' S2-M4^{6G} (*open squares*), or GluA1' S2-M4^{8G} (*solid triangles*). Points were fit with the Hill equation (see Experimental Procedure) yielding EC_{50}s and Hill coefficients of 4.1 ± 0.2 mM & 1.4 ± 0.1 for GluA1' (n = 7); 3.5 ± 0.2 mM & 1.5 ± 0.1 for S2-M4^{2G} (n = 5); 3.1 ± 0.2 mM & 1.2 ± 0.1 for S2-M4^{4G} (n = 7); 3.2 ± 0.3 mM & 1.5 ± 0.1 for S2-M4^{6G} (n = 4); and 2.7 ± 0.2 mM & 1.4 ± 0.1 for S2-M4^{8G} (n = 5).

(E) Currents recorded from outside-out patches, isolated from HEK 293 cells, expressing GluA1 or GluA1 S2-M4^{8G}. Solid bar indicates the time of the fast glutamate application (3 mM) (see Experimental Procedures). Holding potential was –60 mV.

(F) Mean values for the entry into desensitization (± SEM) for GluA1 or S2-M4 polyglycine-inserted GluA1 subunits.

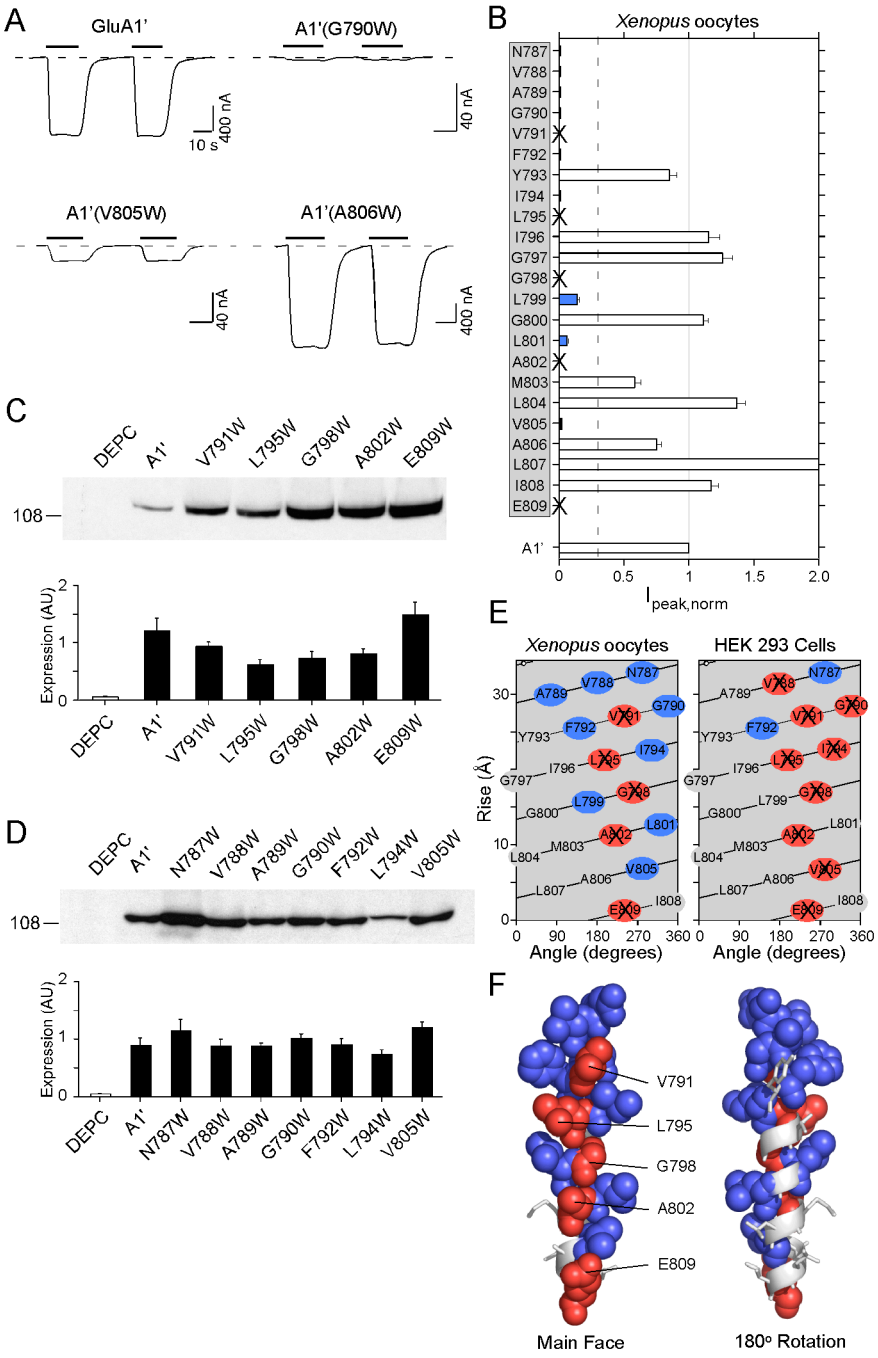

FIGURE 3.5. Tryptophan mutagenesis scan of residues in the M4 segment.

(A) Representative whole-cell currents recorded from *Xenopus* oocytes injected with GluA1', GluA1'(G790W), GluA1'(V805W) or GluA1'(A806W).

(B) Mean current amplitudes (± SEM) at –60 mV and in 1 mM glutamate normalized to those obtained GluA1' injected and recorded during the same cycle for tryptophan substitutions (n > 7). GluA1' current amplitudes were -2120 ± 39 nA (n = 32). Positions that did not show detectable glutamate-activated currents are demarcated by an 'X'. Positions that showed current amplitudes <0.3 of wild-type are colored blue.

(C & D) Immunoblots of oocytes membranes injected either with DEPC water (DEPC), GluA1', or various tryptophan-substituted GluA1' receptors either those that showed no glutamate-activated current (C) or very low levels of current (< 0.3 of wild-type) (D).

(E) Helical net representation of the results for *Xenopus* oocytes (non-desensitizing background) (B) or HEK 293 cells (wild-type background) (Table 3.2). Only positions tested are shown. Positions when substituted with tryptophan that did not show glutamate-activated current are highlighted in Red. Those that showed greatly reduced current amplitudes (<0.1 of wild-type) are highlighted in Blue.

(F) Results from *Xenopus* oocytes (B) mapped onto the M4 segment of GluA2 ($GluA2_{cryst}$; PDB ID 3KG2) (Sobolevsky, Rosconi et al. 2009). Coloring scheme as in (E) with affected positions space-filled and with those not showing glutamate-activated currents in *Xenopus* oocytes labeled in the left panel. Positions where a tryptophan substitution had no effect on current amplitudes are in light gray.

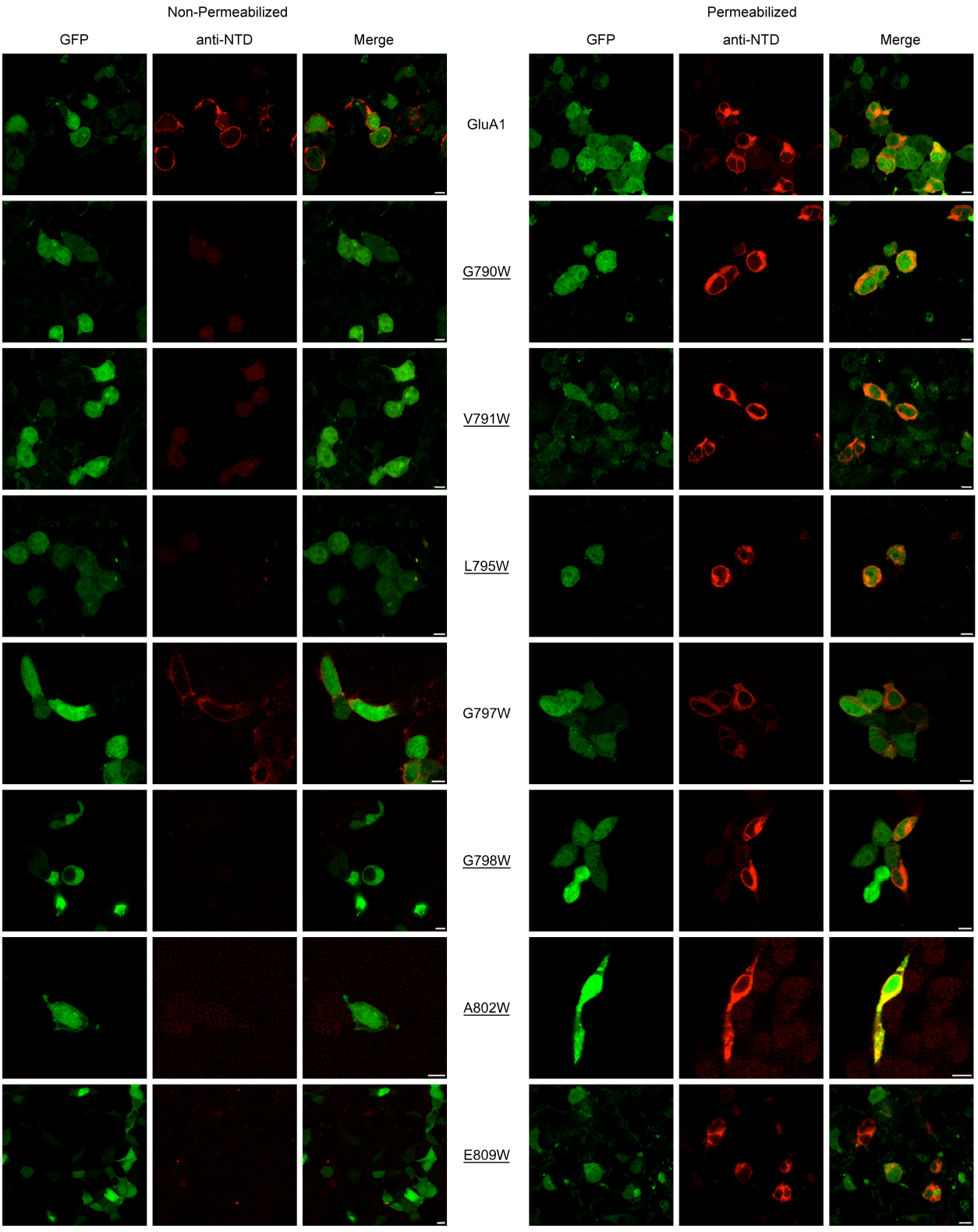

FIGURE 3.6. Tryptophan-substituted receptors that do not show glutamate-activated currents are not expressed at the membrane.

Immunocytochemistry of HEK 293 cells co-transfected with GFP and either wild-type GluA1 (*upper row*) or tryptophan-substituted GluA1 subunits (wild-type background) under non-permeabilized (*left*) or permeabilized (*right*) conditions. Tryptophan-substituted receptors V791W, L795W, G7898W, A802W, and E809W (underlined) showed no detectable glutamate-activated current either in oocytes or HEK cells (Figure 3.5B; Table 3.2) and no surface expression could be detected (Non-permeabilized conditions). Current amplitudes for G790W (underlined) were extremely small (oocytes) or not detected (HEK 293 cells). As a control, G797W showed wild-type-like current amplitudes and robust surface expression. All transfected constructs showed robust intracellular protein expression (Permeabilized conditions). Scale bars represent 10 microns.

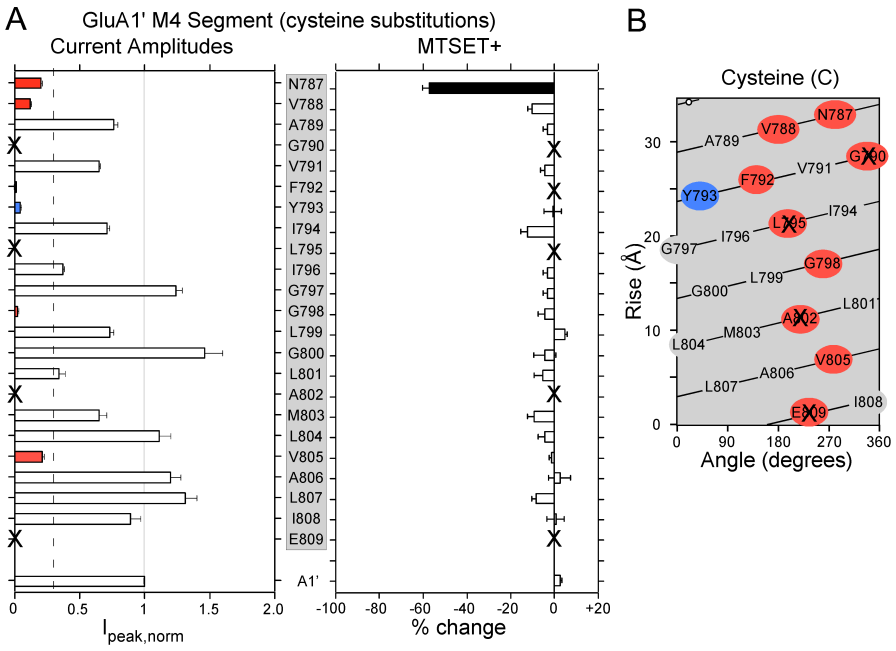

FIGURE 3.7. Cysteine mutagenesis scan of residues in the M4 segment.

(A, left panel) Mean current amplitudes (± SEM) at –60 mV and in 1 mM glutamate normalized to those obtained for GluA1' injected and recorded during the same cycle for cysteine substitutions (n > 7) (all recordings were made in oocytes). GluA1' current amplitudes were -1100 ± 41 nA (n = 32). Positions that did not show detectable glutamate-activated currents are demarcated by a 'X'. Positions that showed current amplitudes <0.3 of wild-type are colored blue.

(A, right panel) Mean percent change (± SEM) in glutamate-activated current amplitudes measured before (*Ipre*) and after (*Ipost*) exposure of wild-type or cysteine-substituted GluA1' subunits to MTSET in the continuous presence of glutamate (MTSET+). Left and right pointing bars indicate inhibition and potentiation, respectively. Filled bars indicate that the value of % change is statistically different from that of wild-type GluA1' ($P < 0.05$).

(B) Helical net representation of current amplitudes for positions substituted with cysteine in the M4 segment recorded in *Xenopus* oocytes (non-desensitizing background). Only positions tested are shown. Receptors containing cysteine-substitutions that did not show glutamate-activated current are highlighted in Red. Those that showed greatly reduced current amplitudes (<0.3 of wild-type) are highlighted in Blue. Outside of Y793, where a tryptophan substitution had no significant effect on current amplitudes, the positions that showed significant effects were a subset of those identified in the tryptophan scan (Figure 3.5E).

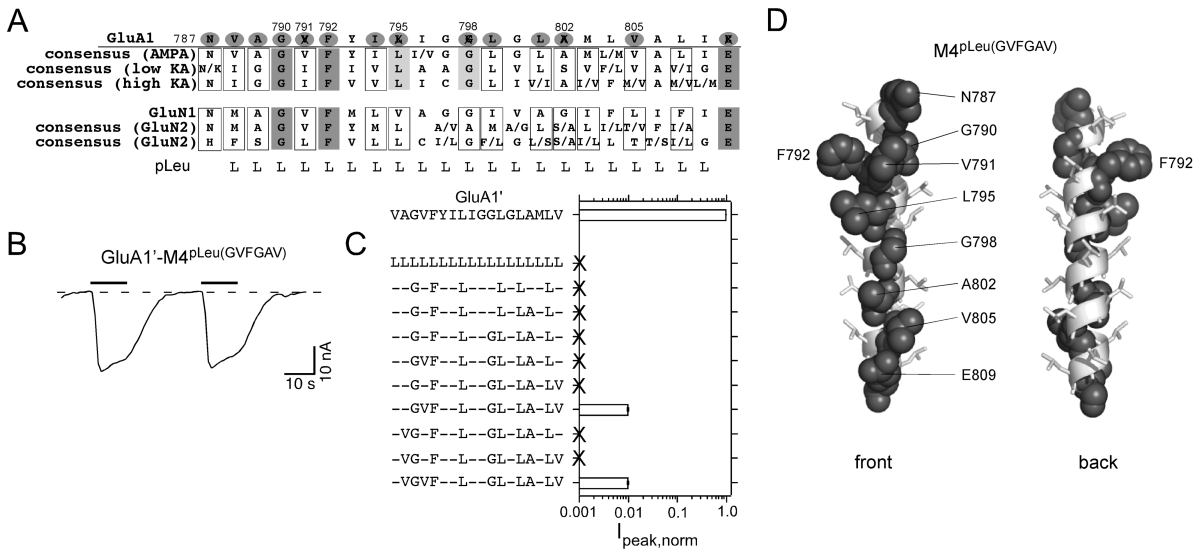

FIGURE 3.8. Recovery of function in the non-surface expressed polyleucine background.

(A) Sequence alignment of residues in and around the M4 segments in mammalian non-NMDA (*upper panel*) and NMDA (*lower panel*) receptor subunits. Outside of GluA1 and GluN1, consensus sequences are shown for AMPA (GluA1-GluA4), low affinity kainate (low KA) (GluK1-GluK3), high affinity kainate (high KA) (GluK4-GluK5), GluN2 (GluN2A-GluN2D), or GluN3 (GluN3A & GluN3B). Positions highlighted in dark gray are conserved across all subunits, light gray are identical for more than 80% of subunits, and boxed are similar in nature. Positions not highlighted are not conserved. Numbering is given only for the GluA1 subunit. GluA1 positions where function was affected in the tryptophan scan in *Xenopus* oocytes are highlighted in dark gray ovals (Figure 3.5; Table 3.2).

(B) Representative whole-cell currents recorded from a *Xenopus* oocyte injected with GluA1'-M4$^{pLeu(GVFGAV)}$. In this construct, the GluA1' M4 segment was in the polyleucine background (see Figure 3.3) but certain positions had been mutated back to their wild-type form: L790G/L791V/L792F/L798G/L802A/L805V (GVFGAV). Currents recorded and displayed as in Figure 3.1A.

(C) Mean glutamate-activated current amplitudes (± SEM) at –60 mV and in 1 mM glutamate normalized to those obtained in wild-type (GluA1') injected and recorded during the same cycle (n > 6). Wild-type current amplitudes were -1760 ± 50 nA (n = 20). Positions that did not show detectable glutamate-activated currents are demarcated by an 'X'. All mutant constructs were in the M4 polyleucine (pLeu) background where certain positions were reverted back to their native residue: GF (L790G/L792F); GFA (GF + L802A); GFGA (GFA + L798G); GFGAV (GFGA + L805V); GVFGA (GFGA + L791V); GVFGAV (GVFGA + L805V); VGFGA (GFGA + L788V); VGFGAV (VGFGA + L805V); and VGVFGAV (VGFGAV + L791V).

(D) The necessary positions (GVFGAV) required to regenerate function in the non-surface expressed pLeu background are shown space-filled and in dark gray on the M4 segment from the GluA2 structure. Note that one of the leucines (L795) was also demarcated red (see Figure 3.5E).

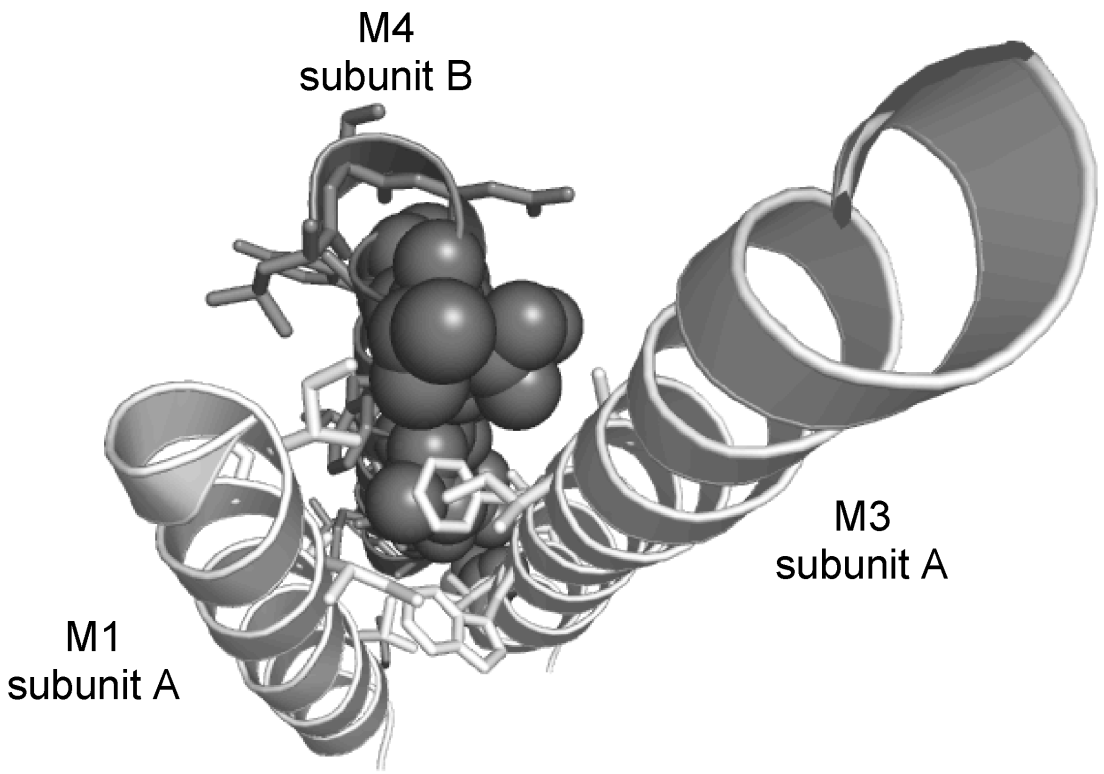

FIGURE 3.9. Interaction of the M4 segment with other transmembrane segments.

Illustration of the interactions of the M4 segment (subunit B) with other transmembrane segments (M1 and M3 from subunit A) (Table 3.3). Positions in M4 that showed significant functional effects in the tryptophan scan in both *Xenopus* oocytes and HEK 293 cells (underlined in Table 3.2) are space-filled and in dark gray.

Table 3.1 Current amplitudes of wild-type and truncated forms of the AMPA receptor GluA1 subunit expressed in *Xenopus* oocytes (GluA1') or HEK 293 cells (GluA1).

	Xenopus *oocytes*		**HEK 293 Cells**	
Construct	**I *(nA)***	**n**	**I (*pA*)**	**n**
GluA1' or GluA1	-1650 ± 75	15	-3010 ± 170	11
A1'-ΔM4 or A1-ΔM4	nd	>20	nd	11
GluA1 + Stargazin	nt		-6850 ± 1500	5
A1-ΔM4 + Stargazin	nt		nd	5
GluA1' or GluA1	-2190 ± 90	11	-71 ± 7	4
A1'-ΔCTD or A1-ΔCTD	-2090 ± 150	10	-15 ± 2	8

Peak glutamate-activated currents (I) for wild-type subunits were measured during the same injection/transfection cycles as corresponding truncated GluA1 subunits. Each construct was also expressed in at least 3 different injection or transfection rounds. In HEK 293 cells, the ΔCTD construct was measured in outside-out patches; the rate of entry into desensitization was 2.3 ± 0.1 ms (n = 4) for wild-type and 2.6 ± 0.1 ms (n = 8) for GluA1-ΔCTD with both showing >99% extent of desensitization (data not shown). A1'-ΔM4 + M4 is the ΔM4 construct co-expressed with the GluA1 M4 segment. Values shown are mean ± SEM. *nd*, no glutamate-activated currents detected. *nt*, not tested. When measuring current amplitudes in HEK 293 cells, where the wild-type background (GluA1) was used, we included cyclothiazide in the recording solution.

Table 3.2 Functional properties of wild-type and tryptophan-substituted GluA1 receptors expressed in *Xenopus* oocytes (GluA1') or HEK 293 cells (GluA1).

	***Xenopus* oocytes**					**HEK 293 Cells**	
Construct	**I *(nA)***	**n**	**EC_{50} *(mM)***	***Hill***	**n**	**I *(pA)***	**n**
GluA1'/A1	-2120 ± 40	32	4.2 ± 0.1	1.6 ± 0.1	14	-1330 ± 50	16
N787W	-14 ± 2	7 (13)	nt			-41 ± 11	4
V788W	-66 ± 2	3 (16)	nt			nd	3
A789W	-15 ± 1	14 (18)	14.8 ± 1.0	1.8 ± 0.1	6	-400 ± 140	4
G790W	-14 ± 2	11 (21)	nt			nd	4
V791W	nd	7	nt			nd	3
F792W	-4 ± 1	2 (9)	nt			-19 ± 7	3
Y793W	-2430 ± 100	11	5.6 ± 0.2	1.5 ± 0.1	6	-234 ± 70	3
I794W	-7 ± 1	7 (16)	nt			nd	3
L795W	nd	10	nt			nd	3
I796W	-3440 ± 160	11	3.0 ± 0.3	1.2 ± 0.1	5	-1330 ± 90	4
G797W	-2940 ± 160	10	3.7 ± 0.2	1.4 ± 0.1	5	-410 ± 120	3
G798W	nd	7	nt			nd	3
L799W	-310 ± 20	13	7.8 ± 0.2	1.5 ± 0.1	8	-490 ± 130	3
G800W	-2970 ± 80	13	3.9 ± 0.1	1.3 ± 0.1	6	-1180 ± 340	3
L801W	-140 ± 10	11	7.2 ± 0.3	1.6 ± 0.1	7	-310 ± 70	3
A802W	nd	7	nt			nd	3
M803W	-1100 ± 60	10	8.0 ± 0.5	1.4 ± 0.1	6	-3490 ± 710	5

L804W	-3350 ± 110	12	3.0 ± 0.1	1.3 ± 0.1	6	-730 ± 400	2
V805W	-36 ± 2	12	11.0 ± 0.3	1.4 ± 0.1	6	nd	3
A806W	-2070 ± 70	10	3.0 ± 0.1	1.5 ± 0.1	5	-430 ± 50	4
L807W	-5670 ± 120	13	3.0 ± 0.1	1.5 ± 0.1	6	-1970 ± 690	4
I808W	-2990 ± 80	12	4.1 ± 0.1	1.3 ± 0.1	6	-440 ± 70	3
E809W	nd	9	nt			nd	3

Values shown and displayed as in Table 3.1. *nd*, no glutamate-activated currents detected. *nt*, not tested. For some mutations, injected oocytes showed either no detectable glutamate-activated currents or very small current amplitudes. In these instances, the *n* values in parentheses indicate the total number of oocytes recorded, whereas the other number indicates those that showed a detectable glutamate-activated current. EC_{50} is the concentration at half-maximal activation and *Hill* the Hill coefficient (see Experimental Procedures). The average current amplitude is only of those recordings that showed detectable currents. Positions underlined showed significant reductions in glutamate-activated current amplitudes in both *Xenopus* oocytes and HEK 293 cells. When measuring current amplitudes in HEK 293 cells, where the wild-type background (GluA1) was used, we included cyclothiazide in the recording solution.

Table 3.3 Residues in the vicinity of the M4 transmembrane segment in the closed state.

M4 Segment *subunit B*	**M1 Segment** *5 Å*	**M3 Segment** *5 Å*
N787	S512 (B) F513 (B)	L616 (B)
V788	I521 (A)	I609 (A) S611 (A)
A789	--	--
G790	V510 (B)	--
X V791 X	F513 (B)	F604 (A) I607 (A)
F792	I521 (A) C524 (A) I525 (A) A528 (A)	F604 (A) I608 (A)
Y793	--	--
I794	--	V600 (A)
X L795 X	A528 (A) V532 (A)	V600 (A) W601 (A) F604 (A)
I796	--	--
G797	--	--
X G798 X	--	I596 (A) V600 (A)
L799	G531 (A) V532 (A) V535 (A)	V597 (A)

G800	--	--
L801	--	I596 (A)
X A802 X	--	S593 (A) I596 (A) V597 (A)
M803	V535 (A) L538 (A)	--
L804	--	--
V805	--	L592 (A) S593 (A)
A806	--	S593 (A)
L807	--	--
I808	--	--
X E809 X	--	L592 (A) S593 (A)

Residues within 5 Å of each individual position in the M4 segment of GluA1 (as a reference subunit B) in the antagonist bound closed state (PDB: 3KG2). All positions tested with tryptophan substitutions are shown (Figure 3.5; Table 3.2). Underlined positions in M4 showed significantly altered current amplitudes in both *Xenopus* oocytes and HEK 293 cells with those yielding no detectable glutamate-activated currents (in oocytes) indicated by an 'X' next to them. Analysis was performed on $GluA2_{cryst}$ using PyMol. For residues located in the M1 and M3 transmembrane segments, we indicate the subunit conformer (A or B) that is positioned within 5 Å of that specific M4 position. A dash indicates that no residues were within this distance. In general, residues in the M4 segment of subunit B are positioned near the M3 segment of subunit A, except at the N-terminal end where they are in close proximity to the M1 and M3 segments of subunit A as well as B. Note that positions that showed no effect on function (not underlined) were generally located remote from other structural elements (except for M803 & A806) and positioned at the lipid interface.

Chapter 4: Concluding Remarks

The elucidation of the first, nearly complete crystal structure of a homomeric AMPA receptor (GluA2) has revolutionized the field of ionotropic glutamate receptor structure/function. The full-length AMPAR crystal structure revealed many surprising and unexpected insights regarding the organization and interaction of subunits in tetrameric iGluR complexes that have deeply impacted my dissertation research. In my first project I utilized the insight that in a receptor formed by four identical GluA2 subunits, individual subunits adopted two distinct conformations – termed A/C and B/D – to address the question of how subunits are arranged in functional NMDARs. Using cysteine mutagenesis, immunoblots, and functional assays, I showed that NMDAR subunits adopt distinct subunit-specific conformations with the GluN1 and GluN2 subunits approximating the A/C and B/D conformations, respectively. My work therefore demonstrated that NMDAR subunits are positioned in a N1/N2/N1/N2 arrangement in functional NMDA receptors, resolving the previous controversy regarding the arrangement of subunits around the ion channel pore.

Second, the novel arrangement and organization of transmembrane segments about the ion channel pore has served as a springboard for the work discussed in Chapter 3, as well as, my present work. Many structural determinants that modulate iGluR biogenesis have been identified in the amino-terminal and ligand-binding domains of iGluR subunits (Chapter 1), but the role of the transmembrane domain in iGluR assembly remains poorly defined. Although it is well accepted that iGluRs are assembled as a dimer of dimers, the mechanism underlying tetramerization – the necessary step for the formation of functional receptors that can be inserted into the

plasma membrane – is unknown. Thus, given that the eukaryotic-specific M4 transmembrane segment is necessary for surface expression of iGluRs (Horak, Chang et al. 2008) and the predicted structural arrangement of the TMD in which the M4 segment of one subunit interacts/associates with the ion channel core of an adjacent subunit (Sobolevsky, Rosconi et al. 2009), we hypothesized that the M4 segment may mediate mammalian iGluR assembly.

The ER is the site of protein maturation ensuring that only properly folded, tetrameric receptors are exported to the Golgi bodies where the receptors undergo post-translational modification prior to insertion into the plasma membrane (Fleck 2006; Heine 2012). To determine where in this secretory pathway the ΔM4 construct was being retained, we visualized permeabilized cells probed with HA, as well as antibodies specific for the ER (calreticulin) or the Golgi bodies (GM130). Immunocytochemical analysis showed that the ΔM4 construct co-localized with the ER marker, but not the Golgi marker, suggesting that it was retained in the ER presumably in some immature, non-functional form (data not shown). Based on this finding, coupled with the knowledge that the rate-limiting step of iGluR biogenesis is the export of properly assembled/oligomerized iGluR assemblies from the ER, we hypothesized that the lack of surface expression of the ΔM4 construct was due to a deficit in receptor oligomerization.

Through the use of blue native-PAGE (BN-PAGE), we assessed the native oligomeric state of ΔM4-containing GluA2 subunits (Figure 4.1A) and in accordance with our hypothesis, showed that ΔM4-containing subunits form dimers, but do not tetramerize. The lack of tetramer formation for the ΔM4 construct is consistent with the

hypothesis that the M4 segment modulates tetramerization. The ΔM4 manipulation, however, is limited in terms of addressing the structural-functional significance of the M4 segment due to its all-or-none action. We therefore focused on an 'interacting' face of the M4 helix – defined by positions (V)aline-(L)eucine-(G)lycine-(A)lanine-(V)aline-(E)glutamate (Figure 4.1C, red positions) (Chapter 3). Tryptophan (W) has a large, bulky side chain that can disrupt helix-helix interactions. Tryptophan substitution of positions in the GluA1 subunit – as well as several adjacent positions, but not of those located on the opposite side of the helix presumably in contact with lipid – prevented surface expression of AMPA receptors (Chapter 3) presumably in a manner comparable to ΔM4. Further, this M4 face is termed 'interacting' because it aligns closely with the ion channel core (transmembrane helices M1 & M3) of an adjacent subunit (Sobolevsky, Rosconi et al. 2009); thus, suggesting that the interaction of M4 with other transmembrane segments is important to its functional role.

Indeed, analysis of the native oligomeric state by BN-PAGE (Figure 4.1B) and/or fluorescence-detection size exclusion chromatography (FSEC) (Figures 4.1D, 4.1E) showed that single-substitutions of the 'interacting' face that disrupt surface expression in both GluA1 (Figure 4.1E) and GluA2 (Figures 4.1B, 4.1D) recapitulate the oligomeric phenotype observed with the ΔM4 construct (Figure 4.1A). An additional technical advantage of FSEC is that it not only provides information regarding the oligomeric state of proteins, but also whether proteins are misfolded. Thus, the lack of higher-order aggregates occurring at earlier time points in the FSEC chromatogram suggests that the loss of tetramerization observed in constructs containing single-substitutions along the

M4 ‘interacting’ face is a result of a disruption in the dimer to tetramer transition, rather than protein misfolding.

Substitutions of the M4 ‘interacting’ face disrupt tetramerization suggesting that the interaction of the M4 segment with the ion channel core of an adjacent subunit is critical in mediating the transition from dimer to tetramer. Thus, alteration of the putative interacting partners in the transmembrane segments of the ion channel core (M1 & M3) should also disrupt tetramer formation. Based on predictions from the GluA2 crystal structure, we identified putative interacting partners in the M3 segment that are positioned within 5 Å of the ‘interacting’ face of M4 (Figure 4.2A). Single-substitutions of these putative interacting partners in the M3 segment disrupted surface expression (Figure 4.2B) and resulted in altered oligomeric profiles by FSEC (Figure 4.2C). Together these data indicate that it is the interaction of the M4 segment with the adjacent ion channel core that is necessary and required for AMPA receptor tetramerization.

Additionally, it should be noted that the although the FSEC experiments shown in Figure 4.1D utilize the unedited form of GluA2 [GluA2(Q)] as the backbone upon which single mutations are introduced into the ‘interacting’ M4 face, the results are phenotypically replicated using the physiologically functional edited form of GluA2(R) by BN-PAGE (Figure 4.1B). Thus, as discussed in Chapter 1, although editing at the Q/R site has been suggested to regulate the export of iGluRs from the ER (Greger, Khatri et al. 2002), the present results suggest that it is not necessary for tetramerization. However, editing at the Q/R site may modulate the efficiency of tetramerization. Therefore, future experiments involving a quantitative analysis of the rate of

tetramerization are needed to determine if editing at the Q/R site has differential effects on the formation and/or stabilization of iGluR tetramerization.

Based on this preliminary data, we propose that the eukaryotic-specific M4 transmembrane segment acts as a tetramerization domain in mammalian iGluRs. Manipulation of the M4 segment does not seem to dramatically affect dimerization, the initial step in iGluR assembly, yet it prevents tetramer formation (Figure 4.1). Dimerization of monomeric subunits is largely a top-down process mediated predominantly by the amino-terminal domains (Leuschner and Hoch 1999; Madry, Mesic et al. 2007; Rossmann, Sukumaran et al. 2011). The transition from dimer to tetramer is complicated by the arrangement of dimer pairs and domain swapping revealed by the recent crystal structure (Sobolevsky, Rosconi et al. 2009). In fact, the predicted dimer pairs at the level of the LBD do not form a dimer interface unless in a tetrameric complex (Sobolevsky, Rosconi et al. 2009; Shanks, Maruo et al. 2010). Thus, based on our preliminary data and the new insights from the crystal structure, we suggest that iGluR tetramerization is a bottom-up process mediated by the TMD. More specifically, we propose that the interaction of the M4 segment with the ion channel core of an adjacent subunit drives and facilitates the domain swapping at the level of the LBD to form a tetrameric complex.

In iGluRs, the core of the ion channel – formed by the M1 and M3 transmembrane segments and an intracellular M2 loop – is structurally and evolutionarily related to inverted two-transmembrane K^+ channels (Arinaminpathy, Biggin et al. 2003). Prokaryotic iGluR (GluR0) subunits share structural and functional similarity with both two-transmembrane K^+ channels and mammalian iGluRs (see **iGluR**

Origins) (Chen, Cui et al. 1999). Like two-transmembrane K^+ channels, GluR0 is composed of two full-pass transmembrane segments and a re-entrant pore loop equivalent to the ion channel core. However, all known eukaryotic iGluR subunits contain an additional transmembrane segment, the M4 segment, C-terminal to the ion channel core.

From a structural standpoint, the addition of the M4 transmembrane segment results in the intracellular positioning of the C-terminus, so that the amino- and carboxy-termini are positioned on opposite faces of the lipid membrane. Additionally, from an evolutionary standpoint, the addition of the M4 transmembrane segment occurred earlier than the evolution of the physiologically critical C-terminal domain. Thus, I speculate that the M4 transmembrane segment evolved to confer and/or provide a biological advantage in vertebrates. GluR0 differs from eukaryotic iGluRs in both its permeation (GluR0, K^+ selective vs. iGluR, cation non-selective) and gating kinetics (GluR0, slow; iGluR, fast) (Chen, Cui et al. 1999; Traynelis, Wollmuth et al. 2010). Thus, the M4 segment presumably facilitates and permits eukaryotic iGluRs to mediate fast, excitatory neurotransmission in the central nervous system.

Although the length of the CTD is variable amongst iGluR subfamilies, the CTD is a functional domain that interacts with intracellular scaffolding proteins (i.e., MAGUKs, TARPs, cornichons) to mediate iGluR trafficking and expression at the synapse (Sheng and Hoogenraad 2007). Dynamic regulation of iGluR expression during synaptic plasticity occurs via C-terminal interactions with scaffolding proteins in a subunit-specific manner (Steigerwald, Schulz et al. 2000; Shi, Hayashi et al. 2001). Previous work has suggested that at least in NMDA receptors, the CTD evolved to accommodate the

expanding complexity of NMDAR-mediated signaling cascades (Ryan, Emes et al. 2008); thereby accounting for species-specific differences in behavior and intellectual fortitude.

Auxiliary protein-mediated changes in iGluR surface expression further support the role of CTD-interacting proteins in iGluR biogenesis. Stargazin, the prototypical TARP, is a transmembrane auxiliary protein that increases the surface expression of AMPA receptors presumably through interactions with the transmembrane domain and/or CTD (Tomita, Adesnik et al. 2005). Further, auxiliary proteins – such as stargazin, PSD-95, and SAP-97 – are present within the secretory pathway and aid in the biogenesis of iGluRs. Thus, due to the intimate relationship of the M4 segment with that of the highly-regulated CTD, M4-mediated tetramerization may be enhanced by C-terminal domain interactions with intracellular auxiliary proteins. Future experiments will explore the mechanisms by which CTD-interacting proteins dynamically regulate iGluR biogenesis.

The identification of the M4 segment as a tetramerization domain in iGluRs represents a new frontier in iGluR biogenesis. Our work demonstrates that the M4 segment acts as a unique functional unit. Alas the question of whether the M4 segment catalyzes or stabilizes iGluR tetramerization is of great interest. Similar to known tetramerization domains in two-transmembrane K^+ channels, the M4 segment interacts with the transmembrane segments of adjacent subunits as well as with the lipid bilayer to presumably mediate tetramerization (Molina, Encinar et al. 2004). We are currently approaching the premise of M4-mediated tetramerization from many fronts including its role in heteromeric assembly, its role as either a catalyzing or stabilizing domain via its

thermodynamic effects, as well as, whether M4-mediated tetramerization can be regulated via interactions with intracellular auxiliary proteins (i.e., stargazin). Understanding the mechanisms regulating tetramerization will allow for the advent of new pharmacological agents that can enhance the formation of new receptors and may alleviate the symptoms of neurological disorders associated with alterations in iGluR biogenesis and/or trafficking.

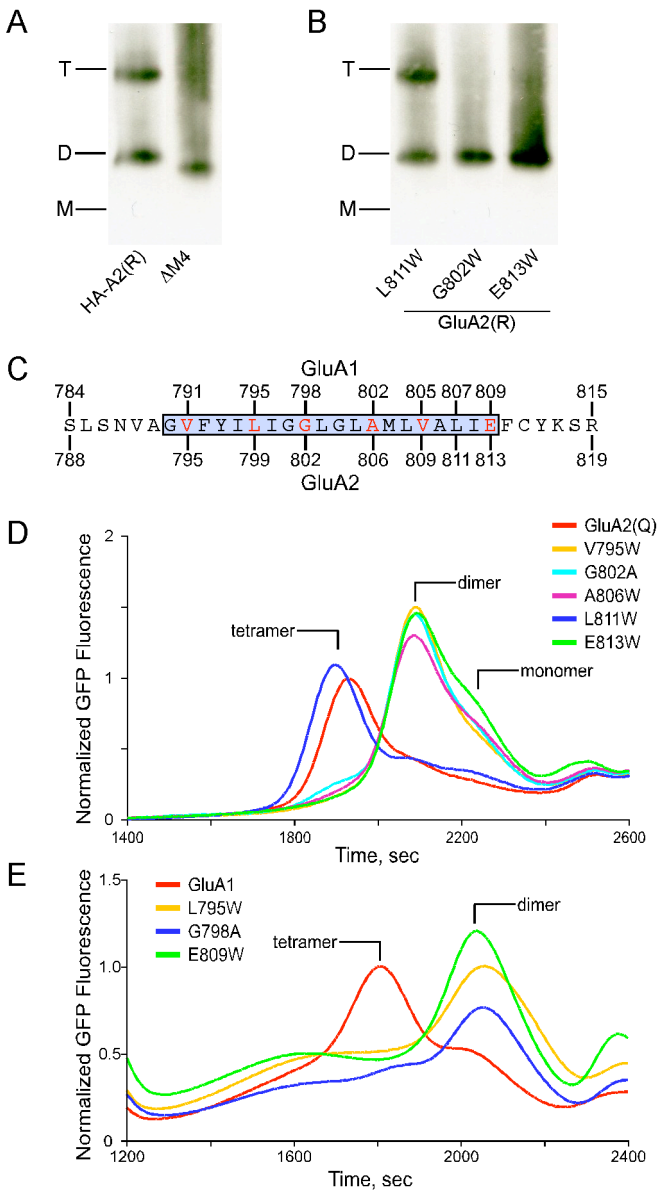

Figure 4.1. The eukaryotic-specific M4 segment is a tetramerization domain in AMPA receptor subunits.

(A), (B), Blue native-PAGE (BN-PAGE) of HA-tagged wild-type, ΔM4-containing (A), or tryptophan-substituted (B) constructs of GluA2(R). Surface-expressing wild-type and L811W subunits show prominent dimer and tetramer bands, whereas, tryptophan-substiutions (G802W or E813W) and ΔM4 constructs that result in no detectable surface expression (Chapter 3) show only dimer formation.

(C), Schematic of the M4 transmembrane segment with those positions substituted with tryptophan (W) shown in blue (enclosed box). The numbering for GluA1 (top) and GluA2 (bottom) subunits is for the mature protein. Residues shown in red define the face of the M4 segment necessary for surface expression – (V)aline-(L)eucine-(G)lycine-(A)lanine-(V)aline-(E)glutamate.

(D), (E), Fluorescence-detection size exclusion chromatograms (FSEC) of GluA2(Q) (D) and GluA1 (E) subunits containing single-tryptophan substitutions in the M4 segment. Surface-expressing wild-type (A2, D; A1, E) and A2(L811W) subunits predominantly formed tetramers, whereas non-surface expressing constructs in both GluA2 (V795W, G802A, A806W, or E813W) (D) and GluA1 (L795W, G798A, or E809W) (E) do not tetramerize, forming almost exclusively dimers. All constructs contained a C-teriminal GFP tag. All constructs were normalized to the observed tetramer peak of wild-type for a given transfection cycle.

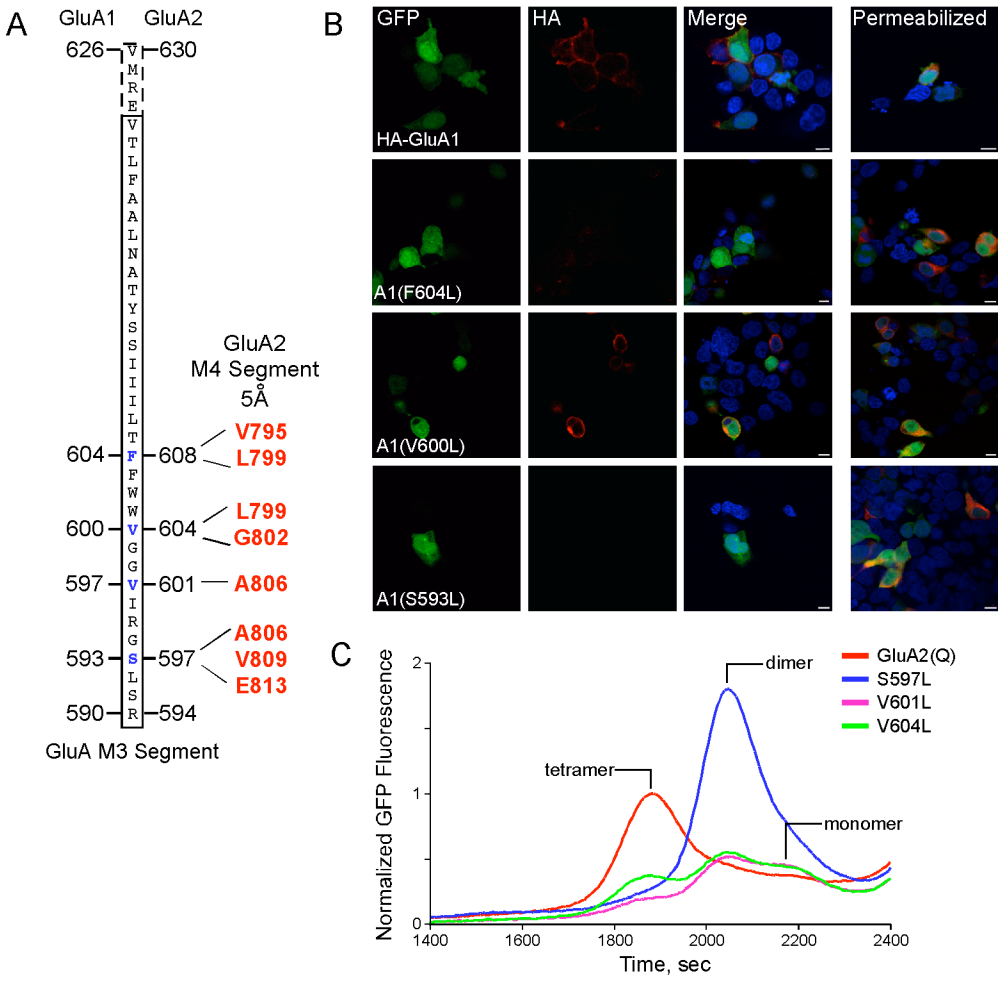

Figure 4.2. Disruption of the putative interacting face in the M3 segment alters tetramerization.

(A), Schematic of the M3 transmembrane segment with the relative numbering of the mature protein for the GluA1 (left) and GluA2 (right) subunits. Residues shown in blue are predicted, based on the GluA2 crystal structure (Sobolevsky, Rosconi et al. 2009) to be positioned within 5Å of the "VLGAVE" face in the M4 segment (red positions).

(B), Immunocytochemistry of HEK 293 cells co-transfected with GFP and either HA-tagged wild-type GluA1 (*upper row*) or leucine-substituted GluA1 subunits (wild-type background) under non-permeabilized (*left*) or permeabilized (*right*) conditions. Leucine-substituted receptors F604L and S593 showed no detectable surface expression. V600L substituted subunits showed intermediate surface expression. All transfected constructs showed robust intracellular protein expression (permeabilized conditions, right). Scale bars represent 10 microns.

(C), Fluorescence-detection size exclusion chromatograms (FSEC) of GluA2(Q) subunits containing single-leucine substitutions in the M3 segment. Surface-expressing wild-type subunits predominantly formed tetramers, whereas non-surface expressing constructs S597L and V601L predominantly formed dimers. V604L, the homologous position to GluA1(V600L) which showed intermediate surface expression by ICC (B), showed slight tetramer formation, but more prominent dimer formation. All constructs contained a C-teriminal GFP tag. All constructs were normalized to the observed tetramer peak of wild-type for a given transfection cycle.

References

Alabi, A. A., M. I. Bahamonde, et al. (2007). "Portability of paddle motif function and pharmacology in voltage sensors." Nature **450**(7168): 370-375.

Anggono, V. and R. L. Huganir (2012). "Regulation of AMPA receptor trafficking and synaptic plasticity." Curr Opin Neurobiol.

Arinaminpathy, Y., P. C. Biggin, et al. (2003). "A prokaryotic glutamate receptor: homology modelling and molecular dynamics simulations of GluR0." FEBS Lett **553**(3): 321-327.

Armstrong, N. and E. Gouaux (2000). "Mechanisms for activation and antagonism of an AMPA-sensitive glutamate receptor: crystal structures of the GluR2 ligand binding core." Neuron **28**(1): 165-181.

Armstrong, N., Y. Sun, et al. (1998). "Structure of a glutamate-receptor ligand-binding core in complex with kainate." Nature **395**(6705): 913-917.

Arvola, M. and K. Keinanen (1996). "Characterization of the ligand-binding domains of glutamate receptor (GluR)-B and GluR-D subunits expressed in Escherichia coli as periplasmic proteins." J Biol Chem **271**(26): 15527-15532.

Ayalon, G., E. Segev, et al. (2005). "Two regions in the N-terminal domain of ionotropic glutamate receptor 3 form the subunit oligomerization interfaces that control subtype-specific receptor assembly." J Biol Chem **280**(15): 15053-15060.

Ayalon, G. and Y. Stern-Bach (2001). "Functional assembly of AMPA and kainate receptors is mediated by several discrete protein-protein interactions." Neuron **31**(1): 103-113.

Banke, T. G. and S. F. Traynelis (2003). "Activation of NR1/NR2B NMDA receptors." Nat Neurosci **6**(2): 144-152.

Benke, T. A., A. Luthi, et al. (1998). "Modulation of AMPA receptor unitary conductance by synaptic activity." Nature **393**(6687): 793-797.

Bitanihirwe, B. K., M. P. Lim, et al. "N-methyl-D-aspartate receptor expression in parvalbumin-containing inhibitory neurons in the prefrontal cortex in bipolar disorder." Bipolar Disord **12**(1): 95-101.

Bito, H. (2010). "The chemical biology of synapses and neuronal circuits." Nat Chem Biol **6**(8): 560-563.

Bjerrum, O. J. and C. Schafer-Nielsen (1986). Analytical Electrophoresis. Weinheim.

Blanke, M. L. and A. M. VanDongen (2008). "Constitutive activation of the N-methyl-D-aspartate receptor via cleft-spanning disulfide bonds." J Biol Chem **283**(31): 21519-21529.

Blanke, M. L. and A. M. VanDongen (2008). "The NR1 M3 domain mediates allosteric coupling in the N-methyl-D-aspartate receptor." Mol Pharmacol **74**(2): 454-465.

Blanpied, T. A., D. B. Scott, et al. (2002). "Dynamics and regulation of clathrin coats at specialized endocytic zones of dendrites and spines." Neuron **36**(3): 435-449.

Boulter, J., M. Hollmann, et al. (1990). "Molecular cloning and functional expression of glutamate receptor subunit genes." Science **249**(4972): 1033-1037.

Brotchie, J. M. (2000). "The neural mechanisms underlying levodopa-induced dyskinesia in Parkinson's disease." Ann Neurol **47**(4 Suppl 1): S105-112; discussion S112-104.

Caputo, G. A. and E. London (2004). "Position and ionization state of Asp in the core of membrane-inserted alpha helices control both the equilibrium between transmembrane and nontransmembrane helix topography and transmembrane helix positioning." Biochemistry **43**(27): 8794-8806.

Careaga, C. L. and J. J. Falke (1992). "Structure and dynamics of Escherichia coli chemosensory receptors. Engineered sulfhydryl studies." Biophys J **62**(1): 209-219.
Chang, H. R. and C. C. Kuo (2008). "The activation gate and gating mechanism of the NMDA receptor." J Neurosci **28**(7): 1546-1556.
Chatterton, J. E., M. Awobuluyi, et al. (2002). "Excitatory glycine receptors containing the NR3 family of NMDA receptor subunits." Nature **415**(6873): 793-798.
Chaudhry, C., M. C. Weston, et al. (2009). "Stability of ligand-binding domain dimer assembly controls kainate receptor desensitization." EMBO J **28**(10): 1518-1530.
Chen, G. Q., C. Cui, et al. (1999). "Functional characterization of a potassium-selective prokaryotic glutamate receptor." Nature **402**(6763): 817-821.
Chen, L., D. M. Chetkovich, et al. (2000). "Stargazin regulates synaptic targeting of AMPA receptors by two distinct mechanisms." Nature **408**(6815): 936-943.
Chen, N., T. Luo, et al. (1999). "Subtype-dependence of NMDA receptor channel open probability." J Neurosci **19**(16): 6844-6854.
Choi, Y. B., L. Tenneti, et al. (2000). "Molecular basis of NMDA receptor-coupled ion channel modulation by S-nitrosylation." Nat Neurosci **3**(1): 15-21.
Citri, A. and R. C. Malenka (2008). "Synaptic plasticity: multiple forms, functions, and mechanisms." Neuropsychopharmacology **33**(1): 18-41.
Clarke, J. and A. R. Fersht (1993). "Engineered disulfide bonds as probes of the folding pathway of barnase: increasing the stability of proteins against the rate of denaturation." Biochemistry **32**(16): 4322-4329.
Clayton, A., C. Siebold, et al. (2009). "Crystal structure of the GluR2 amino-terminal domain provides insights into the architecture and assembly of ionotropic glutamate receptors." J Mol Biol **392**(5): 1125-1132.
Coleman, S. K., T. Moykkynen, et al. (2006). "Isoform-specific early trafficking of AMPA receptor flip and flop variants." J Neurosci **26**(43): 11220-11229.
Coleman, S. K., T. Moykkynen, et al. (2010). "Ligand-binding domain determines endoplasmic reticulum exit of AMPA receptors." J Biol Chem **285**(46): 36032-36039.
Collingridge, G. L., R. W. Olsen, et al. (2009). "A nomenclature for ligand-gated ion channels." Neuropharmacology **56**(1): 2-5.
Contractor, A., C. Mulle, et al. (2011). "Kainate receptors coming of age: milestones of two decades of research." Trends Neurosci **34**(3): 154-163.
Cui-Wang, T., C. Hanus, et al. (2012). "Local zones of endoplasmic reticulum complexity confine cargo in neuronal dendrites." Cell **148**(1-2): 309-321.
Cull-Candy, S. G. and D. N. Leszkiewicz (2004). "Role of distinct NMDA receptor subtypes at central synapses." Sci STKE **2004**(255): re16.
Derkach, V. A., M. C. Oh, et al. (2007). "Regulatory mechanisms of AMPA receptors in synaptic plasticity." Nat Rev Neurosci **8**(2): 101-113.
Deutsch, C. (2002). "Potassium channel ontogeny." Annu Rev Physiol **64**: 19-46.
Di Maio, V. (2008). "Regulation of information passing by synaptic transmission: a short review." Brain Res **1225**: 26-38.
Dingledine, R., K. Borges, et al. (1999). "The glutamate receptor ion channels." Pharmacol Rev **51**(1): 7-61.
du Bois, T. M. and X. F. Huang (2007). "Early brain development disruption from NMDA receptor hypofunction: relevance to schizophrenia." Brain Res Rev **53**(2): 260-270.

Ellgaard, L. and A. Helenius (2003). "Quality control in the endoplasmic reticulum." Nat Rev Mol Cell Biol **4**(3): 181-191.
Erreger, K., P. E. Chen, et al. (2004). "Glutamate receptor gating." Crit Rev Neurobiol **16**: 187-224.
Farina, A. N., K. Y. Blain, et al. (2011). "Separation of domain contacts is required for heterotetrameric assembly of functional NMDA receptors." J Neurosci **31**(10): 3565-3579.
Fishell, G. and B. Rudy (2011). "Mechanisms of inhibition within the telencephalon: "where the wild things are"." Annu Rev Neurosci **34**: 535-567.
Fleck, M. W. (2006). "Glutamate receptors and endoplasmic reticulum quality control: looking beneath the surface." Neuroscientist **12**(3): 232-244.
Furukawa, H., S. K. Singh, et al. (2005). "Subunit arrangement and function in NMDA receptors." Nature **438**(7065): 185-192.
Gambrill, A. C. and A. Barria (2011). "NMDA receptor subunit composition controls synaptogenesis and synapse stabilization." Proc Natl Acad Sci U S A **108**(14): 5855-5860.
Gardoni, F., B. Picconi, et al. (2006). "A critical interaction between NR2B and MAGUK in L-DOPA induced dyskinesia." J Neurosci **26**(11): 2914-2922.
Gaspar, P. A., M. L. Bustamante, et al. (2009). "Molecular mechanisms underlying glutamatergic dysfunction in schizophrenia: therapeutic implications." J Neurochem **111**(4): 891-900.
Geiger, J. R., T. Melcher, et al. (1995). "Relative abundance of subunit mRNAs determines gating and Ca2+ permeability of AMPA receptors in principal neurons and interneurons in rat CNS." Neuron **15**(1): 193-204.
Gielen, M., A. Le Goff, et al. (2008). "Structural Rearrangements of NR1/NR2A NMDA Receptors during Allosteric Inhibition." Neuron **57**(1): 80-93.
Gielen, M., B. Siegler Retchless, et al. (2009). "Mechanism of differential control of NMDA receptor activity by NR2 subunits." Nature **459**(7247): 703-707.
Gill, M. B., P. Vivithanaporn, et al. (2009). "Glutamate binding and conformational flexibility of ligand-binding domains are critical early determinants of efficient kainate receptor biogenesis." J Biol Chem **284**(21): 14503-14512.
Greger, I. H., P. Akamine, et al. (2006). "Developmentally regulated, combinatorial RNA processing modulates AMPA receptor biogenesis." Neuron **51**(1): 85-97.
Greger, I. H., L. Khatri, et al. (2002). "RNA editing at arg607 controls AMPA receptor exit from the endoplasmic reticulum." Neuron **34**(5): 759-772.
Greger, I. H., E. B. Ziff, et al. (2007). "Molecular determinants of AMPA receptor subunit assembly." Trends Neurosci **30**(8): 407-416.
Groc, L., M. Heine, et al. (2006). "NMDA receptor surface mobility depends on NR2A-2B subunits." Proc Natl Acad Sci U S A **103**(49): 18769-18774.
Hansen, K. B., H. Furukawa, et al. (2010). "Control of assembly and function of glutamate receptors by the amino-terminal domain." Mol Pharmacol **78**(4): 535-549.
Hardingham, G. E. (2009). "Coupling of the NMDA receptor to neuroprotective and neurodestructive events." Biochem Soc Trans **37**(Pt 6): 1147-1160.
Hardingham, G. E. and H. Bading (2010). "Synaptic versus extrasynaptic NMDA receptor signalling: implications for neurodegenerative disorders." Nat Rev Neurosci **11**(10): 682-696.

Haucke, V., E. Neher, et al. (2011). "Protein scaffolds in the coupling of synaptic exocytosis and endocytosis." Nat Rev Neurosci **12**(3): 127-138.
Hazell, A. S. (2007). "Excitotoxic mechanisms in stroke: an update of concepts and treatment strategies." Neurochem Int **50**(7-8): 941-953.
Heine, M. (2012). "Surface traffic in synaptic membranes." Adv Exp Med Biol **970**: 197-219.
Horak, M., R. A. Al-Hallaq, et al. (2008). "Role of the fourth membrane domain of the NR2B subunit in the assembly of the NMDA receptor." Channels (Austin) **2**(3): 159-160.
Horak, M., K. Chang, et al. (2008). "Masking of the endoplasmic reticulum retention signals during assembly of the NMDA receptor." J Neurosci **28**(13): 3500-3509.
Horning, M. S. and M. L. Mayer (2004). "Regulation of AMPA receptor gating by ligand binding core dimers." Neuron **41**: 379-388.
Hunt, D. L. and P. E. Castillo (2012). "Synaptic plasticity of NMDA receptors: mechanisms and functional implications." Curr Opin Neurobiol.
Janovjak, H., G. Sandoz, et al. (2011). "A modern ionotropic glutamate receptor with a K(+) selectivity signature sequence." Nat Commun **2**: 232.
Jin, R., S. K. Singh, et al. (2009). "Crystal structure and association behaviour of the GluR2 amino-terminal domain." EMBO J **28**(12): 1812-1823.
Johnson, J. W. and P. Ascher (1987). "Glycine potentiates the NMDA response in cultured mouse brain neurons." Nature **325**(6104): 529-531.
Jonas, P., C. Racca, et al. (1994). "Differences in Ca2+ permeability of AMPA-type glutamate receptor channels in neocortical neurons caused by differential GluR-B subunit expression." Neuron **12**(6): 1281-1289.
Jones, K. S., H. M. VanDongen, et al. (2002). "The NMDA receptor M3 segment is a conserved transduction element coupling ligand binding to channel opening." J Neurosci **22**(6): 2044-2053.
Kalia, L. V., S. K. Kalia, et al. (2008). "NMDA receptors in clinical neurology: excitatory times ahead." Lancet Neurol **7**(8): 742-755.
Kandel, E. R., Schwartz, J.H., and Jessell T.M. (2000). Principles of Neural Science. New York, McGraw-Hill.
Karakas, E., N. Simorowski, et al. (2009). "Structure of the zinc-bound amino-terminal domain of the NMDA receptor NR2B subunit." EMBO J **28**(24): 3910-3920.
Karakas, E., N. Simorowski, et al. (2011). "Subunit arrangement and phenylethanolamine binding in GluN1/GluN2B NMDA receptors." Nature **475**(7355): 249-253.
Kaufman, A. M., A. J. Milnerwood, et al. (2012). "Opposing Roles of Synaptic and Extrasynaptic NMDA Receptor Signaling in Cocultured Striatal and Cortical Neurons." J Neurosci **32**(12): 3992-4003.
Keinanen, K., W. Wisden, et al. (1990). "A family of AMPA-selective glutamate receptors." Science **249**(4968): 556-560.
Kirkwood, A., A. Silva, et al. (1997). "Age-dependent decrease of synaptic plasticity in the neocortex of alphaCaMKII mutant mice." Proc Natl Acad Sci U S A **94**(7): 3380-3383.
Kriegenburg, F., L. Ellgaard, et al. (2012). "Molecular chaperones in targeting misfolded proteins for ubiquitin-dependent degradation." FEBS J **279**(4): 532-542.
Krupp, J. J., B. Vissel, et al. (1996). "Calcium-dependent inactivation of recombinant N-methyl-D-aspartate receptors is NR2 subunit specific." Mol Pharmacol **50**(6): 1680-1688.

Krystal, J. H., L. P. Karper, et al. (1994). "Subanesthetic effects of the noncompetitive NMDA antagonist, ketamine, in humans. Psychotomimetic, perceptual, cognitive, and neuroendocrine responses." Arch Gen Psychiatry **51**(3): 199-214.
Kumar, J., P. Schuck, et al. (2009). "The N-terminal domain of GluR6-subtype glutamate receptor ion channels." Nat Struct Mol Biol **16**(6): 631-638.
Kumar, J., P. Schuck, et al. (2011). "Structure and assembly mechanism for heteromeric kainate receptors." Neuron **71**(2): 319-331.
Kussius, C. L. and G. K. Popescu (2009). "Kinetic basis of partial agonism at NMDA receptors." Nat Neurosci **12**(9): 1114-1120.
Lau, C. G. and R. S. Zukin (2007). "NMDA receptor trafficking in synaptic plasticity and neuropsychiatric disorders." Nat Rev Neurosci **8**(6): 413-426.
Lee, C. H. and E. Gouaux (2011). "Amino terminal domains of the NMDA receptor are organized as local heterodimers." PLoS One **6**(4): e19180.
Lester, R. A., J. D. Clements, et al. (1990). "Channel kinetics determine the time course of NMDA receptor-mediated synaptic currents." Nature **346**(6284): 565-567.
Leuschner, W. D. and W. Hoch (1999). "Subtype-specific assembly of alpha-amino-3-hydroxy-5-methyl-4-isoxazole propionic acid receptor subunits is mediated by their n-terminal domains." J Biol Chem **274**(24): 16907-16916.
Liao, D., N. A. Hessler, et al. (1995). "Activation of postsynaptically silent synapses during pairing-induced LTP in CA1 region of hippocampal slice." Nature **375**(6530): 400-404.
Lipton, S. A. (2004). "Failures and successes of NMDA receptor antagonists: molecular basis for the use of open-channel blockers like memantine in the treatment of acute and chronic neurologic insults." NeuroRx **1**(1): 101-110.
Liu, S. J. and R. S. Zukin (2007). "Ca2+-permeable AMPA receptors in synaptic plasticity and neuronal death." Trends Neurosci **30**(3): 126-134.
Liu, W., M. Eilers, et al. (2004). "Helix packing moments reveal diversity and conservation in membrane protein structure." J Mol Biol **337**(3): 713-729.
Loftis, J. M. and A. Janowsky (2003). "The N-methyl-D-aspartate receptor subunit NR2B: localization, functional properties, regulation, and clinical implications." Pharmacol Ther **97**(1): 55-85.
Ma, B., C. J. Tsai, et al. (2011). "Dynamic allostery: linkers are not merely flexible." Structure **19**(7): 907-917.
Madry, C., I. Mesic, et al. (2007). "The N-terminal domains of both NR1 and NR2 subunits determine allosteric Zn2+ inhibition and glycine affinity of N-methyl-D-aspartate receptors." Mol Pharmacol **72**(6): 1535-1544.
Mah, S. J., E. Cornell, et al. (2005). "Glutamate receptor trafficking: endoplasmic reticulum quality control involves ligand binding and receptor function." J Neurosci **25**(9): 2215-2225.
Malenka, R. C. and M. F. Bear (2004). "LTP and LTD: an embarrassment of riches." Neuron **44**(1): 5-21.
Malhotra, A. K., D. A. Pinals, et al. (1996). "NMDA receptor function and human cognition: the effects of ketamine in healthy volunteers." Neuropsychopharmacology **14**(5): 301-307.
Malinow, R. and R. C. Malenka (2002). "AMPA receptor trafficking and synaptic plasticity." Annu Rev Neurosci **25**: 103-126.
Mansour, M., N. Nagarajan, et al. (2001). "Heteromeric AMPA receptors assemble with a preferred subunit stoichiometry and spatial arrangement." Neuron **32**(5): 841-853.

Martin, S. J., P. D. Grimwood, et al. (2000). "Synaptic plasticity and memory: an evaluation of the hypothesis." Annu Rev Neurosci **23**: 649-711.
Massey, P. V., B. E. Johnson, et al. (2004). "Differential roles of NR2A and NR2B-containing NMDA receptors in cortical long-term potentiation and long-term depression." J Neurosci **24**(36): 7821-7828.
Matsuzaki, M., G. C. Ellis-Davies, et al. (2001). "Dendritic spine geometry is critical for AMPA receptor expression in hippocampal CA1 pyramidal neurons." Nat Neurosci **4**(11): 1086-1092.
Mattson, M. P. (2008). "Glutamate and neurotrophic factors in neuronal plasticity and disease." Ann N Y Acad Sci **1144**: 97-112.
Mayer, M. L. (2005). "Crystal structures of the GluR5 and GluR6 ligand binding cores: molecular mechanisms underlying kainate receptor selectivity." Neuron **45**(4): 539-552.
Mayer, M. L. (2006). "Glutamate receptors at atomic resolution." Nature **440**(7083): 456-462.
Mayer, M. L. (2011). "Structure and mechanism of glutamate receptor ion channel assembly, activation and modulation." Curr Opin Neurobiol **21**(2): 283-290.
Molina, M. L., J. A. Encinar, et al. (2004). "Influence of C-terminal protein domains and protein-lipid interactions on tetramerization and stability of the potassium channel KcsA." Biochemistry **43**(47): 14924-14931.
Mony, L., J. N. Kew, et al. (2009). "Allosteric modulators of NR2B-containing NMDA receptors: molecular mechanisms and therapeutic potential." Br J Pharmacol **157**(8): 1301-1317.
Monyer, H., N. Burnashev, et al. (1994). "Developmental and regional expression in the rat brain and functional properties of four NMDA receptors." Neuron **12**(3): 529-540.
Monyer, H., R. Sprengel, et al. (1992). "Heteromeric NMDA receptors: molecular and functional distinction of subtypes." Science **256**(5060): 1217-1221.
Moore, D. T., B. W. Berger, et al. (2008). "Protein-protein interactions in the membrane: sequence, structural, and biological motifs." Structure **16**(7): 991-1001.
Nash, J. E., T. H. Johnston, et al. (2005). "Subcellular redistribution of the synapse-associated proteins PSD-95 and SAP97 in animal models of Parkinson's disease and L-DOPA-induced dyskinesia." FASEB J **19**(6): 583-585.
Newpher, T. M. and M. D. Ehlers (2008). "Glutamate receptor dynamics in dendritic microdomains." Neuron **58**(4): 472-497.
Nicoletti, F., A. Arcella, et al. (2007). "Metabotropic glutamate receptors: new targets for the control of tumor growth?" Trends Pharmacol Sci **28**(5): 206-213.
Nowak, L., P. Bregestovski, et al. (1984). "Magnesium gates glutamate-activated channels in mouse central neurones." Nature **307**(5950): 462-465.
Oertner, T. G., B. L. Sabatini, et al. (2002). "Facilitation at single synapses probed with optical quantal analysis." Nat Neurosci **5**(7): 657-664.
Okamoto, S., M. A. Pouladi, et al. (2009). "Balance between synaptic versus extrasynaptic NMDA receptor activity influences inclusions and neurotoxicity of mutant huntingtin." Nat Med **15**(12): 1407-1413.
Opazo, P., M. Sainlos, et al. (2011). "Regulation of AMPA receptor surface diffusion by PSD-95 slots." Curr Opin Neurobiol.
Oswald, R. E., A. Ahmed, et al. (2007). "Structure of glutamate receptors." Curr Drug Targets **8**(5): 573-582.

Paille, V., B. Picconi, et al. (2010). "Distinct levels of dopamine denervation differentially alter striatal synaptic plasticity and NMDA receptor subunit composition." J Neurosci **30**(42): 14182-14193.
Paoletti, P. and J. Neyton (2007). "NMDA receptor subunits: function and pharmacology." Curr Opin Pharmacol **7**(1): 39-47.
Papadakis, M., L. M. Hawkins, et al. (2004). "Appropriate NR1-NR1 disulfide-linked homodimer formation is requisite for efficient expression of functional, cell surface N-methyl-D-aspartate NR1/NR2 receptors." J Biol Chem **279**(15): 14703-14712.
Pardo, C. A. and C. G. Eberhart (2007). "The neurobiology of autism." Brain Pathol **17**(4): 434-447.
Passafaro, M., V. Piech, et al. (2001). "Subunit-specific temporal and spatial patterns of AMPA receptor exocytosis in hippocampal neurons." Nat Neurosci **4**(9): 917-926.
Pasternack, A., S. K. Coleman, et al. (2002). "Alpha-amino-3-hydroxy-5-methyl-4-isoxazolepropionic acid (AMPA) receptor channels lacking the N-terminal domain." J Biol Chem **277**: 49662-49667.
Penn, A. C., S. R. Williams, et al. (2008). "Gating motions underlie AMPA receptor secretion from the endoplasmic reticulum." EMBO J **27**(22): 3056-3068.
Picconi, B., G. Piccoli, et al. (2012). "Synaptic dysfunction in Parkinson's disease." Adv Exp Med Biol **970**: 553-572.
Pina-Crespo, J. C., M. Talantova, et al. (2010). "Excitatory glycine responses of CNS myelin mediated by NR1/NR3 "NMDA" receptor subunits." J Neurosci **30**(34): 11501-11505.
Priel, A., S. Selak, et al. (2006). "Block of kainate receptor desensitization uncovers a key trafficking checkpoint." Neuron **52**(6): 1037-1046.
Rambhadran, A., J. Gonzalez, et al. (2010). "Subunit arrangement in N-methyl-D-aspartate (NMDA) receptors." J Biol Chem **285**(20): 15296-15301.
Ren, H., Y. Honse, et al. (2003). "A site in the fourth membrane-associated domain of the N-methyl-D-aspartate receptor regulates desensitization and ion channel gating." J Biol Chem **278**: 276-283.
Ren, H., A. K. Salous, et al. (2008). "Functional interactions of alcohol-sensitive sites in the N-methyl-D-aspartate receptor M3 and M4 domains." J Biol Chem **283**(13): 8250-8257.
Rossmann, M., M. Sukumaran, et al. (2011). "Subunit-selective N-terminal domain associations organize the formation of AMPA receptor heteromers." EMBO J **30**(5): 959-971.
Russ, W. P. and D. M. Engelman (2000). "The GxxxG motif: a framework for transmembrane helix-helix association." J Mol Biol **296**(3): 911-919.
Ryan, T. J., R. D. Emes, et al. (2008). "Evolution of NMDA receptor cytoplasmic interaction domains: implications for organisation of synaptic signalling complexes." BMC Neurosci **9**: 6.
Schmid, S. M., C. Korber, et al. (2007). "A domain linking the AMPA receptor agonist binding site to the ion pore controls gating and causes lurcher properties when mutated." J Neurosci **27**(45): 12230-12241.
Schmid, S. M., C. Korber, et al. (2007). "A domain linking the AMPA receptor agonist binding site to the ion pore controls gating and causes lurcher properties when mutated." J Neurosci **27**(45): 12230-12241.
Schorge, S. and D. Colquhoun (2003). "Studies of NMDA receptor function and stoichiometry with truncated and tandem subunits." J Neurosci **23**(4): 1151-1158.

Schuler, T., I. Mesic, et al. (2008). "Formation of NR1/NR2 and NR1/NR3 heterodimers constitutes the initial step in N-methyl-D-aspartate receptor assembly." J Biol Chem **283**(1): 37-46.
Schwappach, B. (2008). "An overview of trafficking and assembly of neurotransmitter receptors and ion channels (Review)." Mol Membr Biol **25**(4): 270-278.
Senes, A., D. E. Engel, et al. (2004). "Folding of helical membrane proteins: the role of polar, GxxxG-like and proline motifs." Curr Opin Struct Biol **14**(4): 465-479.
Shanks, N. F., T. Maruo, et al. (2010). "Contribution of the global subunit structure and stargazin on the maturation of AMPA receptors." J Neurosci **30**(7): 2728-2740.
Sheng, M. and C. C. Hoogenraad (2007). "The postsynaptic architecture of excitatory synapses: a more quantitative view." Annu Rev Biochem **76**: 823-847.
Shi, S., Y. Hayashi, et al. (2001). "Subunit-specific rules governing AMPA receptor trafficking to synapses in hippocampal pyramidal neurons." Cell **105**(3): 331-343.
Sobolevsky, A. I., C. Beck, et al. (2002). "Molecular rearrangements of the extracellular vestibule in NMDAR channels during gating." Neuron **33**(1): 75-85.
Sobolevsky, A. I., M. L. Prodromou, et al. (2007). "Subunit-specific contribution of pore-forming domains to NMDA receptor channel structure and gating." J Gen Physiol **129**(6): 509-525.
Sobolevsky, A. I., M. P. Rosconi, et al. (2009). "X-ray structure, symmetry and mechanism of an AMPA-subtype glutamate receptor." Nature **462**(7274): 745-756.
Sommer, B., M. Kohler, et al. (1991). "RNA editing in brain controls a determinant of ion flow in glutamate-gated channels." Cell **67**(1): 11-19.
Steigerwald, F., T. W. Schulz, et al. (2000). "C-Terminal truncation of NR2A subunits impairs synaptic but not extrasynaptic localization of NMDA receptors." J Neurosci **20**(12): 4573-4581.
Stern-Bach, Y., B. Bettler, et al. (1994). "Agonist selectivity of glutamate receptors is specified by two domains structurally related to bacterial amino acid-binding proteins." Neuron **13**(6): 1345-1357.
Stern-Bach, Y., S. Russo, et al. (1998). "A point mutation in the glutamate binding site blocks desensitization of AMPA receptors." Neuron **21**(4): 907-918.
Stroebel, D., S. Carvalho, et al. (2010). "Functional evidence for a twisted conformation of the NMDA receptor GluN2A subunit N-terminal domain." Neuropharmacology **60**(1): 151-158.
Sukumaran, M., A. C. Penn, et al. (2012). "AMPA receptor assembly: atomic determinants and built-in modulators." Adv Exp Med Biol **970**: 241-264.
Sun, Y., R. Olson, et al. (2002). "Mechanism of glutamate receptor desensitization." Nature **417**(6886): 245-253.
Suzuki, E., M. Kessler, et al. (2005). "C-terminal truncation affects kinetic properties of GluR1 receptors." Mol Cell Neurosci **29**(1): 1-10.
Swanson, G. T., T. Green, et al. (2002). "Differential activation of individual subunits in heteromeric kainate receptors." Neuron **34**(4): 589-598.
Talukder, I., P. Borker, et al. (2010). "Specific sites within the ligand-binding domain and ion channel linkers modulate NMDA receptor gating." J Neurosci **30**(35): 11792-11804.
Talukder, I. and L. P. Wollmuth (2011). "Local constraints in either the GluN1 or GluN2 subunit equally impair NMDA receptor pore opening." J Gen Physiol **138**(2): 179-194.

Terhag, J., K. Gottschling, et al. (2010). "The Transmembrane Domain C of AMPA Receptors is Critically Involved in Receptor Function and Modulation." Front Mol Neurosci **3**: 117.
Tomita, S., H. Adesnik, et al. (2005). "Stargazin modulates AMPA receptor gating and trafficking by distinct domains." Nature **435**(7045): 1052-1058.
Traynelis, S. F., L. P. Wollmuth, et al. (2010). "Glutamate receptor ion channels: structure, regulation, and function." Pharmacol Rev **62**(3): 405-496.
Tu, L. and C. Deutsch (1999). "Evidence for dimerization of dimers in K+ channel assembly." Biophys J **76**(4): 2004-2017.
Valluru, L., J. Xu, et al. (2005). "Ligand binding is a critical requirement for plasma membrane expression of heteromeric kainate receptors." J Biol Chem **280**(7): 6085-6093.
Watanabe, J., C. Beck, et al. (2002). "DRPEER: A motif in the extracellular vestibule conferring high Ca^{2+} flux rates in NMDA receptor channels." J Neurosci **22**(23): 10209-10216.
Waxman, E. A. and D. R. Lynch (2005). "N-methyl-D-aspartate receptor subtypes: multiple roles in excitotoxicity and neurological disease." Neuroscientist **11**(1): 37-49.
Wenthold, R. J., R. S. Petralia, et al. (1996). "Evidence for multiple AMPA receptor complexes in hippocampal CA1/CA2 neurons." J Neurosci **16**(6): 1982-1989.
Wo, Z. G. and R. E. Oswald (1994). "Transmembrane topology of two kainate receptor subunits revealed by N-glycosylation." Proc Natl Acad Sci U S A **91**(15): 7154-7158.
Wo, Z. G. and R. E. Oswald (1995). "Unraveling the modular design of glutamate-gated ion channels." Trends Neurosci. **18**: 161-168.
Wo, Z. G. and R. E. Oswald (1995). "Unraveling the modular design of glutamate-gated ion channels." Trends Neurosci **18**(4): 161-168.
Wollmuth, L. P. and S. F. Traynelis (2009). "Neuroscience: Excitatory view of a receptor." Nature **462**(7274): 729-731.
Wood, M. W., H. M. A. VanDongen, et al. (1995). "Structural conservation of ion conduction pathways in K channels and glutamate receptors." Proc. Nat. Acad. Sci. (USA) **92**: 4882-4886.
Woolf, C. J. and M. W. Salter (2000). "Neuronal plasticity: increasing the gain in pain." Science **288**(5472): 1765-1769.
Yao, G., Y. Zong, et al. (2011). "Crystal structure of the glutamate receptor GluA1 N-terminal domain." Biochem J **438**(2): 255-263.
Yashiro, K. and B. D. Philpot (2008). "Regulation of NMDA receptor subunit expression and its implications for LTD, LTP, and metaplasticity." Neuropharmacology **55**(7): 1081-1094.
Yelshansky, M. V., A. I. Sobolevsky, et al. (2004). "Block of AMPA receptor desensitization by a point mutation outside the ligand-binding domain." J Neurosci **24**: 4728-4736.
Yuan, H., K. B. Hansen, et al. (2009). "Control of NMDA receptor function by the NR2 subunit amino-terminal domain." J Neurosci **29**(39): 12045-12058.
Zhang, S. J., M. N. Steijaert, et al. (2007). "Decoding NMDA receptor signaling: identification of genomic programs specifying neuronal survival and death." Neuron **53**(4): 549-562.
Zhou, F. X., H. J. Merianos, et al. (2001). "Polar residues drive association of polyleucine transmembrane helices." Proc Natl Acad Sci U S A **98**: 2250-2255. Epub 2001 Feb 2213.